1 General remark

The reply is structured as follows:

- Referee comment

  ⇒ Authors reply

  → Modification(s) in the manuscript. "old" → "new"

2 Reply to Referee #1

2.1 General comments

- The authors present a new sinking scheme for marine aggregates that takes into account selected important effects of aggregate microstructure (such as estimates of porosity, TEP content, and density based on the aggregate composition, which is derived from HAMOCC tracer concentrations) and of the resulting estimated aggregate size distribution. The authors achieve this without the use of an explicit aggregation model, and without introducing different particle size classes, thereby keeping the scheme very affordable, affordable enough for long-term global carbon cycle modelling. Because several of the incorporated mechanisms that affect the sinking of particulate carbon in the ocean were previously neglected in global carbon cycle models, the presented work is a welcome contribution to the field and should be published.
  While the presented sensitivity experiments with respect to selected parameters of the sinking scheme seem well-placed in the manuscript, I would suggest to reconsider wether the CO2 -sensitivity experiments would be better-placed in a separate manuscript, 1) given the length of the manuscript, 2) given that the title does at least not explicitly reflect those results, and 3) given some inconsistencies compared to atmosphere–ocean CO2 flux observations described below that may be better addressed in more detail in a separate manuscript, specifically aiming at the role of aggregate and sinking speed changes in response to greenhouse gas emissions and climate change.
  The manuscript provides a large amount of sinking-relevant background information that is interesting on its own, and necessary to understand the (incorporated or neglected) processes in the new sinking

scheme. The description of the new sinking scheme itself is also very detailed, making the results reproducible – also with the help of the very well-documented supplementary material. This, combined with the presented extensive analysis and selected parameter sensitivity experiments, understandably leads to a rather long manuscript. However, I do believe that the manuscript can still be shortened and readability can be improved by clarifying / simplifying some formulations (see comments on selected sentences below).
Some additional minor comments to improve/clarify the manuscript prior to publication, as well as some typos are listed below.

⇒ We thank the reviewer for her/his comprehensive, constructive and positive review. With respect to the section on atmosphere-ocean carbon dioxide fluxes (Sect. 3.8 Regional CO_2 uptake), we admit having used an erroneous y-label for Fig. 14 a. Indeed, it is Gt C yr^{-1} for the cumulative zonal CO_2 fluxes. We apologize for the confusion. Apart from that, we are confident that the results are in agreement with present knowledge, which we comment on below. Since the CO_2 fluxes are of clear interest in an ESM framework and a benchmark for the development of such a comprehensive aggregate-representing model component, we decided to keep this present section. For the sake of clarity, we changed the section title.

→ Changed the unit (see Fig.1).
Section Title: "Regional CO_2 uptake" → "Regional CO_2 fluxes"

2.2 Minor comments

- Abstract, line 10: I would suggest to replace "which has been recently constrained by" by "as recently constrained by", to clarify that this particular latitudinal pattern of POC transfer efficiency is reproduced. I think it would be appropriate to mention (here or at least later on page 3 around lines 6-12 or 29-31) that previous estimates of transfer efficiency showed an opposing latitudinal pattern (Henson et al. 2012).

⇒ Thanks for your suggestions. We did the replacement accordingly. In addition, we now mention the opposing pattern on page 3, line 30, see also below.

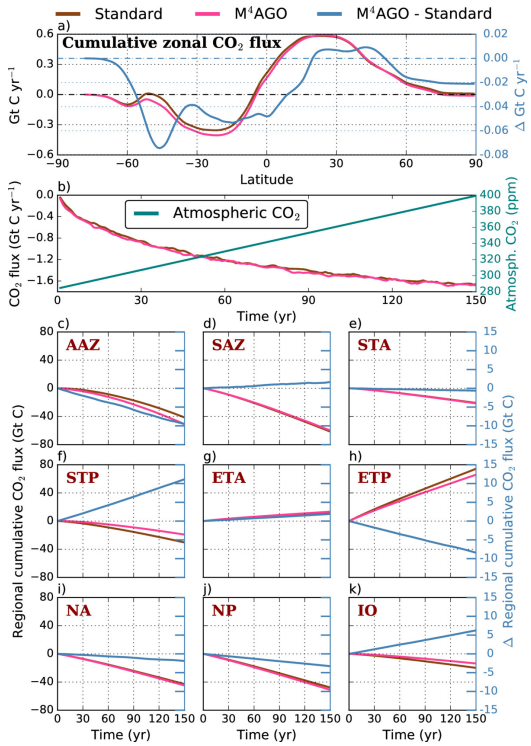

Figure 1: Units from manuscript Fig. 14 a corrected ("Gt C yr^{-1} deg^{-1}" → "Gt C yr^{-1}").

→ "which has been recently constrained by" → "as recently constrained by",
"…more reliable than previous estimates (e. g. Henson et al., 2012; Marsay et al., 2015)" → "…more reliable than previous estimates with partly opposing latitudinal pattern (e. g. Henson et al., 2012; Marsay et al., 2015)"

- Abstract, lines 14-16: Please rephrase. In standalone runs with rising carbon dioxide... M^4AGO only alters the simulated fluxes. Sentences could maybe also be shortened, e.g.: Using M^4AGO in standalone runs with prescribed rising CO2 concentrations (with-out climate feedback) leads to higher CO2 uptake in the Southern Ocean, and to lower CO2 uptake in the subtropical gyres compared to the standard run, while the global oceanic CO2 uptake remains the same.

⇒ Rephrased.

→ "In ocean standalone runs and rising carbon dioxide (CO_2) without CO_2 climate feedback, M^4AGO alters the regional ocean-atmosphere CO_2 fluxes compared to the standard model." → "Prescribing rising carbon dioxide (CO_2) concentrations in standalone runs (without climate feedback), M^4AGO alters the regional ocean atmosphere CO_2 fluxes compared to the standard model."

- Abstract, lines 12-13: Please rephrase / clarify. Are temperature effects contributing ("driving factor") to the simulated transfer efficiency pattern? Wouldn't at least the temperature effect on viscosity counteract the simulated pattern? Or does this refer to the newly introduced temperature-dependent remineralization of POC, which, if I understand correctly, least counteracts the high sinking speeds in the high latitudes (countours in Fig. 9b)?

  ⇒ Thanks. We referred here to the temperature effect on remineralization. We clarified it.

  → "a driving factor" → "a driving factor for remineralization"

- Page 2, line 17, "The sinking velocity of aggregates is primarily determined by their size." I understand that aggregate size does matter, but is it really the main factor? Reference? Even very large aggregates can be rather buoyant (e.g., Riebesell 1992).

  ⇒ This is an interesting comment and we realize, also by the same comment of reviewer #2, that there seems to be much confusion about the controlling factors for sinking velocity, which deserves a publication on its own (being in progress). We want to emphasize here that we clearly state in the follow-up sentence that structure and composition of aggregates regulate the excess density and can thus have a high impact on sinking velocity (we now provide a reference for it). Nevertheless, we would here argue from the mathematical perspective. For simplicity and neglecting the changing drag coefficient for particles with higher Reynolds particle numbers,

let's consider the Stokes sinking velocity for low particle Reynolds numbers:

$$w_s(d, \rho_f, \ldots) = \frac{1}{18\,\mu}\,(\rho_f - \rho)\,g\,d^2 \tag{1}$$

where d is the diameter, μ the molecular dynamic viscosity, ρ_f the aggregate density, ρ is the density of the ambient fluid, and g is the gravitational acceleration constant. It is obvious that $w_s \propto (\rho_f - \rho)$ and $w_s \propto d^2$. Hence, sinking velocity only linearly increases with aggregate density, while it increases with a power law relationship of the diameter. This suggests that size is indeed the primary factor controlling sinking velocity. If we consider the fractal scaling relationship for excess density (Eq. (5) and (8) in our manuscript), this clarity becomes blurred, because the aggregate excess density is itself size-dependent. However, if we further consider that natural aggregate size ranges over more than an order of magnitude (from sizes of about $0.45 \cdot 10^{-6}\,\mathrm{m}$, which is operationally defined by typical filter pore sizes for POM filtration, to size of $O(10^{-2}\,\mathrm{m})$), while aggregate excess density $(\rho_f - \rho)$ typically ranges only between zero (neutrally buoyant) and $O(100\,\mathrm{kg\,m^{-3}})$, it is obvious that size is the dominant factor (for non-neutrally buoyant aggregates), while, as we clearly state, excess density can entail high variability of sinking velocity. This is also, what e. g. Iversen & Robert (2015)[1] imply, when writing '2- to 3-fold higher **size-specific** sinking velocities' for mineral ballasted aggregates.

→ We add the reference Iversen & Robert 2015 to the follow-up sentence: "...entail high variability of excess density and thus sinking speed of aggregates (Iversen & Robert, 2015)"

- Page 3, line 15: Please replace "while ignoring" with "while neglecting" (the effects are still discussed).

  ⇒ Thanks.

  → Changed.

[1] Iversen & Robert 2015: *Ballasting effects of smectite on aggregate formation and export from a natural plankton community.* Marine Chemistry 175, 18 - 27.

- Page 3, lines 29-31: As mentioned above, I would point out that Henson et al. (2012) suggested an opposing pattern. Would it be possible to reproduce also this opposing pattern with M^{4}AGO? I think a brief discussion of this issue would be interesting – potentially regarding the presented sensitivity experiment with smaller diatom frustules showing much lower transfer efficiencies in high latitudes?

  ⇒ As stated above, we now mention the opposing latitudinal pattern explicitly. From our present knowledge about the model responses, the pattern proposed by Henson et al. 2012 could be likely reproduced by applying unreasonable parameter values. However, an investigation of this question would require multiple model simulations, which is a computationally costly task and out of the scope of our manuscript. We therefore only provide reasons to relate our model results to Weber et al. 2016 (an order of magnitude more phosphate than direct flux observations, which makes the transfer efficiency calculations of Weber et al. more reliable), and don't discuss the pattern proposed by Henson et al. intensively, which may be a future work.

  → Changed as described above. We now mention the opposing pattern.

- Page 4, line 28: Please consider including the equation for opal dissolution explicitly, also to better understand the given dissolution rates in Table 1. As far as I understand / looking at the HAMOCC code, the opal dissolution rate given in Table 1 corresponds to 7 °C?

  ⇒ The reviewer is right, and we agree that this information is useful. We hence provide the equation. However, we believe, it is better placed on p. 12, l18, where the new Q_{10}-dependent remineralization has been introduced. While doing so, we realized that we haven't introduced the symbols r_{opal}, T, T_{ref} and r_{POC} which we additionally added.

  → Added after Eq. (30):
  "where r_{opal} is the opal dissolution rate at the reference water temperature $T_{\mathrm{ref,opal}}$ and T is the ambient water temperature."

"In the standard version, we remain with the former linearly temperature-dependent opal dissolution (Ragueneau et al., 2000, Segschneider and Bendtsen, 2013)" $\rightarrow$ "In the standard version, we remain with the former linearly temperature-dependent opal dissolution ($\partial_t[\text{opal}] = -r_{\text{opal}}\,(0.1\,(T+3))\,[\text{opal}]$) (Ragueneau et al., 2000, Segschneider and Bendtsen, 2013)"

"...where K_{O_2} is the half saturation constant in Michaelis-Menten kinetics" $\rightarrow$ "...where K_{O_2} is the half saturation constant in Michaelis-Menten kinetics, and r_{POC} is the remineralization rate at reference temperature $T_{\text{ref,POC}}$

- Page 5, line 9-11: Please rephrase; e.g., ... is eventually computed from a number distribution that is truncated at the minimum and maximum aggregate diameters ..., and expressions for the mass and sinking velocity of aggregates of a particular diameter:

  $\Rightarrow$ Thanks. Rephrased accordingly and accounted for the reviewers #2 comment on integration differential.

  $\rightarrow$ "...determined by a truncated number distribution, Eq. (2), through the minimum and maximum aggregates sizes, d_{min} and d_{max}, respectively, the aggregate mass, $m(d)$, and the sinking velocity of single aggregates, $w_s(d)$" $\rightarrow$ "...computed from the number distribution, Eq. (2), that is truncated at the minimum and maximum aggregate sizes, d_{min} and d_{max}, respectively, and expressions for the aggregate mass, $m(d)$, and the sinking velocity of aggregates, $w_s(d)$, of a particular diameter, d. Integration over the aggregate size spectrum yields $\langle w_s \rangle$,"

- Page 5, line 26: It would be helpful to define the diameter d of an aggregate more accurately here. For example, is the diameter of an aggregate with df =1 (i.e., a chain) just given by its length?

  $\Rightarrow$ Yes. Adding a sub-clause.

  $\rightarrow$ A $d_f = 1$ would depict a chain of aggregate constituents, where the length equals the aggregate diameter, ..."

- Page 6, line 7: Please move reference to "well known" Stokes (1851) here.

  ⇒ Ok. Done.

  → Moved the reference.

- Page 6, line 26: I am a little lost here. What is the motivation for this paragraph? What is n? And why is that equation only true for $n \neq n_p$?

  ⇒ We here derive the mean primary particle size, based on the encapsulated solid volumes of individual, poly-sized primary particles inside the fractal aggregate, to conserve the total solid volume and thus the porosity. This comes at the cost that the theoretical number of primary particles of mean primary particle diameter $\langle d_\mathrm{p} \rangle$ is not necessarily the same as the number of individual primary particles (which would only be the case for mono-sized primary particles). This, however, is negligible for the calculations that follow. We now give some more explanation that clarifies the issue.

  → "while $n \cdot \langle d_p \rangle^3 = \sum_i n_i \, d_{p,i}^3$ with $n \neq \sum_i n_i$, and thus the porosity of the aggregate is unimpaired." → "and thus the porosity of the aggregate is unimpaired, while the calculation does not presume equal number of mean, n, and individual primary particles, $\sum_i n_i$, (hence, $n \cdot \langle d_p \rangle^3 = \sum_i n_i \, d_{p,i}^3$ with $n \neq \sum_i n_i$ for poly-sized primary particles), which is negligible in the following as we don't consider n any further."

- Page 6, line 27: Do I understand correctly that "same heterogeneity in a size spectrum" means that all aggregates of a particular composition / in a particular grid cell are assumed to have the same heterogeneity/microstructure/dp (for all aggregate diameters d)?

  ⇒ Yes.

  → Seems, as there is no change needed. Remained.

- Page 7, line 9: Please define Vp,i more accurately; volume of the primary particles per unit volume of sea water?

⇒ $V_{p,i} = \frac{1}{6}\,\pi\,d_{p,i}^3$ is the individual primary particle volume. We clarified it.

→ "$V_{p,i}$" → "$V_{p,i} = \frac{1}{6}\,\pi\,d_{p,i}^3$"

- Page 7, line 6-8: Maybe shorten to "... tracer Ci, namely detritus, opal, calcite and dust."

  ⇒ Thanks, but we remained with the extra sentence, since we believe it is an important information that shouldn't be given in a sub-clause.

  → Remained.

- Page 7, line 15: Add "Multiplication by the volume of the mean primary particle then yields..."; helps the reader / I didn't see this at first.

  ⇒ Changed.

  → "the mass of a mean primary particle can be written as" → "multiplication by the volume of the mean primary particle then yields the mass of a mean primary particle"

- Page 8, line 3: Please add reference to traditional scaling relationship.

  ⇒ Added the previously given references.

  → added: (Logan and Wilkinson, 1990; Kranenburg, 1994)

- Page 9, line 1: For consistency, if j=0..3 here, also add definitions of a/bj=0 in last paragraph of page 8.

  ⇒ We added a sub-clause at the end of the whole paragraph, p.9, l.7, since the application of $a_{j=0}$ and $b_{j=0}$ is only useful in the context of how the lower integration boundary of the mean sinking velocity is defined. Further, we introduce $a_{j=0} = b_{j=0} = 1$, since dividing by zero in case of $a_{j=0} = b_{j=0} = 0$ is not defined.

  → is the maximum diameter of aggregate, and by applying $a_{j=0} = b_{j=0} = 1$, the lower integration boundary equals the mean primary particle diameter

- Page 9, line 13: It is not clear to me what "dynamic steady state" means.

  ⇒ We extended the sentence to specify that the dynamic steady state is between aggregation and fragmentation

    → "Instead of modeling the processes of aggregation and fragmentation explicitly or prescribing b, we assume dynamic steady state for the slope of the number distribution" → "Instead of modeling the processes of aggregation and fragmentation explicitly or prescribing b, we assume dynamic steady state between aggregation and fragmentation to describe the slope of the number distribution."

- Page 9, line 20-21: I am wondering why the assumption of Reynolds numbers between 0.1 and 10 here is okay, while the authors go through the extra trouble of deriving expressions for the sinking speed for even smaller and even larger Reynolds numbers in Section 2.2.2. Is there a reason for this?

  ⇒ Thanks for pointing out the lacking information. Since we are aware of and discuss the limitations of the dynamic steady state size distribution, we here avoided extra complexity where little benefit as compared to an explicit representation of the dynamic size distribution is expected (see Sect. 3.10: Current limitations of M^{4}AGO, where we discuss the limitations of our current approach versus an explicit representation of a dynamic size distribution). We therefore simplify at this point and remain with text.
  With regards to the drag formulation: in a previous model version of M^{4}AGO, we applied the simple Stokes sinking velocity ($c_D = 24/Re_p$) and disregarded the restriction to $Re_p < 0.1$, with similar well results for the transfer efficiency, but clearly underestimated the maximum diameter of aggregates and thus the represented size range of aggregates. For future applications of M^{4}AGO, this can be of relevance. In order to point out this advantage, we add a sentence in the previous paragraph (p.8,l.24) and remove sub-clause on p.9, l.4

→ "We approximate this representation by" → "This drag representation leads to smaller settling velocities for large aggregates than the classical Stokes drag ($c_D = 24/Re_p$). Hence, aggregates can grow larger, until they reach the globally fixed critical Re_p for fragmentation, Re_{crit}, which leads to a more realistic representation of the size range of aggregates. We approximate the White drag representation by"
Removed: "where Re_{crit} is the globally fixed critical Re_{p} for fragmentation."

- Page 10, line 6: Please clarify / see above comment on "in a size spectrum": ... as one value across all aggregate sizes.?

  ⇒ Modified.

  → "as one value across a particle size spectra" → as one value across all aggregate sizes

- Page 11, line 10: Shouldn't it read: When detritus from the frustules is remineralized, it is replaced...?

  ⇒ No, since there can be more detritus available than needed to fill the void.

  → Remained.

- Page 12, line 2: Please rephrase: ...thus decrease the fractal dimension of aggregates, and ii) ...

  ⇒ Done.

  → "thus fractal dimension of aggregates is small" → "thus decrease the fractal dimension of aggregates"

- Page 15, Table 1: Is it correct that the applied opal dissolution rate in the setup with M^4AGO is larger than that in the standard model setup? What is the resulting effect of the temperature-dependency here? Wouldn't the larger remineralization rate combined with the slower opal sinking speeds in the euphotic zone lead to very high opal production, and consequently to very low calcite production?

⇒ The reviewer is right that the dissolution rate is larger in M^4AGO than in the standard model setup. However, the RLSs for opal (the ratio between sinking velocity and dissolution rate) eventually determine the silicate retention in the water column. As briefly discussed in Sect. 3.6: Regional fluxes & rain ratios, the opal RLSs are indeed shorter in surface waters, but longer in regions of the mesopelagic zone and below. In total, the attenuation of opal fluxes with depth remain similar in most regions (see Fig. 11). Hence, HAMOCC with M^4AGO doesn't show much difference in the global opal to $CaCO_3$ production ratio, which can also be seen in the flux ratios, shown in Fig. 5.

→ Remained with the present state of description.

- Page 16, line 7: I am not sure if I understand correctly: Is dp,calc chosen particularly small to avoid an overestimate of the volumetric density effect? If so, for clarity, while accounting for could be rephrased: We set dp,calc ..., to account for ....

⇒ Modified accordingly.

→ ", and hence, we set $d_{p,\mathrm{calc}} = 3\,\mu\mathrm{m}$, which is thus at the lower bound of the observed range while accounting for the volumetric density effect of non-spherical plate-like coccoliths." → "We set $d_{p,\mathrm{calc}} = 3\,\mu\mathrm{m}$, which is thus at the lower bound of the observed range, to account for the volumetric density effect of non-spherical plate-like coccoliths."

- Page 16, line 24: Sentence unclear to me; ...distinction between parameter tuning and model evaluation, when... (?)

⇒ We aimed at clarification and rephrased the sentence.

→ "The close connection between the parametrized processes of sinking and remineralization, the transfer efficiency and the climatological nutrient field hampers the clear distinction between tuning and evaluation data when comparing the model results to literature values for transfer efficiency" → "The newly parametrized

processes of sinking and remineralization directly affect the transfer efficiency, and thus the climatological nutrient fields. This close connectedness hampers the clear distinction between data employed for model tuning or for model evaluation, when comparing the model results to literature values for transfer efficiency."

- Page 16, line 33: Please rephrase: Since the adaptation of the sinking velocity and thus of the transfer efficiency to the remineralization and dissolution rates occurs within a few years, parameter variations aiming at a quantitative agreement with the transfer efficiency of Weber et al. were feasible. (?)

  ⇒ For clarity, we split the sentence.

  → "Since the adaptation of the sinking velocity versus the remineralization and dissolution rates, and thus the transfer efficiency, was within a few years, parameter variations aiming at a quantitative agreement with the transfer efficiency of Weber et al. (2016) enabled a useful strategy to select for promising parameter sets." → "We performed parameter variations aiming at a quantitative agreement with the transfer efficiency of Weber et al. (2016). Since the adjustment of the sinking velocity versus the remineralization and dissolution rates, and thus the transfer efficiency, occurs within a few years, this strategy was useful to select for promising parameter sets."

- Page 17, lines 8-13: Move to results section / next paragraph?

  ⇒ Since this part includes methodological aspects, we follow your suggestion to start a new paragraph in the methods section.

  → New paragraph started.

- Page 17, lines 12-13: The annual mean of only one year seems rather short. Have you checked how sensitive your results are with respect to interannual variability due to, e.g., ENSO or deepwater formation variability?

⇒ We are using a climatological forcing, which, by definition, does not resolve interannual events such as ENSO. However, internal variability of ocean circulation still happens and we here therefore provide the climatological 100 a mean of the transfer efficiency and its respective standard deviation (Fig. 2). As can be seen, the standard deviation is small for most ocean regions and exhibits higher values in the Antarctic polar regions. These are likely linked to the shifting of polar fronts through the internal variability of ocean circulation that imprints on the ocean biogeochemistry. However, the overall latitudinal mean pattern of the transfer efficiency resembles the one of Fig. 8 in the manuscript. In our manuscript, we are not concerned with the internal variability and focused on the general potential effects of aggregate composition and microstructure on POC fluxes as explanatory factors for the global pattern of transfer efficiency. We may revisit the aspect of internal variability in a follow up work and don't want to lengthen the manuscript further at this stage. We therefore remain with the present status.

→ Remained.

- Page 18, lines 1-3: Please rephrase / correct sentence structure ("features" can not refer to "In the M^4AGO run").

  ⇒ Thanks. Rephrased accordingly.

  → "In the M^4AGO run, the equatorial Pacific exhibits the lowest export efficiencies, features maximum values of about 0.14-0.16 in the subtropical gyres and about 0.20 in the Arctic region (Fig. 4 d)" → "In the M^4AGO run, the equatorial Pacific exhibits the lowest export efficiencies, the subtropical gyres feature maximum values of about 0.14-0.16, and the Arctic region about 0.20 (Fig. 4 d)"

- Page 18, lines 3-4: It is difficult to say from Fig. 4 wether the use of M^4AGO really leads to smaller latitudinal variability, since the minima and the global mean p-ratio also seem lower than in the standard run. Maybe remove this statement or double-check?

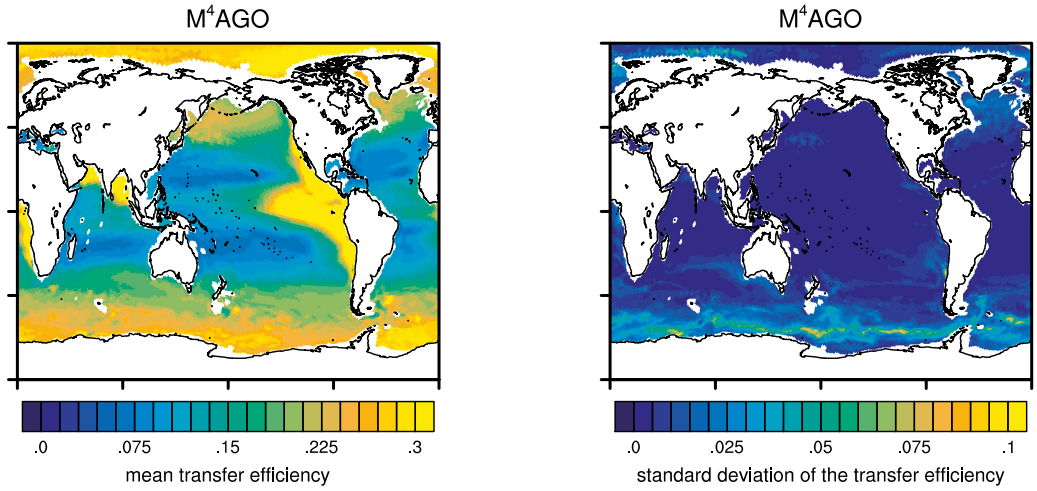

Figure 2: 100 a climatology of the transfer efficiency (left) and the standard deviation (right). Shifting of polar fronts due to internal variability of ocean circulation and the affected biogeochmistry are likely the cause for higher standard deviation of the transfer efficiency in the Antarctic polar region than in the rest of the ocean. The overall mean transfer efficiency pattern resembles the one shown in Fig. 8 in our manuscript.

⇒ We double-checked. The standard has even smaller minimum p-ratios than the M^{4}AGO run. We therefore remain with the text.

→ Remained.

- Page 20, line 8: This is only shown in Fig. 7a, not in Fig. 7d.

⇒ Thanks.

→ Modified: "7 a,d" → "7 a"

- Page 21, Figure 7 (and page 26, Fig. 9): It would be helpful to show (or at least describe) the location of WOA transect P16.

⇒ We now describe the location in the caption. Caption changed:

→ "Modeled marine aggregate properties on WOA transect P16" → "Modeled marine aggregate properties on the Pacific WOA transect P16, which is located at about 150 °W"

- Page 23, line 7: Sentence unclear to me: ... we neglect this effect versus? Maybe delete versus the lower primary particle binding forces? What are those forces?

  ⇒ We aimed at clarification and rephrased the sentence.

  → "While compaction likely enhances the internal number of binding links in aggregates, we neglect this effect versus the lower primary particle binding forces on the overall susceptibility to shear stress and thus kept Re_{crit} globally constant." → "Compaction can coincide with an increasing number of binding links in aggregates, which can lower the overall susceptibility of aggregates to shear stress. In M^{4}AGO, we disregard this effect and keep Re_{crit} globally constant.

- Page 23, line 8: "we neglect... and kept" For clarity, I would suggest to consistently stick to present-tense for the work performed for this study, and to past tense for previous results.

  ⇒ We rephrased the sentence and now stick to present tense. See above.

  → As reformulated in the previous comment.

- Page 25, line 26: Shouldn't it read "...decay to 1/e of its initial value, ..."?

  ⇒ The reviewer is right. Thank you very much! We modified it accordingly

  → "half" → "$1/e$ ($\approx 37\,\%$)"

- Page 27, line 9 / Figure 9: The lower remineralization rates described here are hard to see in Figure 9b, also due to the missing label on the -30% (?) contour; maybe smaller contour intervals would help.

  ⇒ For clarity, we add the 30 % contour label, see Fig. 3.

  → Contour label added.

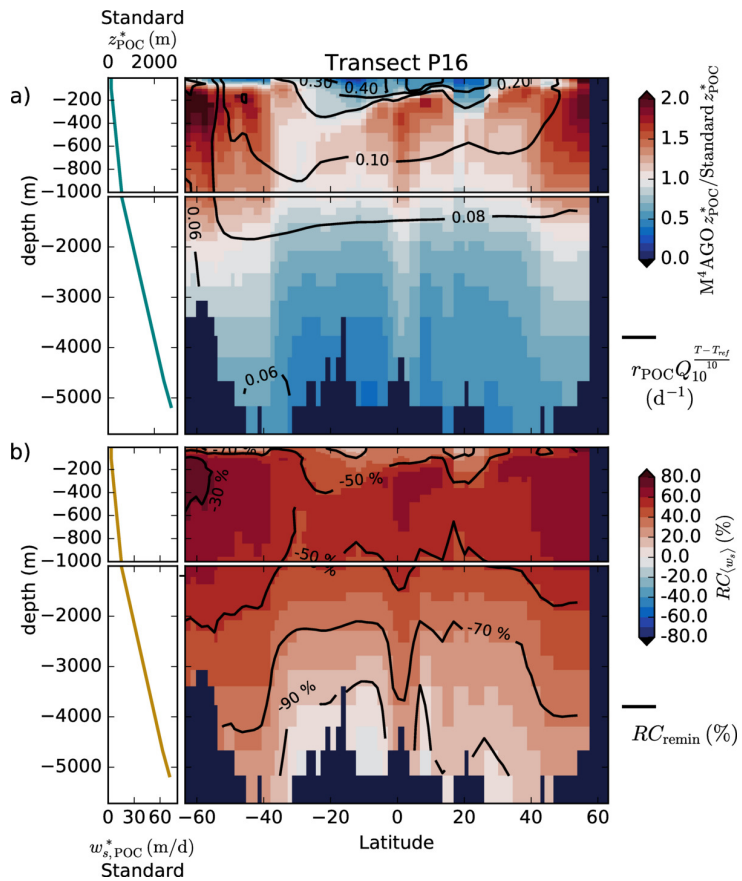

Figure 3: Added "-30 %" contour level label in b)

- Page 27, lines 29-30: Maybe clearer: The relative contributions provide information about the main driving factors for local sinking speed deviations from the global mean.

  ⇒ We modified the sentence.

  → "The relative contributions provide an information on the main driving factors, expressed as percentage, for the local $\langle w_s \rangle$ as compared to global average aggregates." → "The relative contributions provide information about the main driving factors for the local $\langle w_s \rangle$ as compared to $\langle w_s \rangle$ of global average aggregates."

- Page 28, lines 23-24: Please rephrase / clarify sentence; e.g.: M^{4}AGO

thus likely underestimates the spatial variability and relative contribution of b to ws.

⇒ Thanks. Done.

→ "likely underestimates the spatial variability of the relative contribution to $\langle w_s \rangle$" → "likely underestimates the spatial variability and relative contribution of b to $\langle w_s \rangle$"

- Page 30, lines 22-23: Unclear sentence structure. Maybe: Similar to POC fluxes, opal fluxes exhibit shorter RLSs in ..., while they exceed the standard RLSs in ...

  ⇒ Modified accordingly.

  → "Similar to the POC remineralization length scales, opal fluxes exhibit shorter opal RLS in the surface waters, while they exceed the standard RLS in the mesopelagic zone and below (not shown)." → "Similar to POC fluxes, opal fluxes exhibit shorter opal RLSs in the surface waters, while they exceed the standard RLSs in the mesopelagic zone and below (not shown)."

- Page 30, line 27: "... fluxes are generally small." Is this true for both model versions? Not shown here, or is it?

  ⇒ It's a result from low opal production in the subtropical gyres, visible in Fig. 5 a,b. We therefore give a reference to Fig. 5a,b

  → added: "(see Fig. 5a,b)

- Page 30, lines 28-29: Please add sedimentation flux in standard model for comparison.

  ⇒ We now provide the global Si flux to sediment for the standard run as well.

  → "$\sim$ 1.03 Gt Si per year" → "$\sim$ 1.03 Gt Si per year ($\sim$ 1.04 Gt Si per year in the standard run)"

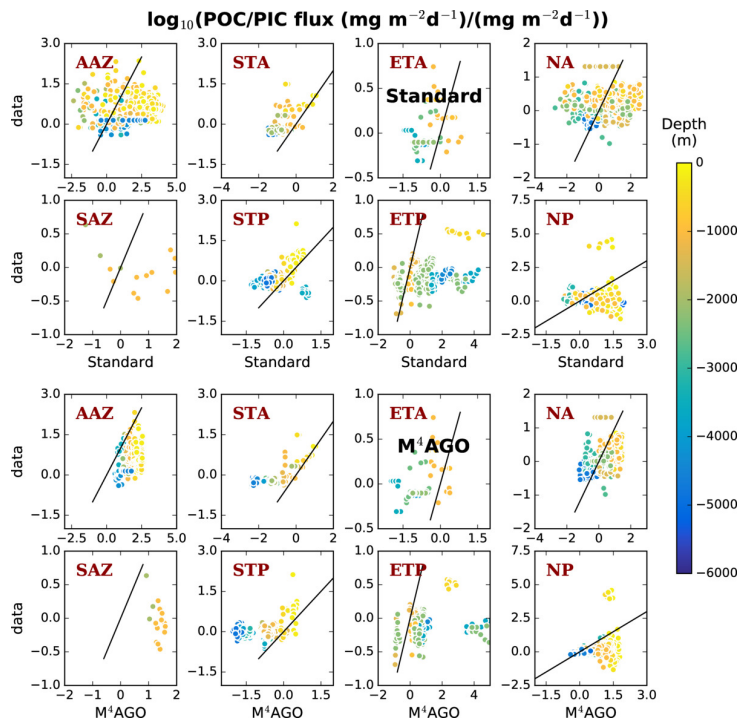

Figure 4: As Fig.12 in the manuscript, but for POC/PIC ratio. Comparison of the standard run and the M^{4}AGO run to the Mouw et al (2016a,b) data set. Standard refers to upper two rows, M^{4}AGO to the lower two rows.

- Page 31, line 7: "The M^{4}AGO run represents the PIC/POC fluxes equally well as the standard run." It would be interesting to know how well that is.

  ⇒ We here provide the PIC/POC fluxes in the reply, see Fig. 4

  → Nothing to be changed.

- Page 31, lines 8 and 11: "... the scatter around the 1:1 line is reduced ..." (line 8) At least for some regions, e.g. for the Sub Antarctic Zone, the points are not really scattered around the 1:1 line. But I agree with the view that M^{4}AGO reduces the variability in the POC/Si ratio (line 11). Isnt't this reduced variability / compression in the POC/Si fluxes expected, because the variability of the fluxes is only due to the

variability of the POC/Si concentrations in M^4AGO (POC and opal sink at the same speed), while in the standard model, variability is also introduced due to differences between Si- and POC-sinking speeds?

⇒ We write at the end of the first paragraph of Sect. 3.6 that M^4AGO couples the timing of mineral and POC fluxes and took that also as motivation for the comparison to data, as lined out on p. 31, l.1 ff. We therefore agree that the compression likely stems from the joint sinking of mineral and POC components, which we also discuss on p. 31, l. 11 ff. We therefore remain with the present text.

→ Remained.

- Page 32, Figure 12: Do I understand correctly that each dot in the figure is a generated monthly mean data point, compared to the respective location and monthly mean of the last year in the model run?

⇒ We modified the caption for clarity.

→ "POC/Si rain ratios in the standard run and M^4AGO compared to the Mouw et al. (2016a,b) data set." → "Monthly POC/Si rain ratios in the standard run and in M^4AGO compared to the monthly climatological mean derived from the Mouw et al. (2016a,b) data set."

- Page 33, line 34: ... and the North American Westcoast (?)

⇒ Yes. Thanks for improving clarity.

→ "North America coast" → "North American West Coast"

- Page 35, lines 20-22 / page 36, Figure 14a: If negative fluxes really do represent a net-CO2 uptake by the ocean in Fig. 14a, as stated in the caption, the southern hemisphere ocean acts as a net sink for atmospheric CO2 (and not a source), and the northern hemisphere ocean acts as a net source (not a sink). Consequently, the oceanic CO2 transport would be from south to north.

⇒ We are generally very sorry for having caused confusion about the units and thus the interpretation of Fig. 14a. It should be Gt C yr^{-1}. For easier interpretation, we add the starting point of the cumulative flux calculation (from south to north). Given that the cumulative fluxes show a positive sign at the equator, the southern hemisphere is a net-source of CO_2. We remain with the general statement and provide additional information on the cumulation procedure in the caption of Fig. 14.

→ "Climatological cumulative zonal CO_2 flux in the standard and the M^4AGO run" → "Climatological cumulative zonal CO_2 flux in the standard and the M^4AGO run (from south to north)"

- Irrespective of the sign / flux direction, these results are in stark contrast to CO2 flux observations of net zonal mean outgassing at the Equator and net ocean CO2 uptake in mid-latitudes (e.g., Figure 14 in Takahashi et al. 2019). Maybe this is just due to a plotting error in Figure 14?

⇒ The plot is in agreement with this general pattern. The cumulative sum shows a positive trend towards the equatorial region (and beyond until about 15 °N), which indicates outgassing in the tropics. We, however, have to admit, that the text gave a different impression, which we change. Many thanks for pointing this out!

→ p.35, l. 24,26: deleted "sub" of "subtropical" → "tropical"

- I also am not sure if I understand the units in Figure 14a. Does the left axis show the net sea–air CO2 flux accumulated over the respective 1° latitude band? If that is true, the values seem very large. I am guessing from Fig. 14a that the ocean CO2 uptake accumulated in the southern hemisphere would then amount to around 0.2 GtC/yr/deg·60deg≈12 GtC/yr, which is an order of magnitude larger than the observed net uptake by the southern hemisphere ocean (south of 14°S) of about 1.1 GtC/yr.

⇒ We are again sorry for the wrong unit, which we correct for. Generally, the uptake in the southern hemisphere is lower than 1.1 GtC/yr, since Fig. 14a corresponds to pre-industrial conditions, as stated at the beginning of Sec. 3.8. We add a sentence to provide references for the qualitative and quantitative agreement.

→ Added the sentence: "In general, the latitudinal zonal CO_2 fluxes and the cross-equatorial southward oceanic CO_2 transport agree qualitatively and quantitatively well with former forward-integrated models for pre-industrial conditions (e. g Sarmiento et al., 2000; Gloor et al., 2003; Mikaloff Fletcher et al., 2007)."

- Page 35, lines 22-24: "In the simulation with M4AGO, a stronger CO2 uptake in the region ... coincides with ... increased transfer efficiency" This is a very interesting point; does it still hold despite the (to my understanding) erroneous Figure 14a? To me it is surprising that the CO2 fluxes do *not* differ more, despite the very different transfer efficiencies. Why do the CO2 fluxes hardly differ south of, say, 55°S, where the transfer efficiency difference is largest? Why is there hardly an effect in the Arctic Ocean?

  ⇒ We are again sorry for the misleading, wrong axis label. At first glance, the strong differences in transfer efficiency contradicts the little changes in atmosphere-ocean CO_2 fluxes in some regions. However, transfer efficiency is not equal to actual POC fluxes. Transfer efficiency only describes, which fraction of exported POC is transferred to certain depth (in our manuscript calculated for about 1000 m). For example, in the Arctic ocean, we find a high transfer efficiency of the exported material, but actual POC fluxes are small. Thus the high transfer efficiency in the Arctic has hardly any impact on the atmosphere-ocean CO_2 fluxes. We now provide a brief explanation for it. With regards to the region south of 55 °S, we hope that with clarification of the units in Fig. 14 a it becomes clear that indeed, a clear effect of the increased transfer efficiency in M^4AGO compared to the standard run is visible. There is a stronger uptake in the AAZ region in M^4AGO (see the difference between M^4AGO and the standard run), as also visible in the rising CO_2 experiments (cmp. Fig. 14 c). This is also described in the text (see p. 37, l.7ff: "Quantitatively, differences of regional cumulative CO_2 fluxes larger than 5 Gt C appear in the Antarctic Zone (AAZ),") We rephrase the sentence and link the transfer efficiency and the primary production pattern.

  → "Qualitatively, this coincides well with the higher transfer efficiencies in these regions (cmp. to Fig. 8)." → "Qualitatively,

this coincides well with the primary production, respective export and the higher transfer efficiencies in these regions (cmp. to Fig. 4 and 8). In regions of higher transfer efficiency, but similar CO_2 fluxes as compared to the standard run, either POC export fluxes are small (e. g. in the Arctic Ocean) or physical processes such as mixing or upwelling dominate over biologically induced CO_2 fluxes (e. g. in the SAZ)."

- Page 39, line 7: Sentence structure. ... body size decreases with increasing water temperature. And increasing water temperature has been suggested to ... (?)

  ⇒ Modified.

  → "...which is suggested..." → ". The increasing water temperature has been suggested..."

- Page 39, line 10: Does "... such eco-physiological responses ..." refer to the primary particle size change, or to other effects?

  ⇒ Yes, such eco-physiological responses refer to the change of primary particle size.

  → Remained with the sentence.

- Page 39, line 29: ... increases the phosphate concentrations in the subtropical gyres by up to 50% (?)

  ⇒ No, it's more than 150 %. The sentence is fine.

  → Remained.

- Page 40, line 1-2: Please rephrase (phosphate increases phosphate concentrations...), e.g. by: ...phosphate ... populates ... and reaches the subtropical gyres.

  ⇒ Modified.

→ "Phosphate previously utilized by diazotrophs in the Panama basin now partially populates the downstream equatorial current and increases the subtropical gyres phosphate concentrations." → "Phosphate previously utilized by diazotrophs in the Panama basin now partially populates the downstream equatorial current and reaches the subtropical gyres."

- Page 41, lines 21-29: This paragraph, describing the main implications of this study, is not formulated very clearly. "Our findings ... suggest a number of implications." Number=2, according to later "first" and "second"? Please rephrase second sentence. E.g., First, the finding that the size ... is a potential contributor to high sinking speeds suggests that the ballast hypothesis needs to be extended to a size-and-ballast hypothesis. What does "it requires" in line 23 refer to?

  ⇒ We rephrased the sentences accordingly.

  → "First, size of aggregate constituents, particularly of diatom frustules, as potential factor for high sinking velocity suggest to widen the perspective of mineral ballast studies towards a size-and-ballast hypothesis." → "First, the finding that the size of aggregate constituents, particularly of diatom frustules, act as potential factor for high sinking velocities, suggests to widen the perspective of mineral ballast studies towards a size-and-ballast hypothesis."
  "it requires" → "such extended size-and-ballast hypothesis requires"

- Page 43, line 9: As far as I understand β is not prescribed in the standard run, but only the sinking speed, i.e., β still depends on the remineralization (which varies with temperature and oxygen concentrations). How do you get to the value of β=1?

  ⇒ In the referred standard run, remineralization is not temperature-dependent, but oxygen-dependent. Thus, β is implicitly prescribed by the gradient of sinking velocity ($\partial_z \bar{w}_s$) and the remineralization rate R_{POC} in oxygenated waters. Following Kriest and Oschlies (2008), the vertical mass concentration exponent is defined

by $R_{\mathrm{POC}}/\partial_z \bar{w}_s + 1 = 2$, (their r/a+1 in Eq. (5)), which is prescribed in HAMOCC. Hence, it translates to a preset $\beta = 1$, which, by internal processes such as reduced R_{POC}, upwelling, but also numerical diffusion, then results in an effective Martin slope $\langle \beta' \rangle$ that is smaller than one. For clarity, we now provide information about the assumption on the oxygenation state.

→ "that is smaller than the prescribed value of $\beta = 1.00$" → "that is smaller than the prescribed value of $\beta = 1.00$ in oxygen-saturated waters"

2.3 Typos

- Page 2, line 32: Primary / fundamental(?) determining factors?

  ⇒ Thanks. Changed.

  → "primer" → "primary"

- Page 3, line 29: ...benefits from an order of...

  ⇒ Thanks. Added.

  → added: "an"

- Page 4, line 23: Bar over ws meaning global mean / annual mean?

  ⇒ It's also the mass concentration-weighted mean sinking velocity, but different from the spatio-temporally variable one in M^4AGO. So, we added the information.

  → "Below z_0, we assume a linearly increasing mean sinking velocity with depth." → "Below z_0, we assume a linearly increasing mass concentration-weighted mean sinking velocity with depth."

- Page 4, line 27: The opal dissolution rate...

  ⇒ Modified.

  → "Opal" → "The opal"

- Page 10, line 27: ... enhance the sinking velocity...

  ⇒ Modified.

  → added: "the"

- Page 18, line 7: ... which also lead (plural)

  ⇒ Thanks. Changed.

  → "lead"

- Page 18, line 8: ... from either satellite data, in situ observations, or models lead to partly contrasting patterns (add "data" and plural "s")

  ⇒ Changed.

  → added "data" and plural "s" in pattern"s"

- Page 19, line 5: Both model simulations show a similar pattern (add "a")

  ⇒ Changed.

  → "Both model simulations show similar pattern of opal to detritus ratio fluxes" → "Both model simulations show a similar pattern of opal to detritus flux ratios"

- Page 22, line 11: Use "By contrast" rather than "In turn"?

  ⇒ Changed.

  → "In turn" → "By contrast"

- Page 22, line 13: ... during the aggregates's descent. (?)

  ⇒ Modified.

  → "aggregates" → "their"

- Page 23, line 3: It is likely that (no comma)

⇒ Changed.

→ removed ","

- Page 23, line 17: linearly increasing

⇒ Changed.

→ "linear" → "linearly"

- Page 23, line 30: ...from the relationship... and the transfer efficiency.

⇒ Changed.

→ "from relationship between the Martin curve slope parameter and transfer efficiency" → "from the relationship between the Martin curve slope parameter and the transfer efficiency"

- Page 24, line 5: M^4AGO posseses...

⇒ Changed.

→ "possess" → "possesses"

- Page 24, line 11: ...allows to more reliably constrain POC transfer efficiency

⇒ Allows for is correct.

→ Remained.

- Page 25, line 5: extent

⇒ Changed.

→ "extend" → "extent"

- Page 25, line 30: ... in surface waters and the upper mesopelagic zone...

⇒ Changed.

→ added: "the"

- Page 25, lines 32-33: ... the RLSs... are similar or slightly (?) longer, or smaller again in ... The longer RLSs in the mesopelagic zone... (plural)

  ⇒ Modified in parts.

  → "In the mesopelagic zone, the RLSs in M^{4}AGO is similar or pronounced longer and decreases" → "In the mesopelagic zone, the RLSs in M^{4}AGO are similar or pronounced longer and decrease" "The longer RLS" → "The longer RLSs"

- Page 27, line 16: In summary, the temperature-dependence...induces...

  ⇒ Changed.

  → "temperature-dependence of remineralization in M^{4}AGO induce" → "the temperature-dependence of remineralization in M^{4}AGO induces"

- Page 27, line 28: ...$X_{i,z}$ is (not as)

  ⇒ Changed.

  → "as" → "is"

- Page 28, line 20: ... given the general importance of the microstructure....

  ⇒ Changed.

  → "given the microstructure general importance" → "given the general importance of the microstructure"

- Page 35, line 29: ... in M^{4}AGO on *the* CO2 uptake ...

  ⇒ Changed.

  → added: "the"

- Page 39, line 34: one *in the* too much; thus leads to (singular)

⇒ Thanks. Changed.

→ "primary production in the in the equatorial upwelling regions (ETA and ETP) thus lead" → "primary production in the equatorial upwelling regions (ETA and ETP) thus leads"

- Page 40, line 13: grazing through zooplankton

  ⇒ Changed.

  → "though" → "through"

- Page 43, line 7: underpins the previously...

  ⇒ Changed.

  → added: "the"

- Page 50, line 33: initials for Núñez-Riboni

  ⇒ Bibliography updated. Thanks.

  → Done.

- Page 53, line 4: Aiko Voigt (not Vogt?)

  ⇒ Yes. Thanks.

  → Done.

- Page 53, line 19: please check reference / entry missing?

  ⇒ Done.

  → added: "PANGAEA"

- Page 55, line 11: please check / C. R. Geoscience

  ⇒ Yes. It's the official abbreviation for 'Comptes Rendus Geoscience'

  → modified to: "Comptes Rendus Geoscience"

1 General remark

The reply is structured as follows:

- Referee comment

  ⇒ Authors reply

  → Modification(s) in the manuscript. "old" → "new"

2 Reply to Referee #2

2.1 General summary

- Review of Maerz et al: *Microstructure and composition of marine aggregates as co-determinants for vertical particulate organic carbon transfer in the global ocean.* The authors present a new scheme for the calculation of the mean sinking velocity of marine aggregates as a function of the aggregate composition and the fractal dimension. This scheme is reported to be cost-efficient and hence useful in large-scale ocean models. The model is described in detail and carefully evaluated. The authors report a substantial improvement in the simulation of the latitudinal pattern of POC transfer efficiency. This is an impressive effort and worth of publication. I have some specific comments that should be addressed before publication. Writing style: Sentences are very long and not always clear. This is particularly true for the introduction and model description.

  ⇒ We thank the reviewer for her/his constructive and positive review. We tried to respond to every single comment and hope to improved the clarity of the manuscript.

  → –

2.2 General comments

- I miss a comparison with the stochastic, Lagrangian model of sinking biogenic aggregates in the ocean (SLAMS) by Jokulsdottir and Archer. Jokulsdottir, T. and Archer, D.: A stochastic, Lagrangian model of

sinking biogenic aggregates in the ocean (SLAMS 1.0): model formulation, validation and sensitivity, Geosci. Model Dev., 9, 1455–1476, https://doi.org/10.5194/gmd-9-1455-2016, 2016.

⇒ Indeed, the model of Jokulsdottir and Archer (2016) is an interesting new model approach. Unfortunately, their Lagrangian model is currently limited to a conceptual 1-D application and is computationally likely too costly for the incorporation in an Earth System Model framework. However, it might provide valuable insights for further development and tuning of M^4AGO or similar models. We pick up on it and briefly discuss it in Sect. 3.10 Current limitations of M^4AGO.

→ Added on p. 40, l. 28 (after . . . "subsequent aggregation (Martin et al., 2011)."): "More detailed models, such as e. g. the 1-D Lagrangian approach of Jokulsdottir and Archer (2016), can likely provide more insights into aggregate dynamics and can help to further improve the aggregate representation in ESM frameworks."

- Please make the model code publicly available. It is not in the repository that you mention.

⇒ The model code was, is and will be publicly available on request. However, we acknowledge that the provided information how and where to request it, was insufficient. We therefore now provide more information i) in the manuscript and ii) in the MPGPuRe repository, how to inquire it. It requires to agree to the MPI-ESM license agreement and registering at the MPI-ESM-Forum. Unfortunately, the license obliges users to this method for accessing the code due to third party rights on the code.

→ "Primary data and code for this study is stored and made available through the Max-Planck-Gesellschaft Publications Repository: https://pure.mpg.de." → "Primary data and code for this study is stored and made available through the Max-Planck-Gesellschaft Publications Repository: https://pure.mpg.de. The respective MPI-OM and HAMOCC model code (revision numbers: r4981 and r5003) is available on request after agreeing

to the MPI-ESM license agreement and registering at the MPI-ESM-Forum (https://www.mpimet.mpg.de/en/science/models/licenses/)."

- explain ALL abbreviations and symbols used in the figures in each and every figure caption.

  ⇒ We carefully went through the manuscript and added the abbreviations and symbols, where we believe, it's necessary. If not otherwise stated in the modifications below, no modifications were performed for the caption.

  → Added in caption of Fig. 1:
  "$V_{p,i}$ is the primary particle volume, $\rho_{p,i}$ is the primary particle density, and $d_{p,i}$ is the primary particle diameter of primary particle type i. $m(d)$ is the mass of an aggregate of diameter d. $\langle d_p \rangle$ and $\langle \rho_p \rangle$ represent mean primary particle diameter and density, respectively."

  Added in caption of Fig. 2:
  "l denotes the thickness of the opal shell with volume V_{opal}, V_{aq} and V_{POM} are the encapsulated volumes of water and POM, respectively. $d_{p,\text{frustule}}$ is the diameter of the diatom frustule."

  Added in caption of Fig. 3: "d_{max}"

  Refrained from adding the symbols explicitly in caption of Fig. 7, since they are given nearby in caption of Fig. 6 and we refer to them explicitly.

  Modifications caption of Fig. 9:
  "z^*_{POC}" → "the remineralization length scales, z^*_{POC},"
  "sinking velocity" → "sinking velocity, $w^*_{s,\text{POC}}$,"
  "temperature-dependent remineralization rates" → "Q_{10} factor temperature-dependent remineralization rates with r_{POC} at reference temperature T_{ref}"
  "Relative contributions of sinking and remineralization" → "Relative contributions of sinking, $RC_{\langle w_s \rangle}$, and remineralization, RC_{remin},"

Added in caption of Fig. 10:
"Mathematical symbols are: $\langle \rho_p \rangle$: mean primary particle density; $\langle d_p \rangle$: mean primary particle diameter; d_f: fractal dimension; μ: dynamic molecular viscosity; $d_{\max}$: maximum aggregate diameter; b: aggregate number distribution slope."

Modified caption of Fig. 13:
"tracers $\rightarrow$ "tracers (oxygen, O_2, nitrate, NO_3^-, phosphate, PO_4^{3-}, silicate, Si)"

Modifications in caption of Fig. 15:
"POC transfer efficiency to $d_{p,\text{frustule}}$" $\rightarrow$ "POC transfer efficiency to diatom frustule size, $d_{p,\text{frustule}}$"
"and d_f" $\rightarrow$ "and fractal dimension, d_f"

- I am quite worried about the high buoyancy of diatom-dominated aggregates through the TEP formulation. This needs more justification. Do you here assume that all organic carbon has the same density as TEP? That would explain your low density of diatom-dominated aggregates. Is there sufficient evidence for such behavior?

  $\Rightarrow$ We acknowledge that our formulation is simplified. We will make the simplification more clear. However, we don't assume that all detritus has the same density as TEPs. We assume that TEPs lower the density of the diatom frustule and parametrize the effect with respect to the model-defined freshness of detritus. In our model framework, we thus focus on the qualitative effect of TEP that has been previously suggested (Mari et al., 2017) and, as we learned, also applied by Jokulsdottir et al. 2016. There are a number of observational and experimental studies that support the general behaviour of TEPs as buoyancy adding agent in marine aggregates. For example, the following experimental and observational studies point to low TEP density or show low buoyancy of aggregates, similar to our modeled diatom-dominated aggregates with mean excess densities of $\Delta\langle \rho_f \rangle_V \approx 2\,\mathrm{kg\,m^{-3}}$

    – Azetsu-Scott and Passow, 2004[2]: $\rho_{\text{TEP}} \approx 700 - 840\,\mathrm{kg\,m^{-3}}$.

[2] Azetsu-Scott, K. and Passow, U.: Ascending marine particles: Significance of trans-

Thus TEPs are lighter than sea water and add buoyancy, if incorporated in aggregates.

- Alldredge & Gottschalk 1988[3]: excess density of median marine aggregates: $0.14\,\mathrm{kg\,m^{-3}}$, and for diatom aggregates (their Fig.2 d): $\approx 10^{-5} - 10^{-4}\,\mathrm{g\,cm^{-3}} = 10^{-2} - 10^{-1}\,\mathrm{kg\,m^{-3}}$ for large, porous diatom-dominated aggregates ($O(1\,\mathrm{cm})$).
- Laurenceau-Cornec et al. 2019[4]: excess density of diatom-dominated aggregates including TEPs (partly also including mineral components): $\approx 0.3 - 5.7\,\mathrm{kg\,m^{-3}}$

Some of the studies don't explicitly mention TEP (since they were not explicitly described at the time of the study), but nowadays TEPs are ubiquitously found in the global ocean and thus possess a likely explanation for the low aggregate excess densities. We believe that the confusion about our modeled diatom-dominated aggregates arises primarily due to the fact that most often diatom-dominated aggregates are reported in the form of marine snow, and hence large aggregates that have high sinking velocities of often more than $> 50\,\mathrm{m\,d^{-1}}$. Our model agrees well with sinking velocities of these individual aggregates, when considering only the respective sizes (and not the mean sinking velocity of the full size spectrum). For example, here using Stokes sinking velocity for simplicity, thus slightly overestimating w_s compared to the White drag parametrization:

$$
\begin{aligned}
& w_s(d = 1\,\mathrm{mm} = 0.001\,\mathrm{m}) = \frac{1}{18\,\mu}\Delta\rho_f\, g\, d^2 \\
& = \frac{1}{18\,\cdot 0.0015\,\frac{\mathrm{kg}}{\mathrm{m\,s}}} \cdot 2\,\frac{\mathrm{kg}}{\mathrm{m^3}} \cdot 9.81\,\frac{\mathrm{kg}}{\mathrm{m}} \cdot (0.001\,\mathrm{m})^2 \cdot 86400\,\frac{\mathrm{s}}{\mathrm{d}} \\
& \approx 62.8\,\mathrm{m\,d^{-1}}
\end{aligned}
$$

parent exopolymer particles (TEP) in the upper ocean, Limnol. Oceanogr., 49, 741–748, 2004

[3]Alldredge, A. L. and Gotschalk, C.: In situ settling behaviour of marine snow, Limnol. Oceanogr., 33, 339-351, 1988

[4]Laurenceau-Cornec, E.C, Moigne, F.A.C., Gallinari, M, Moriceau, B., Toullec, J., Iversen, M.I., Engel, A., De La Rocha, C.L.: New guidelines for the application of Stokes' models to the sinking velocity of marine aggregates, Limnol. Oceanogr., 2019, doi:10.1002/lno.11388

The due to Stokes slightly overestimated value of $\approx 62.8\,\mathrm{m\,d^{-1}}$ is of the same order as e. g. the measurements by Alldredge & Gottschalk (1988), who found the settling velocities can be best described by $50 \cdot (d[\text{in mm}])^{0.26}$ (their Fig. 3 a) which would be $\approx 50\,\mathrm{m\,d^{-1}}$ for our example diameter of 1 mm.

As a consequence of the reviewers comment, we now give the reference to Jokulsdottir and Archer (2016) and Mari et al. (2017) closer to the description of our diatom density description. Both author teams explicitly described the potential of TEPs to add buoyancy through the TEPs lower density than water ($\rho_{\mathrm{TEP}} \approx 700 - 840\,\mathrm{kg\,m^{-3}}$, Azetsu-Scott and Passow, 2004). In addition, we emphasize our simplification of TEP representation. We add the reference to Laurenceau-Cornec at the point, where we discuss the diatom-dominated aggregate excess density. To further clarify the fact that mean sinking velocity can differ significantly from reported large marine snow aggregates of sizes of typically $> 1\,\mathrm{mm}$, we add a note in the caption of Fig. 6. Further, we add a sentence on p. 22 l.2, where we present the sinking velocities.

→ "The density of diatoms becomes" → "To account for the additional buoyancy through TEPs (Jokulsdottir and Archer, 2016; Mari et al., 2017), we here simplify and assume that the frustule density is lowered by TEPs in dependency on the freshness of detritus. Eventually, the diatom density, ρ_{diatom}, becomes"

Added in caption of Fig. 6 (after concentration-weighted mean sinking velocity of aggregates):
"Note that $\langle w_s \rangle$ comprises the full range of many micrometer-sized to rare, large aggregates with low ($O(1\,\mathrm{m\,d^{-1}})$) and high ($O(> 100\,\mathrm{m\,d^{-1}})$) sinking velocities, respectively."

Added reference to: "Laurenceau-Cornec et al., 2019" on p. 22,l.20/21

"Particle properties and molecular dynamic viscosity determine the concentration-weighted mean sinking velocity of aggregates, $\langle w_s \rangle$ (Fig. 6 f,l), for particle sizes ranging from few micrometers

to millimeters." → "Particle properties and molecular dynamic viscosity determine the concentration-weighted mean sinking velocity of aggregates, $\langle w_s \rangle$ (Fig. 6 f,l). For $\langle w_s \rangle$, M^{4}AGO considers particle sizes ranging from few micrometers to millimeters and thus the full size spectrum, where sinking velocities of $O(1\,\mathrm{m\,d^{-1}})$ to $O(> 100\,\mathrm{m\,d^{-1}})$ are represented. $\langle w_s \rangle$ thus can significantly differ from reported sinking velocities for large individual aggregates."

2.3 Abstract

- Line 14: too much information given: delete rising CO2 and without CO2 climate feedback.

  ⇒ We rephrased the sentence and hope, that it is now better readable.

  → "In ocean standalone runs and rising carbon dioxide (CO_2) without CO_2 climate feedback, M^{4}AGO alters the regional ocean-atmosphere CO_2 fluxes compared to the standard model." → "Prescribing rising carbon dioxide (CO_2) concentrations in standalone runs (without climate feedback), M^{4}AGO alters the regional ocean atmosphere CO_2 fluxes compared to the standard model."

2.4 Introduction

- P.2 Please give more references for your statements, especially in the first paragraph. No reference given between line 5 and 11.

  ⇒ Given the general principles stated in the paragraph, we now provide a reference to the excellent book of Williams and Follows 2011: Ocean Dynamics and the Carbon Cycle: Principles and Mechanisms.

  → added reference: "(Williams and Follows, 2011)"

- P. 2, line 17: "The sinking velocity of aggregates is primarily determined by their size". This needs a reference. I would argue it is density, e.g. Iversen and Robert,http://dx.doi.org/10.1016/j.marchem.2015.04.009 . The next sentence also needs a reference (line 19)

⇒ A similar comment has been done by reviewer #1. We answered his/her comment and provide the answer here:
This is an interesting comment and we realize, also by the same comment of reviewer #2, that there seems to be much confusion about the controlling factors for sinking velocity, which deserves a publication on its own (being in progress). We want to emphasize here that we clearly state in the follow-up sentence that structure and composition of aggregates regulate the excess density and can thus have a high impact on sinking velocity (we now provide a reference for it). Nevertheless, we would here argue from the mathematical perspective. For simplicity and neglecting the changing drag coefficient for particles with higher Reynolds particle numbers, let's consider the Stokes sinking velocity for low particle Reynolds numbers:

$$w_s(d, \rho_f, \ldots) = \frac{1}{18\,\mu}\,(\rho_f - \rho)\,g\,d^2 \tag{2}$$

where d is the diameter, μ the molecular dynamic viscosity, ρ_f the aggregate density, ρ is the density of the ambient fluid, and g is the gravitational acceleration constant. It is obvious that $w_s \propto (\rho_f - \rho)$ and $w_s \propto d^2$. Hence, sinking velocity only linearly increases with aggregate density, while it increases with a power law relationship of the diameter. This suggests that size is indeed the primary factor controlling sinking velocity. If we consider the fractal scaling relationship for excess density (Eq. (5) and (8) in our manuscript), this clarity becomes blurred, because the aggregate excess density is itself size-dependent. However, if we further consider that natural aggregate size ranges over more than an order of magnitude (from sizes of about $0.45 \cdot 10^{-6}\,\mathrm{m}$, which is operationally defined by typical filter pore sizes for POM filtration, to size of $O(10^{-2}\,\mathrm{m})$), while aggregate excess density $(\rho_f - \rho)$ typically ranges only between zero (neutrally buoyant) and $O(100\,\mathrm{kg\,m^{-3}})$, it is obvious that size is the dominant factor (for non-neutrally buoyant aggregates), while, as we clearly state, excess density can entail high variability of sinking velocity. This is also, what e. g. Iversen & Robert (2015)[5] imply, when writing '2- to 3-fold higher **size-specific** sinking velocities'

[5]Iversen & Robert 2015: *Ballasting effects of smectite on aggregate formation and export from a natural plankton community.* Marine Chemistry 175, 18 - 27.

for mineral ballasted aggregates.

→ We add the reference Iversen & Robert 2015 to the follow-up sentence: "...entail high variability of excess density and thus sinking speed of aggregates (Iversen & Robert, 2015)"

- P. 2, line 32: primer → primary?

  ⇒ Changed.

  → "primer" → "primary"

2.5 Model description

- It would be very helpful to have a table with all symbols used in the equations at the beginning of section 2.1

  ⇒ We will provide the table in the appendix.

  → Adding table. At end of first paragraph of Sect. 2: Model description, p. 4, l.15, we add: "A table with the used mathematical symbols can be found in App. D, Tab. D1"

- P. 5, line 2, what is meant with "terminal sinking velocity"? I suggest to delete "terminal"

  ⇒ Terminal sinking velocity is the sinking velocity of any particle in steady state, when all involved forces balance. This is the classical assumption, when applying e. g. the Stokes formula for sinking velocity (or any other drag formulation in the provided Eq. (7)). By writing 'terminal sinking velocity', we make it clear that we are not attempting to solve the Maxey-Riley equation (M.R. Maxey & J.J. Riley 1983: Equation of motion for a small rigid sphere in a nonuniform flow. The Physics of Fluids 26, 883, https://doi.org/10.1063/1.864230). We thus remain with the present formulation.

  → Remained with the formulation.

- Eq. 3: I can guess what is meant with dd, but it is easily misunderstandable.

⇒ In agreement with reviewer #1 and aiming at clarity, we rephrased this part and now make clear that $\langle w_s \rangle$ is derived from integration over the size spectrum.

→ "The local concentration-weighted mean sinking velocity, $\langle w_s \rangle$, in M^{4}AGO is eventually determined by a truncated number distribution, Eq. (2), through the minimum and maximum aggregates sizes, d_{min} and d_{max}, respectively, the aggregate mass, $m(d)$, and the sinking velocity of single aggregates, $w_s(d)$" → The local concentration-weighted mean sinking velocity, $\langle w_s \rangle$, in M^{4}AGO is eventually computed from the number distribution, Eq. (2), that is truncated at the minimum and maximum aggregate sizes, d_{min} and d_{max}, respectively, and expressions for the aggregate mass, $m(d)$, and the sinking velocity of aggregates, $w_s(d)$, of a particular diameter, d. Integration over the aggregate size spectrum yields $\langle w_s \rangle$,"

- P. 5, line 28: What is meant by a "primary particle". How does that differ from "a particle"?

⇒ Primary particles are the modelled (smallest) entities of which an aggregate is composed of. As we state in p.5, line 28, we consider e.g. phytoplankton cells or coccolithophore shells as primary particles. We render the definition of primary particles more precisely on p. 6, l.17-19, when we introduce the theory for heterogeneously composed aggregates. There, we state:
"With M^{4}AGO, we represent aggregates composed of poly-dense, poly-sized primary particles under the assumption of a singled value fractal dimension throughout the aggregate size spectrum. This allows for representing heterogeneous primary particles such as diatom frustules, coccoliths, dust particles, and detritus as principal components of marine aggregates. ".
'Particle' is a more general term and can refer, depending on context, to a primary particle or an aggregate. As a consequence of the reviewer's question, we carefully checked throughout the manuscript, if we always refer correctly to primary particles.

→ We remained with the text.

- P. 7, line 1: What is meant by “the total number of one primary particle type” ? The total number of one should be one. Do you mean “of particles of one particle type”?

  ⇒ Yes. We modified the sentence accordingly.

  → "between the total number of one primary particle type" → "between the total number of primary particles of one particle type"

- P. 8, line 5: “mean primary particle size, (. . .) which we apply as a lower integration bound”. Please give a justification for this choice.

  ⇒ The fractal scaling law breaks for aggregates smaller than the smallest composing entity, i. e. the primary particle size. For $\lim d \rightarrow \langle d_p \rangle$, the aggregate is composed of one single primary particle. Hence, the lower limit must be $\langle d_p \rangle$. Anyhow, we now provide an additional reference to Kriest and Evans (1999).

  → Added reference: "and hence, $d_{\min} = \langle d_p \rangle$" → "and hence, $d_{\min} = \langle d_p \rangle$ (following Kriest and Evans, 1999)"

- P. 10, line 5: no reference to Engel et al 2004? Engel, A. , Thoms, S., Riebesell,U. , Rochelle-Newall, E. and Zondervan, I. (2004) Polysaccharide aggregation as a potential sink of marine dissolved organic carbon. Nature, 428 . pp. 929-932. DOI 10.1038/nature02453.

  ⇒ Thanks for the reference. Added it.

  → Added: "Engel et al., 2004"

- Figure 2: explain abbreviations and symbols in each and every figure caption.

  ⇒ Where needed, we now do it. See the remark in the general comments section of the same reviewer.

  → Particularly for Fig. 2, we added to the caption:
  "l denotes the thickness of the opal shell with volume V_{opal}, V_{aq} and V_{POM} are the encapsulated volumes of water and POM, respectively. $d_{p,\text{frustule}}$ is the diameter of the diatom frustule."

- P. 11, line 18: how is m_e and $m_{\text{potential}}$ calculated? I can't follow whether the masses of opal and of TEP are taken into account correctly to calculate the density of the diatom-aggregate. Do you here assume that all organic carbon has the same density as TEP? That would explain your low density of diatom-dominated aggregates. Please clarify.

  ⇒ We do not assume that diatom frustule-associated detritus has the same density as TEP. We first calculate the frustule density according to Eq. (27), which is based on the density of opal, ρ_{opal}, and POM ρ_{POM} (now corrected to ρ_{det}). We admit that we should have written ρ_{det} instead of ρ_{POM}, which we change. For the eventual density of the diatom ρ_{diatom}, we assume that the amount of diatom frustule-associated detritus is proportionally linked to the presence of TEP, which makes the diatom frustule lighter. We apologize for not having provided the equations for m_e and $m_{\text{potential}}$, which we now provide. Our modeled primary particle densities in silicifier-dominated waters like the Southern Ocean are about $1060\,\text{kg}\,\text{m}^{-3}$ to $1100\,\text{kg}\,\text{m}^{-3}$ (values based on re-checked monthly mean model output) are in a normal range of detritus. We are certain that the calculated excess density of rather fresh, porous diatom-dominated aggregates in surface waters is with about $2\,\text{kg}\,\text{m}^{-3}$ in the range of previously measured excess densities of diatom aggregates. For example, a range of about 0 to $\sim 10\,\text{kg}\,\text{m}^{-3}$ is given by Alldredge and Gottschalk, 1988, Ploug et al. 2008 and Iversen and Ploug 2013 (as cited in the manuscript). Please see also the reply to the general comments of the same reviewer. Further, the modeled excess density of diatom-dominated aggregates increases with ongoing remineralization during the decent through the mesopelagic zone (Fig. 7 d).
  We clearly state in Sect. 3.10 (Current limitations of M^{4}AGO) that TEPs are only simplistically considered. We make it more clear now in Sect. 2.2.5, p. 11, l.16. Given the potential role of TEPs in aggregate formation, we currently consider to include TEPs explicitly.

  → "ρ_{POM}" → "ρ_{det}"

  "defined as the mass ratio between the actual amount of de-

tritus m_e and the potential mass of detritus linked to opal production $m_{\text{potential}}$." → "defined as the mass ratio between the actual amount of detritus, $m_e = n_{\text{frustule}} V_{\text{POM}} \rho_{\text{det}}$ and the potential mass of detritus linked to diatom frustules $m_{\text{potential}} = n_{\text{frustule}} (V_{\text{POM}} + V_{\text{aq}}) \rho_{\text{det}}$."

"The density of diatoms becomes" → "To account for the additional buoyancy through TEPs (Jokulsdottir and Archer, 2016; Mari et al., 2017), we , we here simplify and assume that the frustule density is lowered by TEPs in dependency on the freshness of detritus. Eventually, the diatom density, ρ_{diatom}, becomes"

- P. 13, line 1: mention that this forcing is based on ERA reanalysis (be specific) and avoid the abbreviation OMIP which you don't explain (or explain it)

  ⇒ We now provide more information on the OMIP forcing and avoid the word OMIP.

  → "We run both, the standard and the M^{4}AGO run, in a GR15/L40-OMIP setup. This translates to a horizontal resolution of about 1.5 °, 40 uneven vertical layers with highest resolution in the first few hundred meters of the ocean. OMIP is a climatological daily atmospheric forcing (Röske, 2005)." → "We run both, the standard and the M^{4}AGO run, in a GR15/L40 setup with climatological forcing. This translates to a horizontal resolution of about 1.5 °, 40 uneven vertical layers with highest resolution in the first few hundred meters of the ocean. The climatological atmospheric boundary conditions are derived from the second European Centre for Medium-Range Weather Forecasts (ECMWF) Re-Analysis project (ERA-40; Simmons and Gibson, 2000; Röske, 2005). The mean annual cycle of i. e. wind stress, heat and freshwater fluxes are resolved on a daily basis. The continental freshwater runoff is provided by means of a runoff model (Röske, 2005)."

- P. 13, line 3/4: are these global numbers? What are corresponding model parameters?

⇒ Yes, these are global number. We rephrased the sentence for clarity . As stated in the text, the values are the weathering rates for the substances: $CaCO_3$, dissolved organic phosphate, and silciate.

→ "The loss of POM, opal, and $CaCO_3$ due to sedimentation and subsequent burial was accounted for through homogeneously applied weathering rates which were adjusted accordingly, namely for the standard / M^4AGO run: $CaCO_3$ ≈17.2 / 26.5 T mol C yr^{-1}, dissolved organic phosphorus ≈99.6 / 101.5 G mol P yr^{-1}, and silicate ≈3.2 / 2.3 T mol Si yr^{-1}" → "The loss of POM, opal, and $CaCO_3$ due to sedimentation and subsequent burial was accounted for through homogeneously applied weathering rates which were adjusted for the standard run (and the M^4AGO run): Globally, we add ≈99.6 (101.5) G mol P yr^{-1} as dissolved organic phosphorus, and ≈3.2 (2.3) T mol Si yr^{-1}. To compensate for the loss of $CaCO_3$, we add ≈17.2 (26.5) T mol C yr^{-1} to surface dissolved inorganic carbon (DIC) and a corresponding amount to surface total alkalinity, A_T, as on DIC:$2A_T$."

- Table 1: caption: "The value for the Martin curve. . ." . Why is this single parameter given in the caption, please add it it to the list of parameters in the main body of the table.

  ⇒ Since the table is about the new M^4AGO parameters, we completely remove the sentence. The value is still provided and discussed in the appendix.

  → Removed.

- P. 16, line 4: "a minor role in biogenic fluxes". This statement needs a reference.

  ⇒ We provide now references.

  → added: "(described by e. g. Berelson et al., 2007; Fischer and Karakaş, 2009, Fischer et al., 2016)"[6].

[6]Berelson, W. M., Balch, W. M., Najjar, R., Feely, R. A., Sabine, C., and Lee, K.: Relating estimates of $CaCO_3$ production, export, and dissolution in the water col-

- P. 16, line 33/34: “adaptation .. within a few years.” Is adaptation the right word here? Maybe “an equilibrium was established”? or its change after a few years was small..

  ⇒ We rephrased the whole sentence and split in in two sentences for clarity. We now use the word ’adjustment’ instead of ’adaptation’.

  → "Since the adaptation of the sinking velocity versus the remineralization and dissolution rates, and thus the transfer efficiency, was within a few years, parameter variations aiming at a quantitative agreement with the transfer efficiency of Weber et al. (2016) enabled a useful strategy to select for promising parameter sets." → "We performed parameter variations aiming at a quantitative agreement with the transfer efficiency of Weber et al. (2016). Since the adjustment of the sinking velocity versus the remineralization and dissolution rates, and thus the transfer efficiency, occurs within a few years, this strategy was useful to select for promising parameter sets."

2.6 Results

- P. 22, line 12-13: “diatom-dominated aggregates feature a high buoyancy through TEP.” Is there any evidence for such behavior or is this a major model bug?

  ⇒ Yes, there is evidence for such behavior and we discuss the low excess densities of diatom-dominated aggregates in l. 19-21 on the same page. TEPs indeed feature high buoyancy (their density has

umn to measurements of $CaCO_3$ rain into sediment traps and dissolution on the sea floor: A revised global carbonate budget, Global Biogeochemical Cycles, 21, GB1024, https://doi.org/10.1029/2006GB0028

Fischer, G. and Karakaş G.: Sinking rates and ballast composition of particles in the Atlantic Ocean: implications for the organic carbon fluxes to the deep ocean , Biogeosciences, 6, 85–102, 2009

Fischer, G., Romero, O., Merkel, U., Donner, B., Iversen, M., Nowald, N., Ratmeyer, V., Ruhland, G., Klann, M., and Wefer, G.: Deep ocean mass fluxes in the coastal upwelling off Mauritania from 1988 to 2012: variability on seasonal to decadal timescales, Biogeosciences, 13, 3071 – 3090, 2016

been estimated to be about 700-840 $\mathrm{kg\,m^{-3}}$, Azetsu-Scott and Passow, 2004 as cited in the mansucript). The excess density of modelled, fresh aggregates in diatom-dominated regions is with about $2\,\mathrm{kg\,m^{-3}}$ in the observed range of about 0 to $\sim 10\,\mathrm{kg\,m^{-3}}$ is given by Alldredge and Gottschalk, 1988, Ploug et al. 2008 and Iversen and Ploug 2013 (as cited in the manuscript). We want to emphasize here again that the sinking velocity provided in Fig. 6 and 7 are mean sinking velocity. Observed sinking velocity of individual, large aggregates cannot be compared directly to the mean sinking velocity. Modeled large aggregates feature substantially higher sinking velocities than reflected by the mean sinking velocity. Large aggregates in our model thus have similar sinking velocity as compared to observed marine snow. See also the reply in the general part.

→ Remained.

- P. 23, line 25: I assume z0 is 100m, please clarify.

  ⇒ Yes, it is. It was introduced z_0 on p. 4, l. 21. We added z_0.

  → "The transfer efficiency of POC from 100 m to" → "The transfer efficiency of POC from $z_0 = 100$ m to"

- Line 26: "to about 1000m" → at 1000 m.

  ⇒ "at" would be wrong for two reasons: first, it is the transfer efficiency from 100 m to (about) 1000 m, and second, we don't interpolate the fluxes to exactly 1000 m, but use the fluxes across the model layer boundary at 960 m depth to calculate the transfer efficiency.

  → Remained.

- P. 28, line 29: this is not shown in Fig 7a, you only show mean density, not the effect of opal on density.

  ⇒ We disagree. Even at deep ocean regions, where detritus is almost remineralized (and thus POM and TEP play only a minor role for

primary particle density), primary particle density of diatom frustules in silicifier-dominated regions (e. g. south of -40 °) is significantly lower than primary particle density in calcifier-dominated regions (e. g. at about -20 °). Hence, opal acts less than $CaCO_3$ as ballasting agent in our model.

→ Remained.

- Line 30: any indication in the literature and any scientific explanation why silicate frustule size affect the sinking speed if not by density?

  ⇒ This is indeed a good question. Unfortunately, observational studies have so far heavily focused on aggregate size-to-sinking velocity relationships. Minor focus has been put on the solid hydrated density. Hence, even less emphasis has been put on the relation of primary particle sizes, microstructure and sinking velocity. However, as we discuss below line 30, studies by e. g. Laurenceau-Cornec et al. 2015 point to a relevance of cell size and morphology, and dominant size of primary producers have been suggested to drive interannual changes in export fluxes (Boyd and Newton, 1995, see the manuscript). From theoretical considerations, the size of primary particles can affect the porosity, Eq. (6), and hence the aggregate excess density (irrespective of the density of the single primary particles). This is described in the manuscript by Eq. (5). We again searched for relevant literature on experimental studies that clearly disentangle these aspects for marine aggregates. A very recent study by Laurenceau-Cornec et al. (2019)[7] provides a summary, how porosity can vary and can have a decisive role for determining the settling velocity. A new study by C. Flintrop is in preparation that will provide further insights into settling dynamics of marine aggregates. We now explicitly refer to the relevant equations to address, why primary particle size can affect the packaging and thus sinking velocity. We add an explanatory sentence and provide the reference to Laurenceau-Cornec et al. (2019).

[7] Laurenceau-Cornec, E. C., Le Moigne, F. A. C., Gallinari, M., Moriceau, B., Toullec, J., Iversen, M. H., Engel, A., and De La Rocha, C. L.: New guidelines for the application of Stokes' models to the sinking velocity of marine aggregates, Limnol. Oceanogr., https://doi.org/10.1002/lno.11388, 2019

→ Adding on p.28, l. 32 (after: "...likely play a role."): "As indicated by Eq. (5) and (6), primary particle size affects the excess density and porosity of aggregates, which have decisive effects on sinking velocity (Laurenceau-Cornec et al., 2019)."

- Fig 10: colorbar label: conribution → contribution(add 't')

  ⇒ Thanks. Changed.

  → added the "t", see Fig. 1

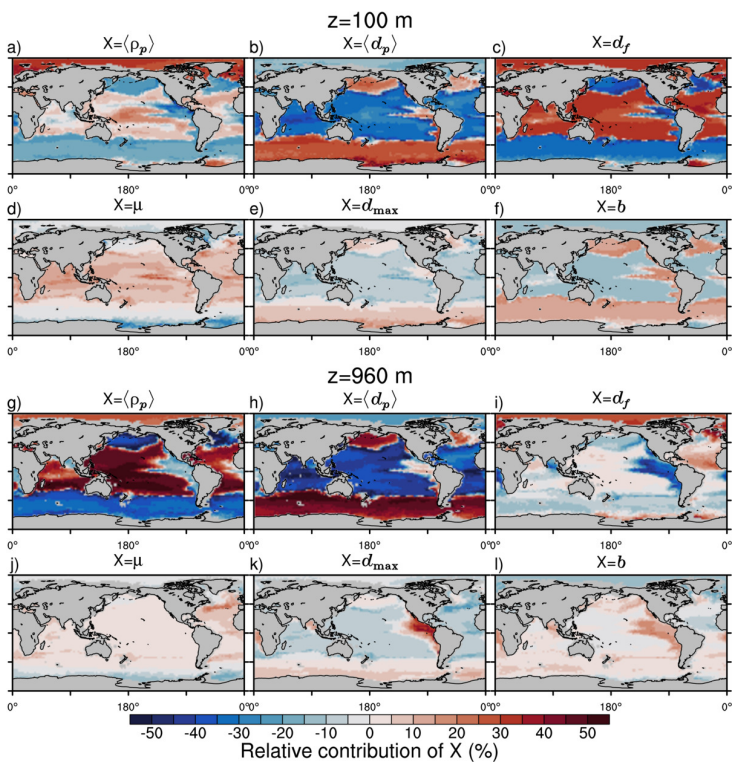

Figure 1: "conribution" → "contribution"

- P. 35 and Figure 14a: what is the reason of showing cumulative CO2 fluxes integrated over latitude? Please show just the zonal means, that's much easier to understand and compare to data. The units should not include per degree if it is cumulative.

⇒ We apologize for the wrong units. However, cumulative fluxes give directly the net-transport across the equator and also provide the information that both model runs are in well spun-up states. We therefore remained with the cumulative fluxes and only corrected the units.

→ Units changed.

- Figure 14c-k: cumulative fluxes make more sense here. I'd prefer actual fluxes/time and then the difference between the two could be cumulative. Then, one y-axis might also be enough.

⇒ We agree with the reviewer that cumulative fluxes make sense here since the subfigures provide a direct insight in how much CO_2 is taken up in the course of the years. We thus remain with the figure as it is.

→ Remained.

- P. 37, line 24: suggested → hypothesize (careful which tense you use). Also, please please back up this hypothesis with literature.

⇒ We here refer to the suggestion made earlier in the manuscript (in Sect. 3.5). We therefore keep 'suggested', and now explicitly refer to the section. In Sect. 3.5, we discuss and cite a number of experimental studies that link sinking velocity of marine aggregates to morphology and size structure of the phytoplankton community. Together with the theoretical derivation of the aggregate excess density (Eq. (5)) and porosity (Eq. (6)), being dependent on primary particle size, these and our study provide reasonable indications that primary particle size (or -diatom- cell size, respectively) potentially affects the sinking velocity of marine aggregates. This led us to suggest primary particle size as an additional factor for aggregate sinking. We are, however, aware that full experimental evidence is, to our best knowledge, lacking and will hopefully be part of future research, where the role of microstructure and composition will be deciphered and disentangled.

→ "We suggested" → "Previously in Sect. 3.5, we suggested"

- P. 38: you have not shown silicate distribution – is that reasonable? You refer to low transfer-efficiency in silicifier-dominate region, but this is not the case in the Southern Ocean, nor do you see much of an impact in Figs 15 a and d in the Southern Ocean, which is THE region dominated by silicifiers. This needs more explanation.

  ⇒ We show in Fig. 5a,c the opal-to-POC flux ratio. As described in the methods part, Sect. 2 (first paragraph), HAMOCCs opal production is directly coupled to silicate availability. The regions of silicifiers are therefore well defined and previously described in the manuscript (and silicate is included in our general Taylor diagram-based analysis of nutrient fields). With respect to the low transfer efficiency, Fig. 15 g clearly shows a drop in transfer efficiency for the AAZ and SAZ regions, once the frustule size of diatoms, $d_{p,\text{frustule}}$ is decreased (cmp. M^{4}AGO run with $S(d_{p,\text{frustule}})$, where $\langle T_{\text{eff}} \rangle$ decreases from about 0.24 to about 0.14 for the Antarctic Zone (AAZ), and from about 0.19 to about 0.11 for the Subantarctic Zone (SAZ)). To make the difference more clear, we rephrase the sentence, where the sensitivity study is compared to the original M^{4}AGO run. We further add the specification, where the largest signal in silicate increase can be found.

  → "As a consequence, the transfer efficiency in silicifier-dominated regions is low (Fig. 15 g). Accordingly, opal dissolves closer to surface waters and the silicate concentration increases with respect to the M^{4}AGO run in silicifier-dominated regions (Fig. 15 d)."
  → "As a consequence, the transfer efficiency in silicifier-dominated regions is lower in $S(d_{p,\text{frustule}})$ than in M^{4}AGO (Fig. 15 g). Accordingly, opal dissolves closer to surface waters and the silicate concentration increases compared to the M^{4}AGO run in silicifier-dominated regions, particularly in and downstream of coastal upwelling regions (Fig. 15 d)."

Microstructure and composition of marine aggregates as co-determinants for vertical particulate organic carbon transfer in the global ocean

Joeran Maerz[1], Katharina D. Six[1], Irene Stemmler[1,3], Soeren Ahmerkamp[2], and Tatiana Ilyina[1]

[1]Max Planck Institute for Meteorology (MPI-M), Hamburg, Germany
[2]Max Planck Institute for Marine Microbiology (MPI-MM), Bremen, Germany
[3]present address: Wobe, Kiel, Germany

Correspondence: Joeran Maerz (joeran.maerz@mpimet.mpg.de)

Abstract.

Marine aggregates are the vector for biogenically bound carbon and nutrients from the euphotic zone to the interior of the oceans. To improve the representation of this biological carbon pump in the global biogeochemical HAMburg Ocean Carbon Cycle (HAMOCC) model, we implemented a novel *Microstructure, Multiscale, Mechanistic, Marine Aggregates in the Global Ocean* (M^4AGO) sinking scheme. M^4AGO explicitly represents the size, microstructure, heterogeneous composition, density, and porosity of aggregates, and ties ballasting mineral and particulate organic carbon (POC) fluxes together. Additionally, we incorporated temperature-dependent remineralization of POC. We compare M^4AGO with the standard HAMOCC version, where POC fluxes follow a Martin curve approach with linearly increasing sinking velocity with depth, and temperature-independent remineralization. Minerals descend separately with a constant speed. In contrast to the standard HAMOCC, M^4AGO reproduces the latitudinal pattern of POC transfer efficiency ~~which has been~~as recently constrained by Weber et al. (2016). High latitudes show transfer efficiencies of $\approx 0.25 \pm 0.04$ and the subtropical gyres show lower values of about 0.10 ± 0.03. In addition to temperature as ~~a driving factor~~a driving factor for remineralization, diatom frustule size co-determines POC fluxes in silicifiers-dominated ocean regions while calcium carbonate enhances the aggregate excess density, and thus sinking velocity in subtropical gyres. ~~In ocean standalone runs and rising carbon dioxide (CO_2) without CO_2 climate feedback, M^4AGO alters the regional ocean-atmosphere CO_2 fluxes compared to the standard model.~~Prescribing rising carbon dioxide (CO_2) concentrations in standalone runs (without climate feedback), M^4AGO alters the regional ocean atmosphere CO_2 fluxes compared to the standard model. M^4AGO exhibits higher CO_2 uptake in the Southern Ocean compared to the standard run while in subtropical gyres, less CO_2 is taken up. Overall, the global oceanic CO_2 uptake remains the same. With the explicit representation of measurable aggregate properties, M^4AGO can serve as a testbed for evaluating the impact of aggregate-associated processes on global biogeochemical cycles, and, in particular, on the biological carbon pump.

Copyright statement. TEXT

1 Introduction

Marine aggregates transfer biologically bound carbon and nutrients from the sunlit surface waters, the euphotic zone, to the interior of the oceans. While uncertainty with respect to primary production estimates exists, about 4.0 Gt C yr^{-1} to 11.2 Gt C yr^{-1} biologically bound carbon are annually exported out of the euphotic zone of the global ocean (Laws et al., 2000; Najjar et al., 2007; Henson et al., 2012). The net-withdrawal of carbon dioxide (CO_2) from the ocean surface through export of carbon bound in particulate organic matter (POM) and biogenic minerals and subsequent release through microbial remineralization and dissolution during aggregates descent determines the strength of the so-called biological carbon pump. The biological carbon pump critically depends on phytoplankton growth, the replenishment of the euphotic zone with nutrients through mixing and upwelling processes, and the efficiency of biologically bound carbon transfer from surface waters to the interior of the oceans (Williams and Follows, 2011). The region and depth of carbon sequestration eventually determines the residence time of the biologically bound carbon upon recurrence at the oceans surface. Representing transport and fate of marine aggregates in Earth System Models (ESMs) is therefore key to quantify the future evolution of biogeochemical cycles, and particularly the biological carbon pump and its feedback on the Earth system under climate change (Ilyina and Friedlingstein, 2016). In the present study, we thus aim at advancing the representation of marine aggregates in an ESM framework.

Marine aggregates are porous entities which are heterogeneously composed of POM, biogenic and inorganic minerals. The sinking velocity of marine aggregates, their microbial remineralization and zooplankton grazing governs the attenuation of vertical particulate organic carbon (POC) fluxes. The sinking velocity of aggregates is primarily determined by their size. In addition, the internal microstructure, defined by the porosity and heterogeneous composition, entail high variability of excess density and thus sinking speed of aggregates (Iversen and Robert, 2015). Biogenic calcium carbonate ($CaCO_3$) and opal structures, primarily formed by coccolithophores and diatoms, act as ballasting minerals in organic aggregates (De La Rocha and Passow, 2007; Armstrong et al., 2002). On the contrary, the available amount of POC, acting as glue, is suggested to limit the uptake capability for ballasting minerals before aggregates disintegrate (Passow, 2004; Passow and De La Rocha, 2006; De La Rocha et al., 2008). Ballasting increases the POC transfer efficiency (Klaas and Archer, 2002; Balch et al., 2010; Cram et al., 2018), defined as the fraction of POC exported out of the euphotic zone that reaches a particular depth, e. g. 1000 m (Francois et al., 2002). As $CaCO_3$ is significantly denser than opal, $CaCO_3$ is suggested to be a more effective ballasting material for marine aggregates (Balch et al., 2010) implying higher POC transfer efficiency in $CaCO_3$ production-dominated regions. Phytoplankton communities possess spatio-temporally varying patterns and prime the sinking flux ratios of detritus to ballasting minerals, i. e. the rain ratios. High $CaCO_3$ to opal ratios are found in oligotrophic regions of the mid-latitude subtropical gyres, while opal is the prevalent ballasting mineral in high latitudes and upwelling-influenced equatorial regions (Balch et al., 2010). However, simple ballasting relationships on aggregates are questioned and the prevailing plankton network is suggested as an additional driver for POC fluxes (Wilson et al., 2012; Henson et al., 2012; Guidi et al., 2016). For example, cell size and morphology present in the phytoplankton community are suggested as ~~primer~~primary determining factor for sinking velocity of marine aggregates (Laurenceau-Cornec et al., 2015; Bach et al., 2016). In turn, the attenuation of POC fluxes is hypothesized to be modulated by microbial remineralization and by zooplankton grazing in oligotrophic and

eutrophic regions, respectively (Guidi et al., 2009). Since temperature controls enzymatic reaction kinetics, and thus microbial remineralization of POC, slower attenuation and thus higher transfer efficiency is suggested in cold high latitudes compared to warm oligotrophic regions (Marsay et al., 2015). For a long time, the aforementioned variable factors and processes, the limited understanding of aggregation and fragmentation processes that shape the aggregate size spectrum, and the sparse amount of data have retarded the emergence of a detailed picture of global pattern of POC fluxes attenuation and thus transfer efficiency.

However, quantification of the regionally varying POC transfer efficiency and their variability is key to understand global biogeochemical cycles, in particular the carbon cycle (Falkowski et al., 1998). Recently, global POC fluxes have been constrained to possess high transfer efficiency in high latitudes and upwelling regions, and lower efficiency in the subtropical gyres (Weber et al., 2016). The underlying controls for the transfer efficiency pattern seem to exhibit a distinct latitudinal variability (Cram et al., 2018). The simplified model study of Cram et al. (2018) suggests aggregate size, ballasting of particles by $CaCO_3$ and opal, temperature effects on microbial aerobic and anaerobic remineralization, water density, and molecular viscosity as major controls of the transfer efficiency pattern.

Processes of marine snow formation, ballasting and sinking are currently underrepresented in ESMs despite the relevance of aggregates for the transfer and sequestration of POC to the deep ocean. Only a few global models explicitly incorporate aggregation of phytoplankton mechanistically (e. g. Gehlen et al., 2006; Schwinger et al., 2016) while ~~ignoring~~neglecting ballasting effects or vice versa (Gehlen et al., 2006; Heinemann et al., 2019). POC sinking velocities in ESMs are typically formulated to reproduce the Martin curve (Martin et al., 1987) or heuristically describe ballasting of POC with opal and $CaCO_3$ (e. g. Gehlen et al., 2006; Heinemann et al., 2019), which limits the process-based adaptation of sinking velocities under changing environmental conditions associated with climate change.

As a first step, we develop the *Microstructure, Multiscale, Mechanistic, Marine Aggregates in the Global Ocean* (M^4AGO) sinking scheme that explicitly represents composition, microstructure and related properties such as porosity and density of aggregates. We aim at consistently defining marine aggregates with their *in situ* measurable properties in an ESM framework. We implement M^4AGO in the global HAMburg Ocean Carbon Cycle (HAMOCC) model which is part of the Max Planck Institute - Earth System Model (MPI-ESM), explicate the emerging pattern of aggregate properties, and examine their effect on sinking velocity and the global pattern of POC transfer efficiency. We particularly aim at: i) representing the POC transfer efficiency pattern of Weber et al. (2016), ii) providing further understanding into the underlying driving factors for this pattern and iii) giving insights on the impact of M^4AGO on the global CO_2 flux pattern. We focus on the transfer efficiency pattern identified by Weber et al. (2016) as it was derived by diagnosing phosphate fluxes from World Ocean Atlas 2009 phosphate concentration via inverse modeling. This approach benefits from ~~an~~order of magnitude more observations than direct flux observations (Usbeck et al., 2003; Weber et al., 2016) and can thus be regarded as, to date, more reliable than previous estimates with partly opposing latitudinal pattern (e. g. Henson et al., 2012; Marsay et al., 2015).

With M^4AGO, we represent marine aggregates at global scale to provide a testbed for future investigations of aggregate-associated processes in ESMs, e. g. particle size-, microstructure- and composition-dependent remineralization rates.

2 Model description

The HAMburg Ocean Carbon Cycle (HAMOCC) model is a global biogeochemical model which features biology and resolves the carbon chemistry (Six and Maier-Reimer, 1996; Ilyina et al., 2013; Paulsen et al., 2017; Mauritsen et al., 2019). HAMOCC assumes a fixed stoichiometry for dead and living organic matter, and represents the nutrients phosphate, nitrate, silicate, and iron. HAMOCCs phytoplankton, namely bulk phytoplankton and diazotrophs, can thus experience nutrient co-limitation. Diazotrophs assimilate gaseous di-nitrogen under nitrate limitation and compete for phosphorus with bulk phytoplankton. Diazotrophs grow slower than bulk phytoplankton and have their optimal growth temperature at about 28 °C (Paulsen et al., 2017, 2018). Zooplankton feeds on bulk phytoplankton and releases POM which enters the common detritus pool. During detritus formation through bulk phytoplankton or zooplankton, opal or $CaCO_3$ is produced depending on silicate availability. This treatment adequately depicts the spatial distribution of silicifying and calcifying plankton communities (Heinze et al., 1999). HAMOCC represents sediment processes (Heinze et al., 1999) and is coupled to the global three dimensional Max Planck Institute Ocean & Sea Ice Model (MPI-OM; Marsland et al., 2003; Jungclaus et al., 2013). HAMOCC is described and evaluated in previous studies, for details see e. g. Six and Maier-Reimer (1996); Ilyina et al. (2013); Paulsen et al. (2017); Mauritsen et al. (2019). In the following, we therefore focus on processes in the standard version, i. e. sinking and remineralization, which we modify with the M^4AGO sinking scheme. A table with the used mathematical symbols can be found in App. D, Tab. D1.

2.1 HAMOCCs standard representation of sinking fluxes & remineralization

The standard version of HAMOCC (Mauritsen et al., 2019) represents sinking fluxes of POC, F_{POC}, at depth $z > z_0$ according to the concept of the Martin curve (Martin et al., 1987; Kriest and Oschlies, 2008)

$$F_{\mathrm{POC}}(z) = F_0 \left(\frac{z}{z_0} \right)^{-\beta} \tag{1}$$

where F_0 is the POC flux out of the euphotic zone at export depth z_0. For simplicity, the export depth is globally defined as being $z_0 = 100\,\mathrm{m}$ in HAMOCC. Above z_0, a constant sinking speed of $3.5\,\mathrm{m\,d^{-1}}$ is assumed. Below z_0, we assume a linearly increasing mass concentration-weighted mean sinking velocity with depth. The ratio between the remineralization rate of POC, $R_{\mathrm{POC,remin}}$ and the vertical gradient of the sinking velocity $\partial_z \bar{w}_s$ determines the POC flux slope $\beta = R_{\mathrm{POC,remin}}/\partial_z \bar{w}_s$ (Kriest and Oschlies, 2008). In the standard version of HAMOCC, remineralization of POC is temperature-independent and comprehends oxygen concentration-dependent aerobic remineralization as well as sulphate reduction and denitrification under sub- and anoxic conditions.

The sinking tracers opal and $CaCO_3$ are treated separately from POC and sink with their own, constant sinking velocity. Aeolian dust is, apart from the release of bioavailable iron in surface waters, inert and sinks slowly through the water column. ~~Opal~~The opal dissolution rate in the standard model is linearly temperature-dependent. HAMOCC accounts for dissolution in carbonate ion under-saturated conditions below the dynamically emerging lysocline. In the following, we refer to this version of HAMOCC as 'standard'.

2.2 The novel M^{4}AGO sinking scheme in HAMOCC

Natural waters exhibit a size spectrum of aggregates whose diameter, d, composition and microstructure determine their terminal sinking velocity. In the M^{4}AGO approach, we explicitly represent microstructure and heterogeneous composition of aggregates. For the aggregate size spectrum, we limit the representation to a variable power law number distribution, $n(d)$, with slope b and power law factor a (following e. g. Kriest and Evans, 1999; Gehlen et al., 2006; Schwinger et al., 2016)

$$n(d) = a\,d^{-b} \tag{2}$$

This way, we avoid the computational costs of size-class based model approaches (Jackson, 1990; Stemmann et al., 2004; Sherwood et al., 2018).

The local concentration-weighted mean sinking velocity, $\langle w_s \rangle$, in M^{4}AGO is eventually ~~determined by a truncated number distribution, Eq. (2), through the minimum and maximum aggregates sizes, $d_{\min}$ and $d_{\max}$, respectively, the aggregate mass, $m(d)$, and the sinking velocity of single aggregates, $w_s(d)$~~computed from the number distribution, Eq. (2), that is truncated at the minimum and maximum aggregate sizes, $d_{\min}$ and $d_{\max}$, respectively, and expressions for the aggregate mass, $m(d)$, and the sinking velocity of aggregates, $w_s(d)$, of a particular diameter, d. Integration over the aggregate size spectrum yields $\langle w_s \rangle$,

$$\langle w_s \rangle = \frac{\int_{d_{\min}}^{d_{\max}} n(d)\,m(d)\,w_s(d)\,\mathrm{d}d}{\int_{d_{\min}}^{d_{\max}} n(d)\,m(d)\,\mathrm{d}d} \tag{3}$$

We only implicitly account for aggregation and fragmentation and explicitly represent the temporally and spatially variable heterogeneity and microstructure of aggregates and their effect on the mean sinking velocity. We refrain from representing the potential heterogeneity of aggregate composition within the local size spectrum (see e. g. Jackson, 1998). Consequently, and in contrast to the standard configuration, the settling tracers in HAMOCC, opal, $CaCO_3$, detritus, and dust, are sinking in M^{4}AGO at the same mean sinking velocity of aggregates, Eq. (3). In contrast to Gehlen et al. (2006); Schwinger et al. (2016); Heinemann et al. (2019), we explicitly incorporate both, variable aggregate size and ballasting through heterogeneous composition. Under the above assumptions, we derive the terms for b, $m(d)$, $w_s(d)$, $d_{\min}$ and $d_{\max}$ in the following sections.

2.2.1 Representation of aggregate microstructure and heterogeneous composition

Marine aggregates are porous (Alldredge and Gotschalk, 1990) and feature a self-similar microstructure which can be described via a fractal dimension d_f (Logan and Wilkinson, 1990; Kranenburg, 1994). A $d_f = 1$ would depict a chain of aggregate constituents, where the length equals the aggregate diameter, and a $d_f = 3$ describes a solid sphere. Consequently, the mass of an aggregate, $m(d)$, grows disproportionately to the aggregates volume and can be expressed as

$$m(d) = m_f\,d^{d_f} \tag{4}$$

where m_f is a mass-factor for the smallest entity. Thus, the density of an aggregate ρ_f decreases with increasing diameter. Aggregates consist of e. g. phytoplankton cells or coccolithophore shells (Alldredge and Gotschalk, 1990) which we consider

as spherical primary particles. Primary particles exhibit their own density ρ_p and diameter d_p. Taking the fractal scaling of aggregate mass into account, the excess density of an aggregate $\Delta\rho_f = \rho_f - \rho$ with respect to surrounding fluid density ρ can be expressed as (Kranenburg, 1994)

$$\Delta\rho_f = (\rho_p - \rho)\left(\frac{d_p}{d}\right)^{3-d_f} \qquad \text{for: } d \geq d_p \tag{5}$$

Furthermore, the aggregate porosity, ϕ, is defined as

$$\phi = 1 - \left(\frac{d_p}{d}\right)^{3-d_f} \qquad \text{for: } d \geq d_p \tag{6}$$

and hence, both, excess density and porosity, are regulated by the fractal dimension and primary particle size. The $\Delta\rho_f$ can be introduced to the well known Stokes (1851) terminal sinking velocity, w_s,

$$w_s = \sqrt{\frac{4}{3}\frac{\Delta\rho_f}{\rho}\frac{g\,d}{c_D}} \tag{7}$$

For small particle Reynolds numbers, $Re_\mathrm{p} = w_s\,d/\nu < 0.1$, the drag coefficient is $c_D = 24/Re_\mathrm{p}$ and the ~~well known Stokes (1851)~~ sinking velocity, w_s, becomes

$$w_s = \frac{1}{18\,\mu}(\rho_p - \rho)\,g\,d_p^{3-d_f}\,d^{d_f-1} \tag{8}$$

where μ and ν are molecular dynamic and kinematic viscosity (Matthäus, 1972), respectively, and g is the gravitational acceleration constant. However, this approach assumes homogeneous, mono-sized primary particles while it displays the potential importance of primary particle size and density as well as aggregate microstructure for sinking velocity. To better represent aggregates in natural systems, the heterogeneity of primary particles was thus far considered either for size or density (Jackson, 1998; Maggi, 2009; Khelifa and Hill, 2006). With M^{4}AGO, we represent aggregates composed of poly-dense, poly-sized primary particles under the assumption of a singled value fractal dimension throughout the aggregate size spectrum. This allows for representing heterogeneous primary particles such as diatom frustules, coccoliths, dust particles, and detritus as principal components of marine aggregates.

Bushell and Amal (1998) derived a representation of the mean primary particle size

$$\langle d_p \rangle = \left(\frac{\sum_i n_i\,d_{p,i}^3}{\sum_i n_i\,d_{p,i}^{d_f}}\right)^{\frac{1}{3-d_f}} \tag{9}$$

for an aggregate that is composed of $n_p = \sum_i n_i$ mono-dense spherical primary particles of different diameters $d_{p,i}$. Poly-sized formed aggregates disobey the traditional mass fractal relationship, but the fractal nature continues to emerge in a power law scaling for the mass present in a radial shell from an occupied point in the aggregate (Bushell and Amal, 1998). The approach of Bushell and Amal (1998) conserves the size of the aggregate and the encapsulated solid volume of the primary particles, ~~while $n \cdot \langle d_p \rangle^3 = \sum_i n_i\,d_{p,i}^3$ with $n \neq \sum_i n_i$, and thus the porosity of the aggregate is unimpaired.~~and thus the porosity of the aggregate is unimpaired, while the calculation does not presume equal number of mean, n, and individual primary particles,

$\sum_i n_i$, (hence, $n \cdot \langle d_p \rangle^3 = \sum_i n_i \, d_{p,i}^3$ with $n \neq \sum_i n_i$ for poly-sized primary particles), which is negligible in the following as we don't consider n any further.

Under the assumption that aggregates feature the same composition and hence same heterogeneity in a size spectrum, the aggregate-composing primary particle types are always the same for any aggregate of diameter d in a unit volume and thus $n_i/n_p = \text{constant}$. This further implies that the ratio K_i, ~~between the total number of one primary particle type~~between the total number of primary particles of one particle type, $n_{i,\text{tot}}$, to the total number of primary particles, $\sum n_{i,\text{tot}}$, in a unit volume is equal to the ratio found in an individual aggregate

$$K_i = \frac{n_i}{\sum_i n_i} = \frac{n_{i,\text{tot}}}{\sum_i n_{i,\text{tot}}} \tag{10}$$

Rewriting, $n_i = K_i \sum_i n_i$ and inserting in Eq. (9) gives

$$\langle d_p \rangle = \left(\frac{\sum_i K_i \, d_{p,i}^3}{\sum_i K_i \, d_{p,i}^{d_f}} \right)^{\frac{1}{3-d_f}} \tag{11}$$

where the factors K_i can be expressed in HAMOCC via the concentration of each aggregate-forming tracer C_i. Namely, we consider the HAMOCC tracers detritus, opal, calcite, and dust in taking part in the formation of heterogeneously composed aggregates. Calculating the number of primary particles from the tracer concentration requires the molecular concentration to mass factor, R_i, the tracer-related primary particle diameter, volume ~~$V_{p,i}$~~$V_{p,i} = \frac{1}{6}\pi \, d_{p,i}^3$, and density $\rho_{p,i}$

$$n_{i,\text{tot}} = \frac{C_i \, R_i}{\rho_{p,i} \, V_{p,i}} \tag{12}$$

The advantage of Eq. (11) is that it allows us to determine the mean primary particle diameter in HAMOCC while solid volume and density of primary particles are conserved. Ensuring mass conservation, we introduce the volume-weighted primary particle mean density

$$\langle \rho_p \rangle = \frac{\sum_i n_{i,\text{tot}} \, V_{p,i} \, \rho_{p,i}}{\sum_i n_{i,\text{tot}} \, V_{p,i}} \tag{13}$$

and hence, ~~the mass of a mean primary particle can be written as~~multiplication by the volume of the mean primary particle then yields the mass of a mean primary particle (see also Fig. 1)

$$m(\langle d_p \rangle) = \frac{1}{6} \pi \langle d_p \rangle^3 \, \langle \rho_p \rangle \tag{14}$$

Substituting Eq. (14) into Eq. (4), we derive the mass-factor for heterogeneous aggregates $m_f = \frac{1}{6}\pi \, \langle d_p \rangle^{3-d_f} \, \langle \rho_p \rangle$. The derivation of the mean primary particle diameter (Eq. 11), density (Eq. 13), and mass (Eq. 14) allows for applying common fractal laws for the calculation of aggregate mass, density, and thus sinking velocity. Hence, $w_s(d, \rho_p, d_p, \ldots)$ can be expressed as $w_s(d, \langle \rho_p \rangle, \langle d_p \rangle, \ldots)$. For a single type of primary particle, all underlying equations reduce to the traditional fractal scaling relationship (Logan and Wilkinson, 1990; Kranenburg, 1994).

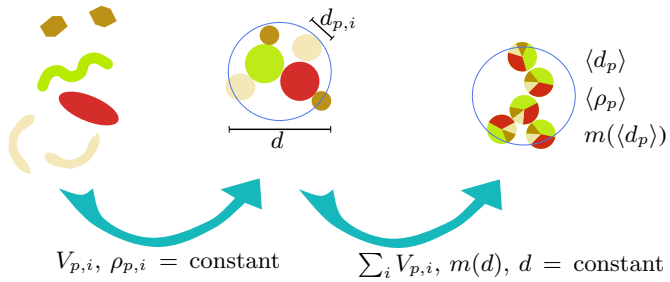

Figure 1. Underlying assumptions for the representation of aggregates composed of poly-dense, poly-sized primary particles. Primary particles, like dust particles, coccoliths, and diatom frustules (left) are assumed to be spherical and exhibit their characteristic density (middle). Once aggregated, we assume the diameter of the aggregate being constant and the total volume and mass of primary particles to be preserved (right). $V_{p,i}$ is the primary particle volume, $\rho_{p,i}$ is the primary particle density, and $d_{p,i}$ is the primary particle diameter of primary particle type i. $m(d)$ is the mass of an aggregate of diameter d. $\langle d_p \rangle$ and $\langle \rho_p \rangle$ represent mean primary particle diameter and density, respectively.

2.2.2 Mean sinking velocity of marine aggregates

In the preceding section, we derived a formulation for the mean primary particle size, Eq. (11), which we apply as a lower integration bound in Eq. (3), and hence, $d_{\min} = \langle d_p \rangle$ (following Kriest and Evans, 1999). The maximum aggregate diameter of the size spectrum, $d_{\max}$, is limited by fragmentation of particles. Several mechanisms can cause fragmentation of aggregates. Flow-induced turbulent shear has been suggested as the dominant process in the upper ocean, where turbulent shear reaches typical values of order $1\,\mathrm{s}^{-1}$ (Jackson, 1990). By contrast, Alldredge et al. (1990) showed that marine aggregates often withstand oceanic turbulence conditions and suggested biological processes as mediating factor for shaping the size distribution. Zooplankton also generates turbulent shear that is strong enough to rupture aggregates (Dilling and Alldredge, 2000). Hill (1998) proposed an alternative control on aggregate size, namely the sinking of aggregates that produces shear of the same order of magnitude as ambient turbulent shear in the ocean (Bagster and Tomi, 1974; Adler, 1979; Alldredge et al., 1990). Sinking could thus cause fragmentation in deeper regions of the ocean, where turbulent shear is small ($O(0.01\,\mathrm{s}^{-1})$; McCave, 1984; Waterhouse et al., 2014). Since modeling of particle-reactive thorium suggests continued fragmentation during particle descent in the deep ocean (Lam and Marchal, 2015), we adopt the hypothesis of sinking-induced fragmentation and limit the size distribution based on the particle Reynolds number, Re_p,

$$Re_\mathrm{p}(d, \langle d_p \rangle, \langle \rho_p \rangle, d_f, \nu) = \frac{d\, w_s(d, \langle d_p \rangle, \langle \rho_p \rangle, d_f)}{\nu} \tag{15}$$

Kiørboe et al. (2001) suggested the particle Reynolds number being in a typical range up to $Re_p = 20$ while e. g. Alldredge and Gotschalk (1988) measured particle Reynolds numbers up to $Re_p = 32$. Aggregates thus can exhibit larger Re_p than the laminar case ($Re_\mathrm{p} < 0.1$). The drag coefficient, c_D, in Eq. (7) can be represented by the expression for solid spheres of White (2005), valid up to $Re_\mathrm{p} < 10^5$

$$c_D = \frac{24}{Re_\mathrm{p}} + \frac{6}{1 + \sqrt{Re_\mathrm{p}}} + 0.4 \tag{16}$$

This drag representation leads to smaller settling velocities for large aggregates than the classical Stokes drag ($c_D = 24/Re_p$). Hence, aggregates can grow larger, until they reach the globally fixed critical Re_p for fragmentation, Re_{crit}, which leads to a more realistic representation of the size range of aggregates. We approximate ~~this~~the White drag representation by (Jiang and Logan, 1991)

$$c_D(Re_{\mathrm{p}}) = a_j\, Re_{\mathrm{p}}^{-b_j} \tag{17}$$

to avoid iteration and to allow for analytical solution of Eq. (3). Applying the parameter values of $a_{j=1} = 24.00,\ b_{j=1} = 1$ for : $Re_{\mathrm{p}} \leq 0.1$; $a_{j=2} = 29.03,\ b_{j=2} = 0.871$ for : $0.1 < Re_{\mathrm{p}} \leq 10$ and $a_{j=3} = 14.15,\ b_{j=3} = 0.547$ for : $10 < Re_{\mathrm{p}} \leq 100$ introduces maximum errors less than 10 % compared to Eq. (16) for $Re_{\mathrm{p}} < 100$ (Jiang and Logan, 1991).

By introducing Eq. (17) in Eq. (7), and applying Eq. (5) using mean primary particle properties, the approximation for the sinking velocity becomes

$$w_s = \left(\frac{4}{3} \frac{\rho_f(d, \langle\rho_p\rangle, \langle d_p\rangle, d_f)\langle\rho_p\rangle - \rho}{\rho} \langle d_p\rangle^{3-d_f}\, g\, \frac{d^{b_j+d_f-2}}{a_j\, \nu^{b_j}} \right)^{\frac{1}{2-b_j}} \tag{18}$$

By substituting Eq. (18) into Eq. (15), the piece-wise integration boundaries, $d_j(Re_{\mathrm{p},j=0..3} = 0, 0.1, 10, Re_{\mathrm{crit}})$, according to the c_D approximation for Eq. (3), become a function of Re_{p}

$$d_j(Re_{\mathrm{p},j}) = \frac{(Re_{\mathrm{p},j}\, \nu)^{\frac{2-b_j}{d_f}}}{\left(\frac{4}{3} \frac{\langle\rho_p\rangle - \rho}{\rho} \langle d_p\rangle^{3-d_f}\, g\, \frac{1}{a_j\, \nu^{b_j}} \right)^{\frac{1}{d_f}}} \tag{19}$$

~~where Re_{crit} is the globally fixed critical Re_{p} for fragmentation.~~ Consequently, the concentration-weighted mean sinking velocity, Eq. (3), can then be expressed as

$$\langle w_s\rangle = \frac{\sum_{j=0}^{2} \left(\int_{\max(\langle d_p\rangle, d_j(Re_{\mathrm{p},j}))}^{d_{j+1}(Re_{\mathrm{p},j+1})} n(d)\, m(d)\, w_s(d, a_{j+1}, b_{j+1})\, \mathrm{d}d \right)}{\int_{\langle d_p\rangle}^{d_{\max}} n(d)\, m(d)\, \mathrm{d}d} \tag{20}$$

where $d_{\max} = d_j(Re_{\mathrm{crit}})$ is the maximum diameter of aggregates, and by applying $a_{j=0} = b_{j=0} = 1$, the lower integration boundary equals the mean primary particle diameter.

2.2.3 The particle distribution slope, *b*

Observed aggregate size spectra in the ocean exhibit a spatio-temporal dependent slope ranging between approximately 3.2 to 5.4 (DeVries et al., 2014) or even lower (≈ 2; Guidi et al., 2009). A smaller slope parameter, b, translates to more large aggregates relative to a larger b and enhances mean sinking velocity. The evolution of the particle size spectra underlies the interacting processes of growth and decay of phytoplankton, aggregation, fragmentation and sinking of aggregates. Instead of modeling the processes of aggregation and fragmentation explicitly or prescribing b, we assume dynamic steady state

~~for~~between aggregation and fragmentation to describe the slope of the number distribution. According to dimensional analysis, the slope of the number distribution in dynamic steady state depends on the fractal dimension of aggregates and the process of aggregation, aggregation due to shear, differential sinking and Brownian motion (Jiang and Logan, 1991). Aggregation due to Brownian motion is only relevant for particles smaller $\approx 1\,\mu\text{m}$ (McCave, 1984) which we neglect here. We further assume that aggregation in the majority of the global ocean is dominated by differential settling and express the particle distribution slope, b, as (Jiang and Logan, 1991)

$$b = \frac{1}{2}\left(3 + d_f + \frac{2 + d_f - \min(2, d_f)}{2 - b_J}\right) \tag{21}$$

where b_J is a fixed parameter for the sinking velocity dependency on the particle Reynolds number that we fix for simplicity to $b_J = b_{j=2}$. The assumption of differential settling-dominated aggregation is likely violated in the euphotic zone, where shear aggregation is probably more relevant and steady state assumption is questionable, which we will address in the discussion (Sec. 3.10).

2.2.4 Heuristic approach to variable aggregate stickiness and fractal dimension

Adhesion properties of particles affect the fractal structure of aggregates and the collision efficiency ('stickiness') of particles (Meakin, 1988; Liu et al., 1990). Theoretical studies show that the stronger the surface adhesive forces are, the higher is the stickiness of particles and the smaller is the intrusion of particles and particle clusters into each other (Liu et al., 1990). As a result, this leads to a looser structure which translates to a small fractal dimension. Stickiness of phytoplankton is species-specific (Hansen and Kiørboe, 1997) and depends on the growth phase (Simon et al., 2014). Furthermore, phytoplankton releases extracellular polymeric substances (EPS; Decho, 1990) such as transparent exopolymer particles (TEPs) which are suggested as aggregation-priming, sticky materials ~~Alldredge et al., 1993; Azam and Malfatti, 2007; Thornton, 2002; Passow, 2002~~(Alldredge et al., 1993; Azam and Malfatti, 2007; Thornton, 2002; Passow, 2002; Engel et al., 2004). The resulting fractal dimension is typically determined as one value across ~~a particle size spectra~~all aggregate sizes. We thus assign a single fractal dimension to an aggregate population and depict the linkage between stickiness and fractal dimension in a qualitative manner. We attribute a stickiness value, α_i, to each of HAMOCCs sinking tracers and calculate a mean stickiness for the aggregates that is then mapped to a fractal dimension. Since adhesion, and thus stickiness, are a surface property, we calculate the mean stickiness

$$\langle\alpha\rangle = \frac{1}{A}\sum_i n_i\, A_i\, \alpha_i \quad \text{where}: A = \sum_i n_i\, A_i \tag{22}$$

weighted by the primary particles surfaces $A_i \propto d_{p,i}^2$. We map the mean stickiness to a range between zero and one

$$\langle\alpha\rangle_{\text{map}} = \frac{\langle\alpha\rangle - \alpha_{\min}}{\alpha_{\max} - \alpha_{\min}} \tag{23}$$

where $\alpha_{\min} = \min(\alpha_i)$ and $\alpha_{\max} = \max(\alpha_i)$.

Nicolás-Carlock et al. (2016) introduced a scaling parameter for the effective aggregation range in microscopic aggregation models to stipulate a defined fractal dimension across aggregate sizes. The scaling parameter can be perceived as an indicator

of stickiness that defines the effective aggregation range, i. e. higher stickiness results in a larger effective aggregation range. We introduce as an analogy for the dependency of the fractal dimension on the scaling parameter of Nicolás-Carlock et al. (2016) a transfer function for the mapped mean stickiness to fractal dimension, $d_f(\langle\alpha\rangle_{\mathrm{map}})$,

$$d_f(\langle\alpha\rangle_{\mathrm{map}}) = d_{f,\max}\exp(\beta_f\,\langle\alpha\rangle_{\mathrm{map}}) \tag{24}$$

with $\beta_f = \log(d_{f,\min}/d_{f,\max})$, where $d_{f,\min}$ and $d_{f,\max}$ are parametrized minimum and maximum fractal dimension of aggregates. Modeled stickier aggregates thus exhibit lower fractal dimensions than non-sticky particles which is in qualitative agreement with previous studies (Meakin, 1988; Liu et al., 1990; Block et al., 1991; Nicolás-Carlock et al., 2016).

2.2.5 Diatoms as a special case of primary particles

Diatoms are silicifying phytoplankton that possesses a hollow opal skeleton, the diatom frustule, and are thus different from a homogeneous, solid primary particle like coccoliths. Diatoms feature a wide range of sizes, with about a few microns to millimeters (Armbrust, 2009). Since sinking velocities of aggregates are proportional to their diameter, primary particle density and size (Eq. 8), aggregate-incorporated large diatom shells likely enhance the sinking velocity of particles. Indeed, un-remineralized, intact diatom frustules were even found in deeper regions of the ocean (Assmy et al., 2013), which is in agreement with previously found high sinking speeds of large diatom aggregates (Alldredge and Gotschalk, 1988). We therefore explicitly account for diatom shells by treating them as hollow opal spheres, filled i) with detritus, and ii) increasing water content with ongoing remineralization while sinking (see Fig. 2).

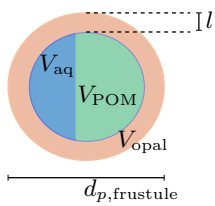

Figure 2. Diatom frustule and the remineralization state-dependent composition of the void. l denotes the thickness of the opal shell with volume V_{opal}, V_{aq} and V_{POM} are the encapsulated volumes of water and POM, respectively. $d_{p,\mathrm{frustule}}$ is the diameter of the diatom frustule.

The opal volume of a modeled diatom is

$$V_{\mathrm{opal}} = \frac{1}{6}\pi\,(d_{p,\mathrm{frustule}}^3 - (d_{p,\mathrm{frustule}} - 2\,l)^3) \tag{25}$$

where $d_{p,\mathrm{fustule}}$ is the diameter of the diatom, whose opal shell thickness l is expressed in terms of the fixed opal-to-phosphorus formation ratio. The number of diatom frustules per unit volume

$$n_{\mathrm{frustule}} = \frac{[\mathrm{opal}]\,R_{\mathrm{opal}}}{\rho_{\mathrm{opal}}\,V_{\mathrm{opal}}} \tag{26}$$

can therefore be deduced from the present opal concentration, [opal], and the opal mol-to-weight factor R_{opal} according to Eq. (12). We assume that the modeled detritus pool can be split into a free external, non-diatom and a diatom frustule-related,

void-filling detritus part. We further assume that the external pool is remineralized before the intra-cellular pool of volume V_{POM} and thus neglect cell lysis observed prior to aggregation (Armbrecht et al., 2014) and rather assume mineral protection of detritus (Hedges et al., 2001). If more detritus is remineralized than the frustules void would hold, it is replaced with the respective volume of water V_{aq} of density ρ. The frustule density thus is

$$\rho_{\mathrm{frustule}} = \frac{V_{\mathrm{opal}}\,\rho_{\mathrm{opal}} + V_{\mathrm{POM}}\,\underline{\rho_{\mathrm{POM}}}\rho_{\mathrm{det}} + V_{\mathrm{aq}}\,\rho}{V(d_{p,\mathrm{frustule}})} \tag{27}$$

During growth and decay, diatoms excrete TEPs which are positively buoyant and possess a density of about $\rho_{\mathrm{TEP}} = 700\,\mathrm{kg\,m^{-3}}$ to $840\,\mathrm{kg\,m^{-3}}$ (Azetsu-Scott and Passow, 2004; Mari et al., 2017). TEPs are suggested to play a prominent role in aggregation processes as they are probably sticky and thus enhance aggregation (Dam and Drapeau, 1995; Passow, 2002). In HAMOCC, phytoplankton excretion of TEPs is not resolved explicitly. We therefore treat TEPs virtually and assume a linear dependency of diatom stickiness and density on the freshness of detritus, ~~defined as the mass ratio between the actual amount of detritus m_e and the potential mass of detritus linked to opal production $m_{\mathrm{potential}}$~~defined as the mass ratio between the actual amount of detritus, $m_e = n_{\mathrm{frustule}}\,V_{\mathrm{POM}}\,\rho_{\mathrm{det}}$ and the potential mass of detritus linked to diatom frustules $m_{\mathrm{potential}} = n_{\mathrm{frustule}}\,(V_{\mathrm{POM}} + V_{\mathrm{aq}})\,\rho_{\mathrm{det}}$. An additional underlying assumption is that TEPs are remineralized with the same rates as normal detritus. Hence, we define the stickiness of diatoms as

$$\alpha_{\mathrm{diatom}} = \frac{m_e}{m_{\mathrm{potential}}}\,\alpha_{\mathrm{TEP}} + \left(1 - \frac{m_e}{m_{\mathrm{potential}}}\right)\alpha_{\mathrm{opal}} \tag{28}$$

for $m_{\mathrm{potential}} > 0$, where α_{TEP} and α_{opal} are the stickiness of TEPs and pure opal, respectively. ~~The density of diatoms becomes~~To account for the additional buoyancy through TEPs (Jokulsdottir and Archer, 2016; Mari et al., 2017), we here simplify and assume that the frustule density is lowered by TEPs in dependency on the freshness of detritus. Eventually, the diatom density, ρ_{diatom}, becomes

$$\rho_{\mathrm{diatom}} = \frac{\rho_{\mathrm{frustule}}\,m_{\mathrm{potential}} + \rho_{\mathrm{TEP}}\,m_e}{m_{\mathrm{potential}} + m_e} \tag{29}$$

TEPs thus have a twofold effect on aggregates in our model: i) TEPs increase stickiness and loosen the aggregate structure, ~~thus fractal dimension of aggregates is small~~thus decrease the fractal dimension of aggregates, and ii) TEPs decrease the fresh diatom frustules density and thus add buoyancy without violating tracer mass conservation (see also model discussion Sec. 3.10).

2.3 Temperature-dependent opal dissolution & POC remineralization

Marine aggregates tie heterogeneous components together that are disparately remineralized or dissolved. By contrast, in the standard model, detritus, opal and $CaCO_3$ were sinking separately from each other and the global remineralization and dissolution rates are tuned independently because the processes are artificially decoupled. In M^4AGO, remineralization of detritus and dissolution of, in particular, opal are tightly linked through the same sinking velocity which let us to re-evaluate and revise the formulations for opal dissolution and remineralization.

Opal dissolution is temperature-dependent (Ragueneau et al., 2000, 2006) and is microbially mediated (Bidle et al., 2002). Intact diatom frustules are protected from dissolution by an organic matrix (Lewin, 1961). Once the organic protection surrounding the silicate frustule becomes utilized by temperature-dependent microbes, they initiate and mediate the dissolution of opal (Bidle et al., 2002). Hence, opal dissolution follows a sequential process: i) an initial temperature-dependent remineralization of the organic coating of the silicate frustule and ii) the microbially mediated dissolution of opal with a temperature dependency of $Q_{10} \approx 2.3$ (Bidle et al., 2002). We here focus on the temperature-dependent microbially mediated dissolution and introduce a Q_{10} temperature-dependent opal dissolution

$$\frac{\partial}{\partial t}[\mathrm{opal}]\Big|_{\mathrm{dissolution}} = -r_{\mathrm{opal}}\, Q_{10,\mathrm{opal}}^{\frac{T-T_{\mathrm{ref,opal}}}{10}}\,[\mathrm{opal}] \tag{30}$$

where r_{opal} is the opal dissolution rate at the reference water temperature $T_{\mathrm{ref,opal}}$ and T is the ambient water temperature. In the standard version, we remain with the former linearly temperature-dependent opal dissolution ($\partial_t[\mathrm{opal}] = -r_{\mathrm{opal}}\,(0.1\,(T+3))\,[\mathrm{opal}]$) (Ragueneau et al., 2000; Segschneider and Bendtsen, 2013).

Analogously to opal, we incorporate a temperature-dependent Q_{10} factor to aerobic POC remineralization (Dell et al., 2011; Mislan et al., 2014) which depends on oxygen concentration, $[O_2]$, (Mauritsen et al., 2019), where K_{O_2} is the half saturation constant in Michaelis-Menten kinetics, and r_{POC} is the remineralization rate at reference temperature $T_{\mathrm{ref,POC}}$

$$R_{\mathrm{POC,remin}} = -r_{\mathrm{POC}}\,\frac{[O_2]}{K_{O_2}+[O_2]}\,Q_{10,\mathrm{POC}}^{\frac{T-T_{\mathrm{ref,POC}}}{10}} \tag{31}$$

We keep the anaerobic remineralization temperature-independent since we do not expect temperature shifts in ocean depths, where oxygen minimum zones appear in HAMOCC. In the standard run, the remineralization rates are temperature-independent ($Q_{10,\mathrm{POC}} = 1$).

2.4 Model setup, parametrization & evaluation

2.4.1 General model setup

The M^{4}AGO sinking scheme was implemented in HAMOCC which is coupled to MPI-OM (Jungclaus et al., 2013). For the flow of calculations in the M^{4}AGO sinking scheme, see Fig. 3. ~~We run both, the standard and the M^{4}AGO run, in a GR15/L40-OMIP setup. This translates to a horizontal resolution of about 1.5 °, 40 uneven vertical layers with highest resolution in the first few hundred meters of the ocean. OMIP is a climatological daily atmospheric forcing (Röske, 2005).~~We run both, the standard and the M^{4}AGO run, in a GR15/L40 setup with climatological forcing. This translates to a horizontal resolution of about 1.5 °, 40 uneven vertical layers with highest resolution in the first few hundred meters of the ocean. The climatological atmospheric boundary conditions are derived from the second European Centre for Medium-Range Weather Forecasts (ECMWF) Re-Analysis project (ERA-40; Simmons and Gibson, 2000; Röske, 2005). The mean annual cycle of i. e. wind stress, heat and freshwater fluxes are resolved on a daily basis. The continental freshwater runoff is provided by means of a runoff model (Röske, 2005). ~~The loss of POM, opal, and $CaCO_3$ due to sedimentation and subsequent burial was accounted for through homogeneously applied weathering rates which were adjusted accordingly, namely for~~

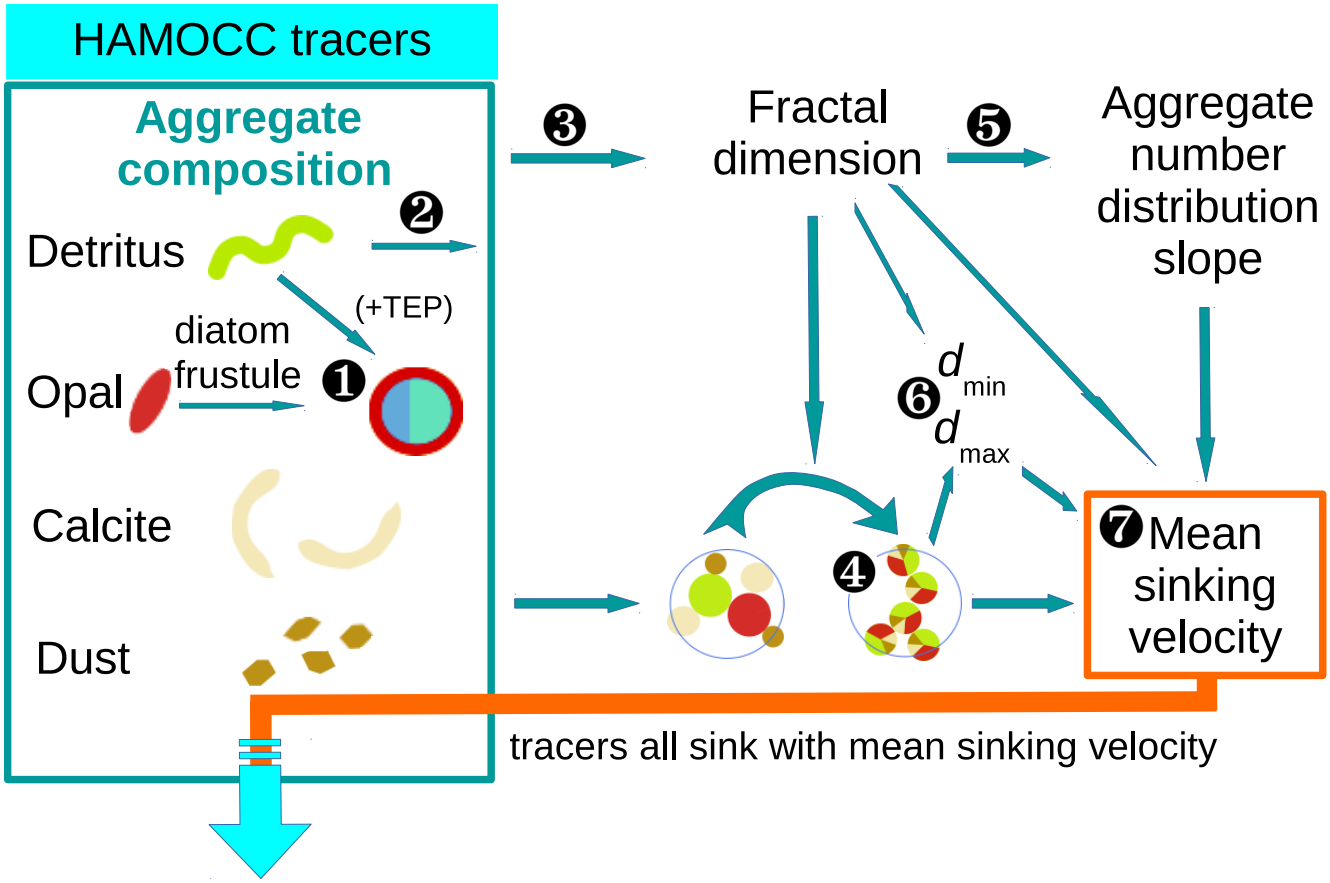

Figure 3. Flow diagram of calculations for the M^{4}AGO sinking scheme carried out at every ocean grid point and time step. Marine aggregates in M^{4}AGO are composed of spherical primary particles derived from HAMOCC tracers. Primary particles featuring size, density, and stickiness are: detritus, diatom frustules, coccoliths ($CaCO_3$), and dust minerals. ❶ The number of diatom frustules, Eq. (26), related diatom density, Eq. (29), and stickiness, Eq. (28), are estimated from opal and detritus concentration. Diatoms are then considered as primary particles which feature particular characteristics. ❷ The remaining detritus is considered as detritus primary particles. ❸ The calculation of the fractal dimension, Eq. (24), and ❹, the calculations of mean primary particle size, Eq. (11), and density, Eq. (13) are carried out. ❺ The fractal dimension determines the number distribution slope, Eq. (21). ❻ The minimum, $d_{\min} = \langle d_p \rangle$, and maximum aggregate diameter, $d_{\max}$ Eq. (19), are estimated. ❼ The mean sinking velocity, Eq. (20), can eventually be determined, with which the tracers sink.

~~the standard / M^{4}AGO run: $CaCO_3$ ≈17.2 / 26.5 T mol C yr^{-1}, dissolved organic phosphorus ≈99.6 / 101.5 G mol P yr^{-1}, and silicate ≈3.2 / 2.3 T mol Si yr^{-1}~~The loss of POM, opal, and $CaCO_3$ due to sedimentation and subsequent burial was accounted for through homogeneously applied weathering rates which were adjusted for the standard run (and the M^{4}AGO run): Globally, we add ≈99.6 (101.5) G mol P yr^{-1} as dissolved organic phosphorus, and ≈3.2 (2.3) T mol Si yr^{-1}. To compensate for the loss of $CaCO_3$, we add ≈17.2 (26.5) T mol C yr^{-1} to surface dissolved inorganic carbon (DIC) and a corresponding amount to

surface total alkalinity, A_T, as on DIC:$2A_T$. We start the M^{4}AGO run from the standard run in steady state and spin it up until steady state is reached in surface and mesopelagic waters, which translates to 1700 model years. Through the long overturning times of the global ocean, we still see drifts of nutrient concentrations in deep, old North Pacific waters at this state (i. e. on average $\sim 7.1\,\mu\mathrm{mol\,P\,m^{-3}\,century^{-1}}$ below 2000 m, which amounts to a centennial change of about 0.25 %). We neglect this drift as we focus on the aggregate properties and their effects on POC fluxes throughout the euphotic and mesopelagic zone.

2.4.2 Parameters of the M^{4}AGO scheme

The M^{4}AGO sinking scheme introduces a set of new parameters, in particular the primary particle characteristics, which require constraining and tuning (summarized in Tab. 1).

We applied HAMOCCs standard sediment densities for opal, $CaCO_3$, and dust to the densities of primary particles, namely $\rho_{\mathrm{opal}} = 2200\,\mathrm{kg\,m^{-3}}$, $\rho_{\mathrm{calc}} = 2600\,\mathrm{kg\,m^{-3}}$ and $\rho_{\mathrm{dust}} = 2600\,\mathrm{kg\,m^{-3}}$. For suspended detritus, we chose $\rho_{\mathrm{det}} = 1100\,\mathrm{kg\,m^{-3}}$ (Fettweis, 2008). As density of TEPs, we applied $\rho_{\mathrm{TEP}} = 800\,\mathrm{kg\,m^{-3}}$, which is within the measured range of $700\,\mathrm{kg\,m^{-3}}$ to $840\,\mathrm{kg\,m^{-3}}$ (Azetsu-Scott and Passow, 2004).

While the density of primary particles is comparably well constrained, the adhesion forces of primary particles, namely related stickiness and fractal dimension of aggregates, are less studied and are weakly constrained. There is yet no standardized way to investigate stickiness, fractal dimension, and their interdependence for aggregates in natural waters. Stickiness is experimentally defined as the interparticle attachment rate divided by the interparticle collision rate. Uncertainties in any of the two rates, e. g. due to ignoring fractal structure of aggregates, aggregate permeability, etc., directly affects the calculated stickiness (Filella, 2007). In addition, stickiness is phytoplankton species-specific (Hansen and Kiørboe, 1997) and depends on the growth phase (Simon et al., 2014). The methodological limitations, the heterogeneity of marine aggregate constituents and their variable formation process lead to a wide spread of indirectly inferred values for stickiness and fractal dimension (see e. g. Filella, 2007, for a broader overview). Diatom aggregates seem to feature a wide spread of fractal dimensions ranging from $d_f \approx 1.26$ to $d_f \approx 2.46$ (Alldredge and Gotschalk, 1988; Guidi et al., 2008) and $\langle\alpha\rangle$ of about 0.03 to 0.88 (Kiørboe et al., 1990; Dam and Drapeau, 1995; Alldredge and McGillivary, 1991). Indirectly inferred fractal dimension for re-worked aggregates exhibit values of $d_f \approx 2.26$ to $d_f \approx 2.46$ (Guidi et al., 2008) and mineral-dominated aggregates also feature high fractal dimensions of about $d_f \approx 2$ (Winterwerp, 1998) to $d_f \approx 2.6$ (Kranenburg, 1999) and low stickiness of $\langle\alpha\rangle \approx O(10^{-2})$ (Tambo and Hozumi, 1979). Since stickiness of *in situ* primary particles is seldom measured, we choose it to our best knowledge and order the stickiness for modeled primary particles according to the mean stickiness of observed aggregate types: $\alpha_{\mathrm{dust}} < \alpha_{\mathrm{opal}} \leq \alpha_{\mathrm{CaCO_3}} < \alpha_{\mathrm{det}} < \alpha_{\mathrm{TEP}}$ (see also Tab. 1). Hence, detritus and TEPs-rich aggregates are modelled with a loose structure and low fractal dimension, while degraded, mineral-rich aggregates are more compact and thus feature a higher fractal dimension (see Eq. 24) which is in congruence with the present conceptual understanding of aggregates becoming compacted during their descent (Mari et al., 2017). For the minimum and maximum fractal dimension of marine aggregates, we chose conservative bounds of 1.6 (Logan and Alldredge, 1989; Li and Logan, 1995; Alldredge, 1998) and 2.4 (in the range of $d_f \approx 2.26$ to 2.46 for reworked aggregates Guidi et al., 2008) which is well within the observed range of 1.26 (Logan and Wilkinson, 1990) to 2.6 (Kranenburg, 1999) for marine particles.

Table 1. Model parameters for M^{4}AGO* and, if adjusted in comparison to the standard HAMOCC, the standard values. ~~The value for the Martin curve of POC fluxes in the standard run, (Eq. 1), is $\beta = 1$.~~

Parameter	Description	Value in HAMOCC standard / M^{4}AGO	Literature range	Unit	References
α_{det}	stickiness of detritus particles	0.10		–	Hansen and Kiørboe (1997); Simon et al. (2014); Filella (2007); Kiørboe et al. (1990); Dam and Drapeau (1995); Alldredge and McGillivary (1991); Tambo and Hozumi (1979)
α_{calc}	stickiness of $CaCO_3$ particles	0.09	for $\langle\alpha\rangle$ of	–	
α_{dust}	stickiness of dust mineral particles	0.07	aggregates,	–	
α_{opal}	stickiness of opal particles	0.08	see text	–	
α_{TEP}	stickiness of TEP particles	0.19		–	
b_J	slope parameter	0.871	0.547, 0.871, 1	–	Jiang and Logan (1991)
$c_{\max}$	maximum fraction of $CaCO_3$ production	0.20 / 0.18	–	–	
$^*d_{p,\mathrm{dust}}$	primary particle diameter of dust minerals	2	< 1 - ≈ 20	µm	Maher et al. (2010); Mahowald et al. (2014)
$^*d_{p,\mathrm{calc}}$	primary particle diameter of $CaCO_3$	3	1.5-15.5	µm	Young and Ziveri (2000); Henderiks (2008)
$^*d_{p,\mathrm{frustule}}$	primary particle diameter of diatom frustule	20	6-29 /O(µm to mm)	µm	Litchman et al. (2009)
$^*d_{p,\mathrm{det}}$	primary particle diameter of detritus	4	–	µm	
$d_{f,\min}$	minimum fractal dimension of aggregates	1.6	1.26 - 2.60	–	Logan and Wilkinson (1990); Kranenburg (1999)
$d_{f,\max}$	maximum fractal dimension of aggregates	2.4			
$^*Q_{10,\mathrm{opal}}$	Q10 factor for opal dissolution	2.6	2.3 (-1.8-17 °C) - 2.9	–	Bidle et al. (2002); based on their values
$^*Q_{10,\mathrm{det}}$	Q10 factor for detritus remineralization	1.0 / 2.1	2-3	–	Mislan et al. (2014); Dell et al. (2011)
$^*r_{\mathrm{opal}}$	dissolution rate opal	0.010 / 0.023	^{a}0.001-0.138 (-1.8 - 33 °C)	d^{-1}	Bidle et al. (2002)
$^*r_{\mathrm{POC}}$	remineralization rate POC	0.026 / 0.120	^{a}0.08-0.21 (at 15 °C)	d^{-1}	Iversen and Ploug (2010)
ρ_{TEP}	density of TEP	800	700-840	$\mathrm{kg\,m^{-3}}$	Azetsu-Scott and Passow (2004)
ρ_{det}	density of detritus	1100	900-1300	$\mathrm{kg\,m^{-3}}$	Fettweis (2008)
ρ_{opal}	density of opal	2200	–	$\mathrm{kg\,m^{-3}}$	
ρ_{calc}	density of $CaCO_3$	2600	2600-2800	$\mathrm{kg\,m^{-3}}$	Fettweis (2008)
ρ_{dust}	density of dust	2600	2300-2800	$\mathrm{kg\,m^{-3}}$	clay, quartz; Fettweis (2008)
R_{opal}	Silicon mol-to-opal-mass factor	60	–	kg SiO_2 (kmol Si)$^{-1}$	
R_{calc}	carbon mol-to-$CaCO_3$-mass factor	100	–	kg $CaCO_3$ (kmol C)$^{-1}$	
R_{det}	P mol-to-detritus-mass factor	3166	–	kg POM (kmol P)$^{-1}$	Takahashi et al. (1985)
$R_{\mathrm{Si:P}}$	silicate to phosphate production ratio	25	–	mol Si (mol P)$^{-1}$	
Re_{crit}	critical particle Reynolds number	20	O(20-30)	–	Alldredge and Gotschalk (1988); Kiørboe et al. (2001)
$T_{\mathrm{ref,x=POC,opal}}$	reference temperature for Q_{10}	10	–	°C	

*: refers to manual tuning of parameter - all other parameters were fixed from beginning

^{a} measured dissolution and remineralization rates include temperature-dependence, which is represented by the Q_{10} factor in M^{4}AGO

For the primary particle sizes, we conceptually assume that the tracer characteristics of opal and $CaCO_3$ are primarily related to phytoplankton mineral structures such as diatom silicate frustules and the coccoliths of coccolithophores. This implies that modeled zooplankton egests biogenic mineral structures of algae while their own larger mineral body structures play, in numbers, a minor role in biogenic mineral fluxes (as described by e. g. Berelson et al., 2007; Ziveri et al., 2007; Fischer and Karakaş, 2009; Fischer et al., 2016). Coccolith diameters range from about 1.5 µm to 15.5 µm (Young and Ziveri, 2000; Henderiks and Pagani, 2008; Henderiks, 2008). The globally ubiquitous coccolithophore *Emiliana Huxleyi* (Read et al., 2013) exhibits coccoliths of about 3 µm to 4 µm in diameter (Young and Ziveri, 2000)~~, and hence, we set $d_{p,\mathrm{calc}} = 3$ µm, which is thus at the lower bound of the observed range while accounting for the volumetric density effect of non-spherical plate-like coccoliths.~~We set $d_{p,\mathrm{calc}} = 3$ µm, which is thus at the lower bound of the observed range, to account for the volumetric density effect of non-spherical plate-like coccoliths. Diatoms frustules feature sizes of a few micrometers to millimeters (Armbrust, 2009) with a dominant size range of about 12 µm to 58 µm (Litchman et al., 2009, equivalent spherical diameter of body volumes 10^3 µm^3-10^5 µm^3). We define the diatom frustule size as $d_{p,\mathrm{frustule}} = 20$ µm. The primary particle size of detritus is weakly constrained and likely ranges from sub-micrometer of microgels and bacteria to millimeter scales of zooplankton body structures (Verdugo et al., 2004). We here chose $d_{p,\mathrm{det}} = 4$ µm. Aeolian dust particles features a typical size ranging from submicron to about 20 µm in size with a mass median diameter of about 1.5 µm to 3 µm (Maher et al., 2010; Mahowald et al., 2014). In summary, we assumed the following order of primary particle sizes for the tracers: $d_{p,\mathrm{dust}} < d_{p,\mathrm{calc}} \leq d_{p,\mathrm{det}} < d_{p,\mathrm{frustule}}$.

The size distribution-limiting maximum aggregate diameter, d_{max}, is variable in the model domain and depends on the critical particle Reynolds number Re_{crit}. Re_{crit} and its potential dependency on aggregate properties is weakly constrained which lets us fix the value globally to $Re_{\mathrm{crit}} = 20$, a conservative value compared to measured maximum particle Reynolds number up to 32 by Alldredge and Gotschalk (1988).

Opal dissolution and detritus remineralization are Q_{10} temperature-dependent in M^{4}AGO. Typically, the Q_{10} factor for biological processes is in the range between 2 and 3. We here chose $Q_{10,\mathrm{POC}} = 2.1$ (similar to Mislan et al., 2014, who applied $Q_{10,\mathrm{POC}} = 2.0$). For opal, we tuned $Q_{10,\mathrm{opal}} = 2.6$ compared to 2.3 suggested by Bidle et al. (2002).

2.4.3 Model tuning and evaluation

~~The close connection between the parametrized processes of sinking and remineralization, the transfer efficiency and the climatological nutrient field hampers the clear distinction between tuning and evaluation data when comparing the model results to literature values for transfer efficiency~~The newly parametrized processes of sinking and remineralization directly affect the transfer efficiency, and thus the climatological nutrient fields. This close connectedness hampers the clear distinction between data employed for model tuning or for model evaluation, when comparing the model results to literature values for transfer efficiency (Weber et al., 2016) and World Ocean Atlas data (Garcia et al., 2014a, b). The transfer efficiency, in combination with the general circulation pattern, affects the nutrient climatology on the long term. In turn, sinking velocity, remineralization and dissolution define the transfer efficiency on time scales of days to months. A direct comparison of modeled to observed sinking velocities and fluxes is challenging, as scale dissimilarities introduce uncertainty for comparisons between models

and observations (Bisson et al., 2018). Furthermore, sediment trap data for POC and mineral fluxes exhibit high uncertainties which complicates model comparisons and even make different parametrizations for vertical fluxes undistinguishable (Cael and Bisson, 2018). As a consequence, we remain with a general evaluation of our model results.

Long simulations with high computational costs to reach steady state are required in the process of model tuning which prevents from intensive parameter variations. ~~Since the adaptation of the sinking velocity versus the remineralization and dissolution rates, and thus the transfer efficiency, was within a few years, parameter variations aiming at a quantitative agreement with the transfer efficiency of Weber et al. (2016) enabled a useful strategy to select for promising parameter sets.~~We performed parameter variations aiming at a quantitative agreement with the transfer efficiency of Weber et al. (2016). Since the adjustment of the sinking velocity versus the remineralization and dissolution rates, and thus the transfer efficiency, occurs within a few years, this strategy was useful to select for promising parameter sets. With respect to the primary particle characteristics, we kept the stickiness values, once chosen to our best knowledge, untouched and minimally varied the primary particle sizes within the range of literature values. We primarily focused on tuning the remineralization and dissolution rates of POC and opal, respectively. We choose this strategy, since reliable remineralization and dissolution rate measurements are available to evaluate the tuned rates (see ranges in Tab. 1). We aimed at keeping global mean values of primary production, export production of POC, opal and $CaCO_3$ as well as their fluxes to sediment within estimated literature ranges. This let us to minimally vary the fraction of maximum $CaCO_3$ production, $c_{\max}$, in M^4AGO compared to the standard run.

We here compare and evaluate the M^4GO run with respect to: i) where possible, the standard run, ii) the regional transfer efficiency as derived by Weber et al. (2016), iii) World Ocean Atlas data from the World Ocean Database (Boyer et al., 2013; Garcia et al., 2014b) and iv) independently to sediment trap-sampled POC and biogenic mineral fluxes compiled by Mouw et al. (2016a, b). The Mouw et al. (2016a, b) data were time- and depth-weighted to receive monthly climatological values for the respective grid boxes in MPIOM, where the sediment trap records were taken. Model results are presented as yearly mean of the last simulated year, unless stated otherwise.

3 Results & Discussion

In the following, we evaluate the global net primary production, the export of POC to the mesopelagic zone and associated pattern of biogenic mineral fluxes (Sect. 3.1). In M^4AGO, the pattern of POC and associated minerals determine the aggregate properties, which we explicate in Sect. 3.2. In Sect. 3.3, we present the global pattern of transfer efficiency. In Sect. 3.4 and 3.5, we examine the contributions of remineralization rates, sinking velocity and aggregate properties to the transfer efficiency pattern. Thereafter, we evaluate the modeled rain ratios (Sect. 3.6) and the biogeochemical tracer distributions (Sect. 3.7). In Sect. 3.8, we discuss the consequence of the transfer efficiency pattern on regional CO_2 fluxes. Subsequently, we examine the sensitivity of the transfer efficiency to selected model parameters (Sect. 3.9), and conclude with a critical review of underlying assumptions of M^4AGO (Sect. 3.10).

3.1 Spatial distribution of POC export fluxes and associated biogenic minerals

The global pattern of the depth-integrated primary production is dominated by global circulation and thus nutrient transport. The global pattern of annual mean integrated primary production therefore remains similar between the standard and the M^{4}AGO run (Fig. 4). Globally integrated, the annual net primary production is $\approx 55.3\,\mathrm{Gt\,C\,yr^{-1}}$ in M^{4}AGO compared to

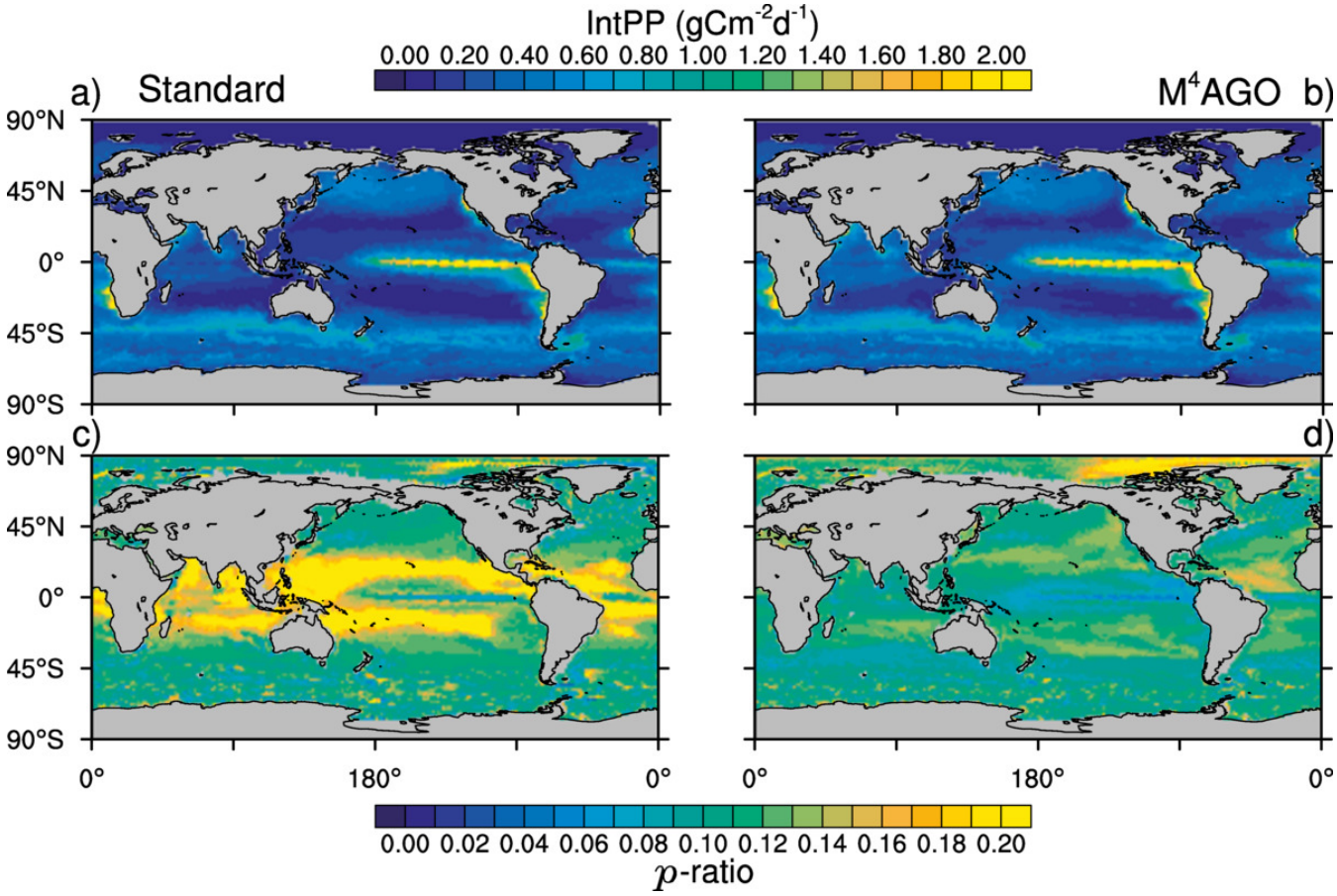

Figure 4. Yearly mean integrated primary production in a) the standard, and b) the M^{4}AGO run. The export efficiency ($p-$ratio) in c) the standard, and d) the M^{4}AGO run.

$\approx 44.7\ \mathrm{Gt\,C\,yr^{-1}}$ in the standard run.

The ratio between carbon export out of the euphotic zone at depth $z_0 = 100\,\mathrm{m}$ and the net primary production, NPP,

$$p-\mathrm{ratio}(z) = \frac{\text{POC flux at depth}\, z = z_0}{\mathrm{NPP}} \tag{32}$$

provides an estimate, of how efficient the export is with respect to the net primary production. Globally, about $5.56\,\mathrm{Gt\,C\,yr^{-1}}$ and $6.28\,\mathrm{Gt\,C\,yr^{-1}}$ are exported out of the euphotic zone in M^{4}AGO and the standard run, respectively. In the standard run, the subtropical gyres exhibit $p-$ratios of more than 0.2 and the high latitudes feature lower export efficiency (Fig. 4 c). ~~In~~

~~the M^{4}AGO run, the equatorial Pacific exhibits the lowest export efficiencies, features maximum values of about 0.14-0.16 in the subtropical gyres and about 0.20 in the Arctic region (Fig. 4 d)~~In the M^{4}AGO run, the equatorial Pacific exhibits the lowest export efficiencies, the subtropical gyres feature maximum values of about 0.14-0.16, and the Arctic region about 0.20 (Fig. 4 d). The M^{4}AGO run thus possesses smaller latitudinal variability of the $p-$ratio compared to the standard run.

In comparison to previous estimates on global primary production, both model runs are well within the range of 30 Gt yr^{-1} to 70 Gt C yr^{-1} and show similar pattern of NPP (Carr et al., 2006). The higher NPP in M^{4}AGO is due to the enhanced remineralization rates in surface waters which also ~~leads~~lead to the lower export efficiencies in the equatorial and subtropical regions. Estimates of the export efficiency from either satellite data, *in situ* observations, or models lead to partly contrasting ~~pattern~~patterns (e. g. Lutz et al., 2002; DeVries and Weber, 2017; Henson et al., 2011, 2012; Buesseler, 1998; Neuer et al., 2002; Siegel et al., 2014; Cram et al., 2018). In contrast to our two model runs, highest $p-$ratios are suggested to be found in the North Pacific and Antarctic Ocean (e. g. Dunne et al., 2005; Henson et al., 2011; DeVries and Weber, 2017). In the tropical and subtropical regions, the M^{4}AGO run reduces the bias with respect to previously found low export efficiencies of about 1 % to 10 % (Buesseler, 1998; Neuer et al., 2002).

The exported POC is accompanied by biogenic minerals and dust. The export flux ratios between opal and detritus exhibit a clear latitudinal pattern, with high values in the high latitudes and upwelling regions compared to the subtropical gyres (Fig. 5 a, b). ~~Both model simulations show similar pattern of opal to detritus ratio fluxes~~Both model simulations show a similar pattern of opal to detritus flux ratios. Higher $CaCO_3$ to detritus flux ratios are confined to equatorial and subtropical regions where silicate depletion favours calcification (Fig. 5 c, d). M^{4}AGO exhibits a higher $CaCO_3$ to detritus mass flux ratio in the western tropical and subtropical Pacific than the standard run. The higher remineralization in the surface waters in this region reduces the amount of detritus that can coalesce with $CaCO_3$. The spatial distribution of sinking tracers and their ratios prime the marine aggregate properties in M^{4}AGO.

3.2 Spatial distribution of marine aggregate properties

The spatial patterns of detritus and mineral fluxes are reflected in the distribution of aggregate properties (cmp. pattern in Fig. 5 b, d to 6 a-f). The primed characteristics further evolve while aggregates descend through the water column and become remineralized. Hence, the information of the tracer distribution in the euphotic zone propagates into the mesopelagic zone. The mean primary particle density, $\langle\rho_p\rangle$, ranges at export depth (100 m) from about 1100 kg m^{-3} in diatom-dominated regions to 1850 kg m^{-3} in the western Pacific where $CaCO_3$ to detritus export ratios are high (Fig. 5 b, d and 6 a). In the Arctic, some regions harbour $\langle\rho_p\rangle$ of max. 2600 kg m^{-3} where aggregates in our model are dominated by dust particles (Fig. 6 a). Particularly in regions of high $CaCO_3$ to detritus export ratios $\langle\rho_p\rangle$ increases with depth (Fig. 6 a,g and 7 ~~a,d~~a). Accordingly, the volume-weighted mean excess aggregate density, $\Delta\langle\rho_f\rangle_V$, exhibits the same pattern as $\langle\rho_p\rangle$, while it ranges from about 2 kg m^{-3} in diatom- to 35 kg m^{-3} in calcifier-dominated regions (Fig. 6 d). Note that we chose $\Delta\langle\rho_f\rangle_V$ to account for the increasing porosity with size, Eq. (6), and thus decreasing aggregate excess density with size, Eq. (5). As a mean value, $\Delta\langle\rho_f\rangle_V$ thus underestimates excess density for small aggregates while it overestimates excess density for large aggregates. Generally both, $\langle\rho_p\rangle$ and $\Delta\langle\rho_f\rangle_V$, tend to increase with depth (Fig. 7a,d). In the Pacific, $CaCO_3$ as ballasting mineral becomes dissolved

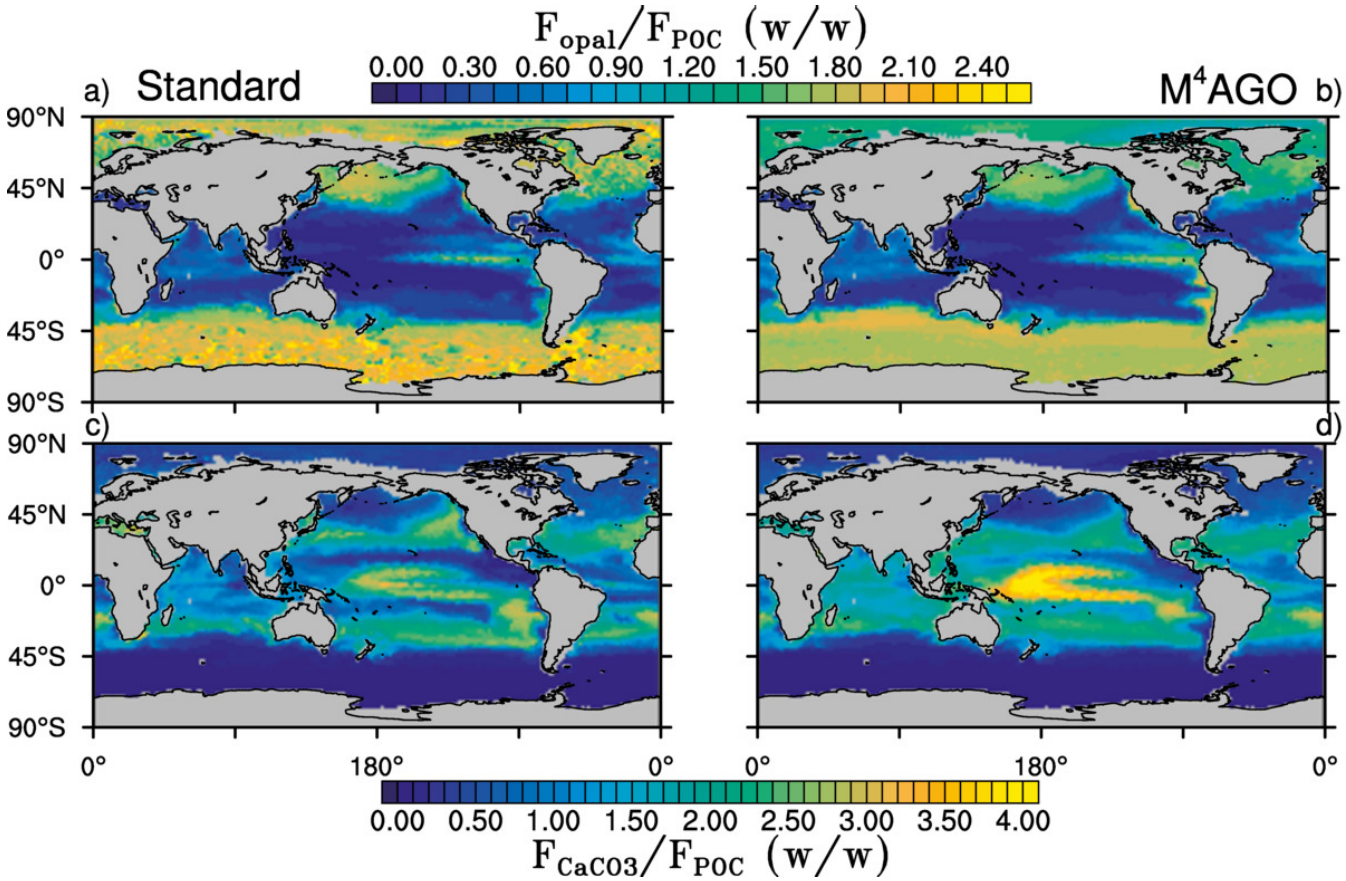

Figure 5. Yearly mean flux ratios of opal (SiO_2) to POC in a) the standard, and b) the M^4AGO run. Yearly mean flux ratios of $CaCO_3$ to POC in c) the standard, and d) the M^4AGO run.

below the lysocline and modeled $\langle \rho_p \rangle$ decreases again in the deep ocean (Fig. 7 a,d). The mean primary particle size, $\langle d_p \rangle$, ranges between the attributed minimum and maximum primary particle size of tracers, 2 µm to 20 µm, respectively. Mean primary particle size shows an opposing pattern to $\langle \rho_p \rangle$ (Fig. 6 a,b,g,h and 7 a,b), since regions are either dominated by small, dense coccoliths or large, less dense diatom frustules. The global pattern of $\langle d_p \rangle$, primed through export fluxes of detritus and minerals, varies only a little throughout the water column (Fig. 7 b) since we assumed invariance of primary particle size to remineralization, dissolution and other processes.

Our simulated $d_{\max}$ are largest in the surface waters of the Southern Ocean and upwelling regions, where TEP-rich aggregates prevail. In calcifier-dominated regions, the maximum aggregate size is small. Generally, $d_{\max}$ tends to decrease with depth (Fig. 7 e).

The microstructure of marine aggregates, modeled as fractal dimension, d_f, shows a pronounced spatial distribution. At 100 m depth, d_f ranges from about 1.7 in upwelling regions and the Southern Ocean to about 2.2 in the western equatorial

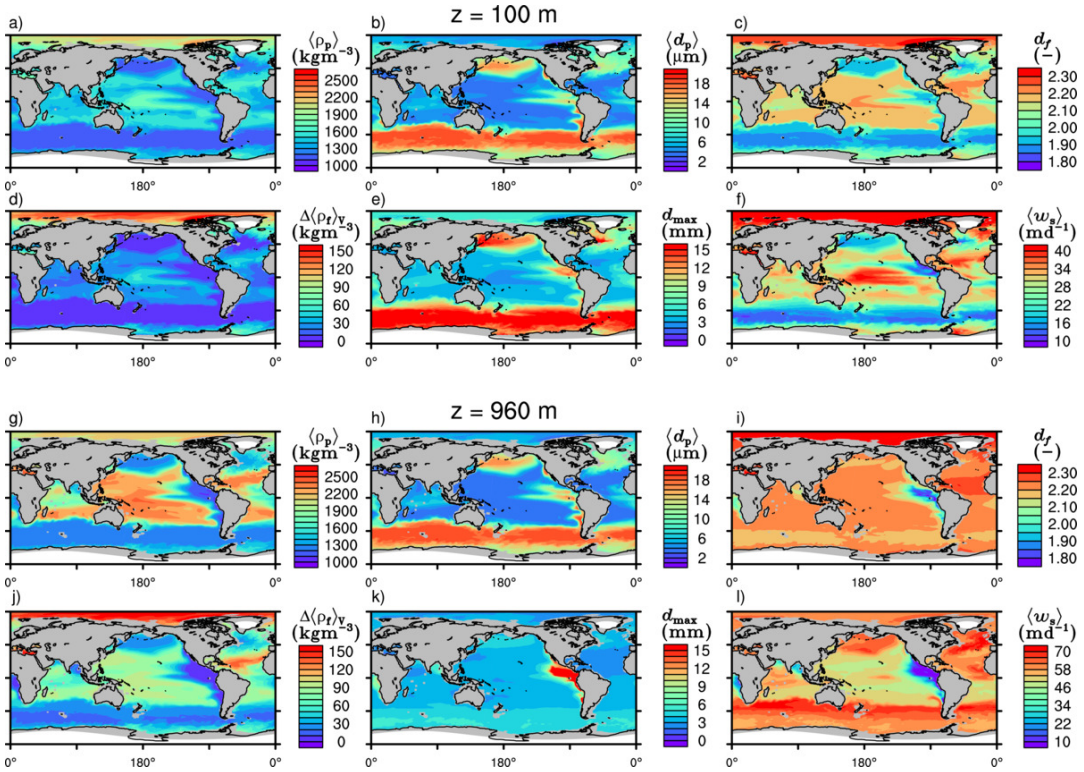

Figure 6. Modeled marine aggregate properties at a)-f) 100 m and g)-l) 960 m depth. Mathematical symbols are: $\langle \rho_\mathrm{p} \rangle$: mean primary particle density, $\langle d_\mathrm{p} \rangle$: mean primary particle diameter; d_f: microstructure (fractal dimension); $\Delta\langle \rho_\mathrm{f} \rangle_\mathrm{V}$: volume-weighted mean excess aggregate density; d_max: maximum aggregate diameter; $\langle w_\mathrm{s} \rangle$: concentration-weighted mean sinking velocity of aggregates. Note that $\langle w_s \rangle$ comprises the full range of many micrometer-sized to rare, large aggregates with low ($O(1\,\mathrm{m\,d^{-1}})$) and high ($O(>100\,\mathrm{m\,d^{-1}})$) sinking velocities, respectively. For the mean stickiness, $\langle \alpha \rangle$, volume-weighted mean porosity, $\langle \phi \rangle_\mathrm{V}$, and the number distribution slope, b, see Fig. A1.

Pacific and features maximum values of 2.38 in Arctic regions (Fig. 6 c). With increasing depth in the mesopelagic zone, aggregates tend to experience a rapid compaction as d_f increases (Fig. 7 c). Ongoing POM remineralization during aggregates descend shifts the aggregate composition towards mineral components which feature lower stickiness in our model. Thus the fractal dimension increases which mimics compaction of aggregates. The global pattern tends to homogenize with depth at about 1000 m, where modeled aggregates feature d_f of about 2.2 (Fig. 6 i). An exception are upwelling regions, where d_f remains low since detritus is slowly remineralized anaerobically in the associated oxygen minimum zones (OMZs). Below 1000 m, d_f only increases slowly with depth (Fig. 7 c).

~~Particle properties and molecular dynamic viscosity determine the concentration-weighted mean sinking velocity of aggregates, $\langle w_s \rangle$ (Fig. 6 f,l), for particle sizes ranging from few micrometers to millimeters.~~Particle properties and molecular dynamic viscosity determine the concentration-weighted mean sinking velocity of aggregates, $\langle w_s \rangle$ (Fig. 6 f,l). For $\langle w_s \rangle$, M^{4}AGO considers particle sizes ranging from few micrometers to millimeters and thus the full size spectrum, where sinking velocities of

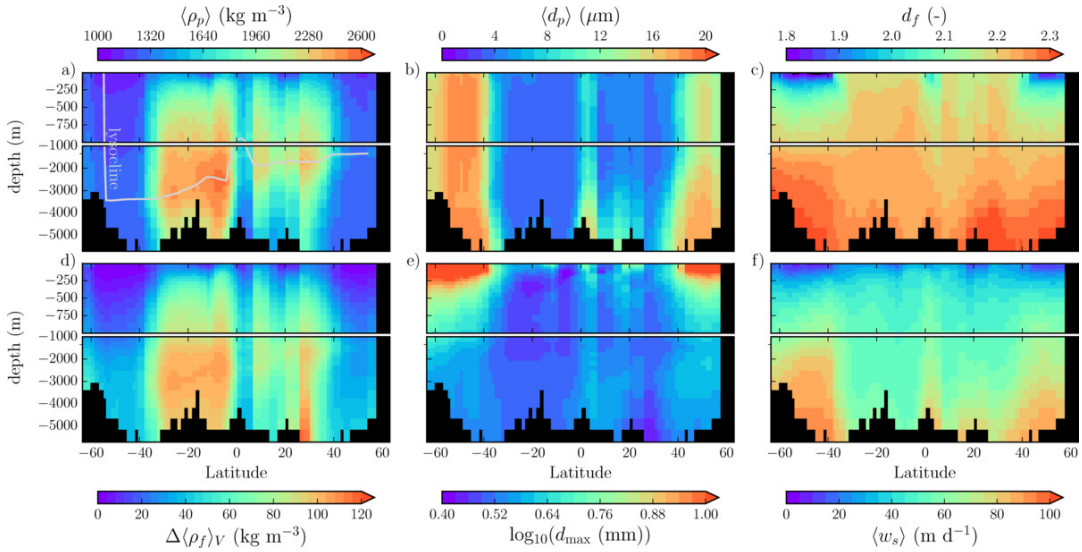

Figure 7. Modeled marine aggregate properties on the Pacific WOA transect P16, which is located at about 150 °W. For symbol descriptions, see caption of Fig. 6.

$O(1\,\mathrm{m\,d^{-1}})$ to $O(>100\,\mathrm{m\,d^{-1}})$ are represented. $\langle w_s \rangle$ thus can significantly differ from reported sinking velocities for large individual aggregates. At the export depth, $\langle w_s \rangle$ ranges from about $10\,\mathrm{m\,d^{-1}}$ in the Southern Ocean and North Pacific region to about $35\,\mathrm{m\,d^{-1}}$ in the western equatorial Pacific and reaches maximum values of $\sim$48 $\mathrm{m\,d^{-1}}$ in dust-dominated Arctic regions (Fig. 6 f,l). Upwelling-influenced surface waters tend to show smaller $\langle w_s \rangle$ than the western equatorial Pacific. Generally, $\langle w_s \rangle$ appears to increase rapidly with depth within the mesopelagic zone (Fig. 7 f). At about 1000 m, the latitudinal pattern changes and the high latitudes, in the Southern Ocean at around 45 °S, exhibit the highest $\langle w_s \rangle$ of about $65\,\mathrm{m\,d^{-1}}$. Along the equator, outside the OMZs, $\langle w_s \rangle$ exhibits similarly high values of about $55\,\mathrm{m\,d^{-1}}$ (Fig. 7 f). Inside the OMZs, where remineralization is slower than in oxygenated waters, the detritus residence time is longer and leads to lower $\langle w_s \rangle$ (Fig. 6l). The subtropical regions, dominated by calcifiers, show a rather homogeneous mean sinking velocity ($\langle w_s \rangle \approx 50\,\mathrm{m\,d^{-1}}$) throughout the water column apart from the first few hundred meters and near bottom regions. ~~In turn~~By contrast, diatom-dominated waters feature a significantly increasing $\langle w_s \rangle$ with depth which reaches values of up to approximately $80\,\mathrm{m\,d^{-1}}$ (Fig. 7 f). Diatom-dominated aggregates in surface waters feature a high buoyancy through TEPs and a loose structure which diminishes with continuous remineralization during ~~aggregates~~their descent.

The aggregate properties entering the M^{4}AGO scheme are all directly or indirectly measurable. The comparison of simulated and measured aggregate properties is, however, difficult as M^{4}AGO depicts mean values of aggregate populations that *in situ* encompass heterogeneous composition among size spectra. In addition, measurements are often limited to particular aggregate characteristics while others remain unconstrained within the same data set. We therefore compare M^{4}AGO to field and laboratory measurements which examine subsets of the simulated aggregate characteristics.

The modeled aggregate excess densities in diatom-dominated regions compare well to former field and laboratory measurements, where marine aggregates showed excess densities of about 0 to $\sim 10\,\mathrm{kg\,m^{-3}}$ ~~(Alldredge and Gotschalk, 1988; Ploug et al., 2008; Iversen and Ploug, 2013).~~ (Alldredge and Gotschalk, 1988; Ploug et al., 2008; Iversen and Ploug, 2013; Laurenceau-Cornec et al., 2019). In calcifier-dominated regions, aggregate excess densities are about $\sim 35\,\mathrm{kg\,m^{-3}}$, which is in the upper range of measured values of $2.1\,\mathrm{kg\,m^{-3}}$ to $41\,\mathrm{kg\,m^{-3}}$ (Engel et al., 2009). The increased excess density of $CaCO_3$-dominated aggregates in about 1000 m depth compares with about $100\,\mathrm{kg\,m^{-3}}$ to $150\,\mathrm{kg\,m^{-3}}$ well with observed fecal pellets egested by coccolith-consuming zooplankton (White et al., 2018). These fecal pellets also show similar mean sinking velocities as our modeled $\langle w_s \rangle \approx 50\,\mathrm{m\,d^{-1}}$. The change of the excess density is linked to the increasing d_f of aggregates with depth that is in qualitative agreement with present conceptual understanding (Mari et al., 2017). The increasing d_f depicts the expected continuous repacking of aggregates and the zooplankton-mediated compaction in fecal pellets. The latter particularly takes place in the upper few hundred meters of the ocean and is a major pathway of coccolith transport (De La Rocha and Passow, 2007; Honjo, 1976).

The general difference in typical size between diatom-rich aggregates and $CaCO_3$ shell-enriched aggregates compares well to observations that also showed smaller $CaCO_3$-dominated aggregates (Biermann and Engel, 2010). The decreasing $d_{\max}$ with depth is in qualitative agreement with observed vertically decreasing aggregate mean diameters (De La Rocha and Passow, 2007). Decreasing maximum aggregate sizes with depth and reduced organic matter content also agree qualitatively well with experiments of Hamm (2002) and Passow and De La Rocha (2006). Both studies showed a significant decrease in aggregate size with increasing mineral components. In their experimental setups, it remains elusive, if a certain threshold of carrying capacity of POM was reached (Passow and De La Rocha, 2006) or if the balance between adhesive forces within the aggregates and the sinking-induced shear forces (Adler, 1979; Brakalov, 1987) was shifted towards smaller aggregates. It is likely~~,~~ that both effects act at the same time since natural polymers possess stronger adhesive surface properties than biogenic minerals (Eisma, 1986). In M^4AGO, only the compaction towards higher fractal dimension through lower internal binding forces, expressed as stickiness of the primary particles, is represented. ~~While compaction likely enhances the internal number of binding links in aggregates, we neglect this effect versus the lower primary particle binding forces on the overall susceptibility to shear stress and thus kept Re_{crit} globally constant.~~Compaction can coincide with an increasing number of binding links in aggregates, which can lower the overall susceptibility of aggregates to shear stress. In M^4AGO, we disregard this effect and keep Re_{crit} globally constant.

In summary, the resulting mean sinking velocity in M^4AGO is of same order of magnitude as found in observations (Alldredge and Gotschalk, 1988; White et al., 2018; Villa-Alfagame et al., 2016). We note, however, that mean sinking velocities estimated from observations potentially overestimate $\langle w_s \rangle$ as they i) are methodologically constrained to particles larger than a lower detection limit, which is typically much larger than primary particle size, and ii) depend on often uncertain size to mass relationships. We emphasize further that our modeled $\langle w_s \rangle$ embraces numerous slowly sinking aggregates of primary particle size ($w_s \approx O(1\,\mathrm{m\,d^{-1}})$) as well as rare, but large, fast sinking aggregates ($w_s \approx O(1000\,\mathrm{m\,d^{-1}})$). This range hence encompasses observations for single cells and coccoliths up to large marine snow aggregates and fecal pellets (Miklasz and Denny, 2010; Alldredge and Gotschalk, 1988; Biermann and Engel, 2010). Generally, the spatio-temporal variability of $\langle w_s \rangle$

in M^{4}AGO differs significantly from the simple underlying assumption of a linearly increasing sinking velocity with depth in the standard run. M^{4}AGO resembles the strongly increasing sinking velocity found in the mesopelagic zone in observations (e. g. Villa-Alfagame et al., 2016) and a modeling approach (DeVries et al., 2014).

3.3 Global pattern of transfer efficiency

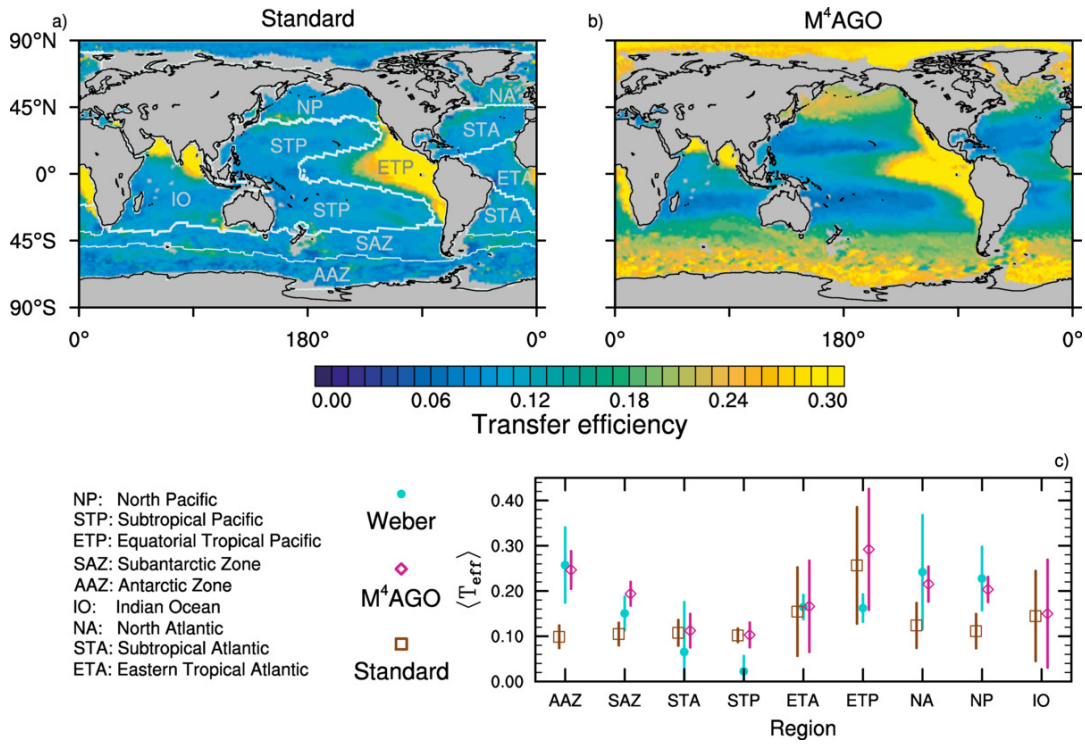

Figure 8. Annual mean transfer efficiency for POC in a) Standard and b) M^{4}AGO from export depth (100 m) to about 1000 m (960 m). In c) the mean transfer efficiency in regions, as defined in a), are compared to the reconstructed transfer efficiency by Weber et al. (2016). Error bars for Weber et al. represent uncertainty for the reconstruction of the regional transfer efficiency. For the model results, error bars indicate the spatial standard deviation. For the resulting effective β' in M^{4}AGO, see Fig. B1. For a seasonal evolution of the transfer efficiency in M^{4}AGO, see Fig. C1.

The transfer efficiency of POC from ~~100 m~~ $z_0 = 100\,\mathrm{m}$ to depth z in the ocean

$$T_{\mathrm{eff,POC},z} = \frac{\text{POC flux at depth } z}{\text{POC flux at depth } 100\,\mathrm{m}} \quad \text{for}: z > z_0 \tag{33}$$

provides an estimate on the fraction of exported POC that reaches a particular depth and is determined by sinking velocity and remineralization. In the Martin curve, Eq. (1), the slope constant, β, prescribes the transfer efficiency

$$T_{\mathrm{eff,POC},z}(\mathrm{Martin}) = \left(\frac{z}{z_0}\right)^{-\beta} \tag{34}$$

to a particular depth and leads to an almost homogeneous global transfer efficiency of $T_{\mathrm{eff,POC},z}(\mathrm{Martin}) \approx 0.12$ to about 1000 m depth in our standard run (Fig. 8a). The lower remineralization rates in sub- or even anoxic OMZs compared to oxygenated regions lead to higher transfer efficiencies, visible in the equatorial eastern Pacific Ocean, upwelling regions off Peru and Africa as well as the northern Indian Ocean. Apart from these regions, the standard run features only little variability as expected from the relationship between the Martin curve slope parameter and the transfer efficiency. The remaining variability is related to ocean currents and spatially variable turbulent mixing. By contrast, the transfer efficiency in M^{4}AGO exhibits a distinct global pattern and possesses higher efficiency in high latitude and upwelling regions compared to the subtropical gyres where low $T_{\mathrm{eff,POC},z}$ appear. Similar to the standard run, the OMZ regions feature high transfer efficiencies in M^{4}AGO. Since local Martin curves provide meaningful information on the attenuation of POC fluxes with depth, we analyzed the effective slope parameter, β' for both, the standard and the M^{4}AGO run. We fitted the Martin curve, Eq. (1), to modeled POC fluxes below z_0 to estimate β'. As expected, the standard run shows little spatial variability apart from the OMZs and features a global, area-weighted mean slope of $\langle\beta'\rangle_{\mathrm{A,Martin}} \approx 0.82$. In agreement with the transfer efficiency pattern, M^{4}AGO possesses a strong latitudinal pattern of the effective slope β' that varies between $\beta' \approx 0.59 - 0.67$ in high latitudes (Antarctic Zone, AAZ; North Pacific, NP; Subantarctic Zone, SAZ), ≈ 0.30 to 0.60 in OMZ regions and max. $\beta' \approx 1.31$ in the subtropical Pacific gyres (Fig. B1).

Recently, Weber et al. (2016) reconstructed the global transfer efficiency pattern by diagnosing particulate organic phosphate fluxes. Reconstructing the transfer efficiency via inverse modeling from phosphate concentrations circumnavigates the obstacle of sparse direct observations of fluxes and allows for a more reliable constrain on POC transfer efficiency (Usbeck et al., 2003; Weber et al., 2016). The comparison of the standard and M^{4}AGO run reveal the inherent inability of the Martin approach to capture the latitudinal variability (Fig. 8 a-c). M^{4}AGO agrees qualitatively and quantitatively well with the reconstructed transfer efficiency pattern of Weber et al. (2016). The overestimation of the transfer efficiency in the equatorial tropical Pacific (ETP) by both, the standard and M^{4}AGO run, is due to the models overestimation of OMZs extensions (Bopp et al., 2013). The large OMZ causes diminished remineralization and, hence, reduced attenuation of POC fluxes. In general, however, the increased transfer efficiency associated to OMZs is in agreement with observations that suggest lower flux attenuation, and hence, small β (Roullier et al., 2014; Löscher et al., 2016; Le Moigne et al., 2017). Lower remineralization in OMZs keeps the POC to ballasting minerals ratio higher as compared to oxygenated waters. Thus, the lower remineralization rates are potentially accompanied by lower sinking velocities which provides a positive feedback loop on the OMZ evolution. The larger the vertical ~~extend~~extent of the OMZ becomes, the longer the retention time becomes through higher POM aggregate content and lower sinking velocities. Eventually, OMZ evolution is balanced by oxygen supply through mixing and transport processes. The global pattern of β' in M^{4}AGO agrees well with the geographical range and pattern found by Buesseler and Boyd (2009) and suggested by Marsay et al. (2015). However, M^{4}AGO shows lower maximum values of $\beta' \approx 1.31$ compared to $\beta' \approx 1.9$ suggested by Marsay et al. (2015). Globally averaged, M^{4}AGO exhibits an effective slope parameter of $\langle\beta'\rangle_{\mathrm{A,M^4AGO}} \approx 0.75$ which is lower than the slope of $\beta' = 0.86$ originally published by Martin et al. (1987) based on local observations. Noticeably, however, the trend of smaller to larger β' values from near- to offshore Pacific US coast is in agreement with the elusive trend

found by Martin et al. (1987). Overall, M^{4}AGO clearly improves the representation of the POC transfer efficiency pattern compared to the standard Martin approach.

3.4 Contributions of $\langle w_s \rangle$ and temperature-dependent remineralization to the transfer efficiency pattern

The attenuation of POC fluxes is primarily regulated by sinking velocity and total remineralization rate of POC. Depth-dependent, sheared lateral transport and vertical water motion can additionally affect the vertical distribution of particulate matter and thus vertical fluxes. We neglect these processes in the following, since i) the timescale of sinking from one layer to the next layer below is typically shorter than the lateral transport at grid resolutions used in our model runs, and ii) sinking velocity is faster than typical vertical motions represented by models with this grid resolution. The remineralization length scale (RLS), z^*_{POC} is given by the local ratio of $\langle w_s \rangle$ to remineralization ($R_{\mathrm{POC,remin}}$),

$$z^*_{\mathrm{POC}} = \frac{\langle w_s \rangle}{R_{\mathrm{POC,remin}}} \tag{35}$$

and defines the vertical distance, in which POC would decay to ~~half~~$1/e$ ($\approx 37\%$) of its initial value, the POC e-folding depth (Cram et al., 2018). RLS can be locally calculated and enables i) to explore the local effects of remineralization and sinking velocity on the attenuation of POC fluxes and ii) to better understand the depth-integrated information provided by the transfer efficiency or Martins effective slope parameter, β'.

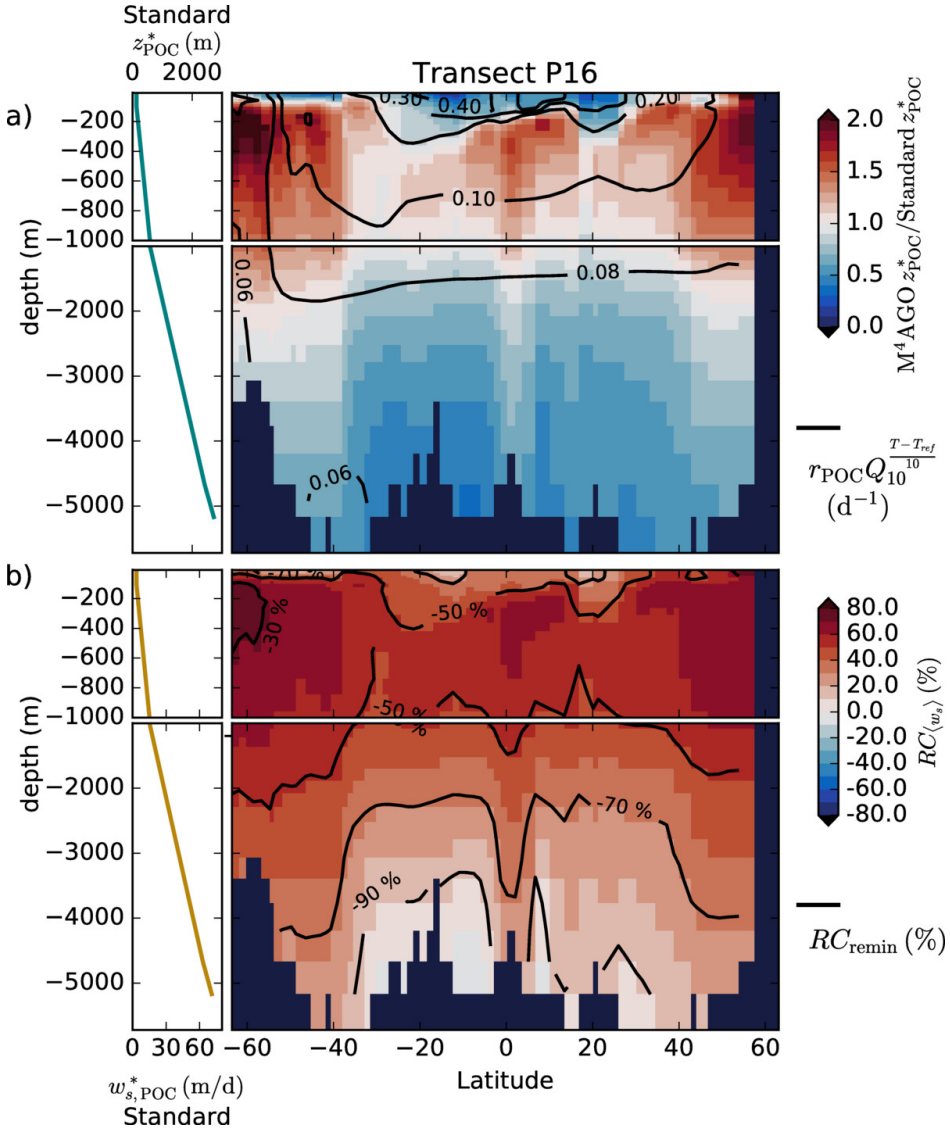

Figure 9. a) Remineralization length scale ratio of M^{4}AGO to the standard model version at the World Ocean Atlas transect P16. We here focus on showcasing the temperature effect on remineralization and calculated ~~z^*_{POC}~~the remineralization length scales, z^*_{POC}, without oxygen limitation of remineralization which cancels out for equal O_2 concentrations. Values smaller than one imply stronger POC flux attenuation in M^{4}AGO than in the standard run. For reference, the RLS in the standard run is given at top left. The standard RLS is increasing due to increasing ~~sinking velocity~~sinking velocity, $w^*_{s,\mathrm{POC}}$, with depth (shown bottom left). Contour lines provide the ~~temperature-dependent remineralization rates~~Q_{10} factor temperature-dependent remineralization rates with r_{POC} at reference temperature T_{ref} in M^{4}AGO. In the standard run, the aerobic rate is globally constant (0.026 d^{-1}). b) ~~Relative contributions of sinking and remineralization~~Relative contributions of sinking, $RC_{\langle w_s \rangle}$, and remineralization, RC_{remin}, to difference between standard and M^{4}AGO run. Contour lines provide the relative contribution of remineralization.

The RLS in surface waters and the upper mesopelagic zone of subtropical and equatorial regions are by more than a factor of two shorter in the M^{4}AGO run than in the standard run (Fig. 9 a). This higher turnover causes the lower p-ratio in M^{4}AGO compared to the standard run in these regions (Fig 4 b). ~~In the mesopelagic zone, the RLSs in M^{4}AGO is similar or pronounced longer and decreases~~In the mesopelagic zone, the RLSs in M^{4}AGO are similar or pronounced longer and decrease again in deeper regions compared to the standard run (Fig. 9 a). ~~The longer RLS~~The longer RLSs in the mesopelagic zone of the high latitude ocean are the reason for the higher transfer efficiency of M^{4}AGO compared to the standard run. In order to analyze which of the two processes, sinking or remineralization, is of primary importance for the change in the RLS and thus the transfer efficiency, we define their relative contributions to the difference between M^{4}AGO and the standard run as

$$RC_{\mathrm{P}_i,\mathbf{x}}[\%] = \frac{\partial_{P_i} z^*_{\mathrm{POC}} \cdot \Delta P_{i,\mathbf{x}}}{\sum_i |\partial_{P_i} z^*_{\mathrm{POC}} \cdot \Delta P_{i,\mathbf{x}}|} \cdot 100 \tag{36}$$

where the processes, $P_i = \{\langle w_s \rangle, R_{\mathrm{POC,remin}}\}$, refer to Eq. (35), ∂_{P_i} is the partial derivative of z^*_{POC} with respect to the process P_i (applying the standard run rates), and $\Delta P_{i,\mathbf{x}}$ is the difference between the value in the M^{4}AGO run and the standard run at spatial point $\mathbf{x}$. M^{4}AGO possesses generally higher remineralization rates than the standard run which would increase the flux attenuation compared to the standard run. The temperature-dependent remineralization in M^{4}AGO shows lower rates in the cold waters of the high latitudes than in the equatorial and subtropical regions (Fig. 9 a). Within M^{4}AGO, this pattern enhances the RLSs, and thus transfer efficiency, in the high latitudes compared to the equatorial regions, which is in agreement with Marsay et al. (2015); Cram et al. (2018). Compared to the standard run, higher $\langle w_s \rangle$ overcompensates the effect of intensified remineralization below the thermocline and leads to longer RLS (Fig. 9 b) in the mesopelagic zone, which is particularly true in diatom-dominated regions. In $CaCO_3$-dominated subtropical gyres, $\langle w_s \rangle$ falls below the sinking velocity of the standard model in regions deeper than 3000 m and thus contributes further to the stronger flux attenuation compared to the standard run. The higher $\langle w_s \rangle$ in M^{4}AGO turns out to dominate over remineralization and increases the RLS, and hence the transfer efficiency, in the mesopelagic zone of the high latitudes. In summary, the temperature-dependence of remineralization in M^{4}AGO induces a latitudinal pattern of longer RLSs, and thus higher transfer efficiency, in high latitudes that is further amplified by high sinking velocities of diatom-dominated aggregates in the mesopelagic zone.

3.5 Impact of mineral size and ballasting effect on sinking velocity

The analysis of RLS changes compared to the standard run emphasizes the role of sinking velocity for longer RLS in the mesopelagic zone in high latitudes and thus for the enhanced transfer efficiency. We therefore aim at a better understanding of the underlying factors that control the mean sinking velocity. We suggest in the following that the size of primary particles might be as important as density of the ballasting material for defining the sinking velocity of aggregates.

M^{4}AGO allows for assessing the contributions of aggregate properties and molecular viscosity on $\langle w_s \rangle$. We define the relative contributions of the modelled particle properties and the molecular viscosity that control $\langle w_s \rangle$ at particular depth z based on a first order approach

$$R_{X_i,z}[\%] = \frac{\partial_{X_i} \langle w_s(\bar{X}_{i,z}) \rangle \cdot \Delta X_{i,z}}{\sum_i \left|\partial_{X_i} \langle w_s(\bar{X}_{i,z}) \rangle \cdot \Delta X_{i,z}\right|} \cdot 100 \tag{37}$$

where $X_i = \{\langle\rho_p\rangle, \langle d_p\rangle, \mu, d_{\max}, b, d_f\}$, $\Delta X_{i,z} = X_{i,z} - \bar{X}_{i,z}$, and $\sum R_{X_i,z} \neq 100$, but $\sum |R_{X_i,z}| = 100$, and $\bar{X}_{i,z}$ ~~as~~is the global mean of the contributing property at depth z. ~~The relative contributions provide an information on the main driving factors, expressed as percentage, for the local $\langle w_s\rangle$ as compared to global average aggregates.~~The relative contributions provide information about the main driving factors for the local $\langle w_s\rangle$ as compared to $\langle w_s\rangle$ of global average aggregates. For example, what is the percentage-wise contribution of denser primary particles than global average to the local sinking velocity. By neglecting the higher order terms, we provide only qualitative insights into the role of the different aggregate properties and molecular viscosity on $\langle w_s\rangle$.

$CaCO_3$ acts as a strong positive, $\langle w_s\rangle$-increasing factor for sinking velocities in the equatorial and subtropical regions due to its high primary particle density (Fig. 10 a). As an exogenous factor, the low molecular viscosity in warm regions contributes positively to sinking velocity (Fig. 10 d). Additionally, in our model, d_f increases particle excess density and thus $\langle w_s\rangle$ in $CaCO_3$-rich areas (Fig. 10 c). In the Southern ocean, North Pacific, North Atlantic, and upwelling regions, particularly the large $\langle d_p\rangle$ in diatom-dominated regions enhances $\langle w_s\rangle$ (Fig. 10 b). According to our model, $d_{\max}$ of aggregates and the number distribution slope, b, contribute positively to $\langle w_s\rangle$ in the high latitudes, except for the Arctic ocean, where mineral material strongly affects the aggregate properties. The pattern of highly variable endogenous and exogenous controls on $\langle w_s\rangle$ emerges particularly in the upper ocean, while in deeper regions of about 1000 m depth, the aggregate properties become more and more homogeneous, except for $\langle d_p\rangle$ and $\langle \rho_p\rangle$ and in OMZs (Fig. 10, lower two panels). With homogenization of most aggregate properties with depth, the contrasting relative contributions of dense mean primary particles and large mean primary particles to $\langle w_s\rangle$ become even more pronounced. Denser, small $CaCO_3$ particles contribute to $\langle w_s\rangle$ in the subtropical, oligotrophic regions of the oceans, while comparably less dense, but larger opal frustules lead to high $\langle w_s\rangle$ in nutrient-rich upwelling and high latitude regions. Even though our formulation for $\langle w_s\rangle$ is highly non-linear, we expect the qualitative pattern of the relative contributions to $\langle w_s\rangle$, particularly through $\langle d_p\rangle$ and $\langle \rho_p\rangle$, to be coherent. In sum, we therefore emphasize the potential role of primary particle size, in particular that of diatom frustules, for determining $\langle w_s\rangle$, and thus POC fluxes.

The effects of microstructure on *in situ* $\langle w_s\rangle$ are not well studied and d_f of aggregates is weakly constrained. It therefore warrants further investigation, especially if a spatially variable d_f effect occurs on *in situ* $\langle w_s\rangle$ in the upper ocean. Vertically varying d_f has been suggested (Mari et al., 2017) and ~~given the microstructure general importance~~given the general importance of the microstructure for sinking velocity, a deeper understanding of the factors and processes influencing d_f is hence highly desirable.

Microstructure d_f directly prescribes the aggregate number distribution slope, b, in M^4AGO (see Fig. A1 c, f for a map of b). Observations show a higher variability of $b \approx 2$ to 5 (Guidi et al., 2009) than in M^4AGO, where b varies between $\approx 3.19 - 3.76$ and thus ~~likely underestimates the spatial variability of the relative contribution to $\langle w_s\rangle$~~likely underestimates the spatial variability and relative contribution of b to $\langle w_s\rangle$. At present, M^4AGO is limited to the steady state size distribution that represents the characteristic processes of aggregation and fragmentation in the system. An explicit modeling of the dynamics of the aggregate size spectrum would be required to cover the variability of measured b which would further enhance the variability of $\langle w_s\rangle$. We briefly discuss this current model limitation in Sec. 3.10.

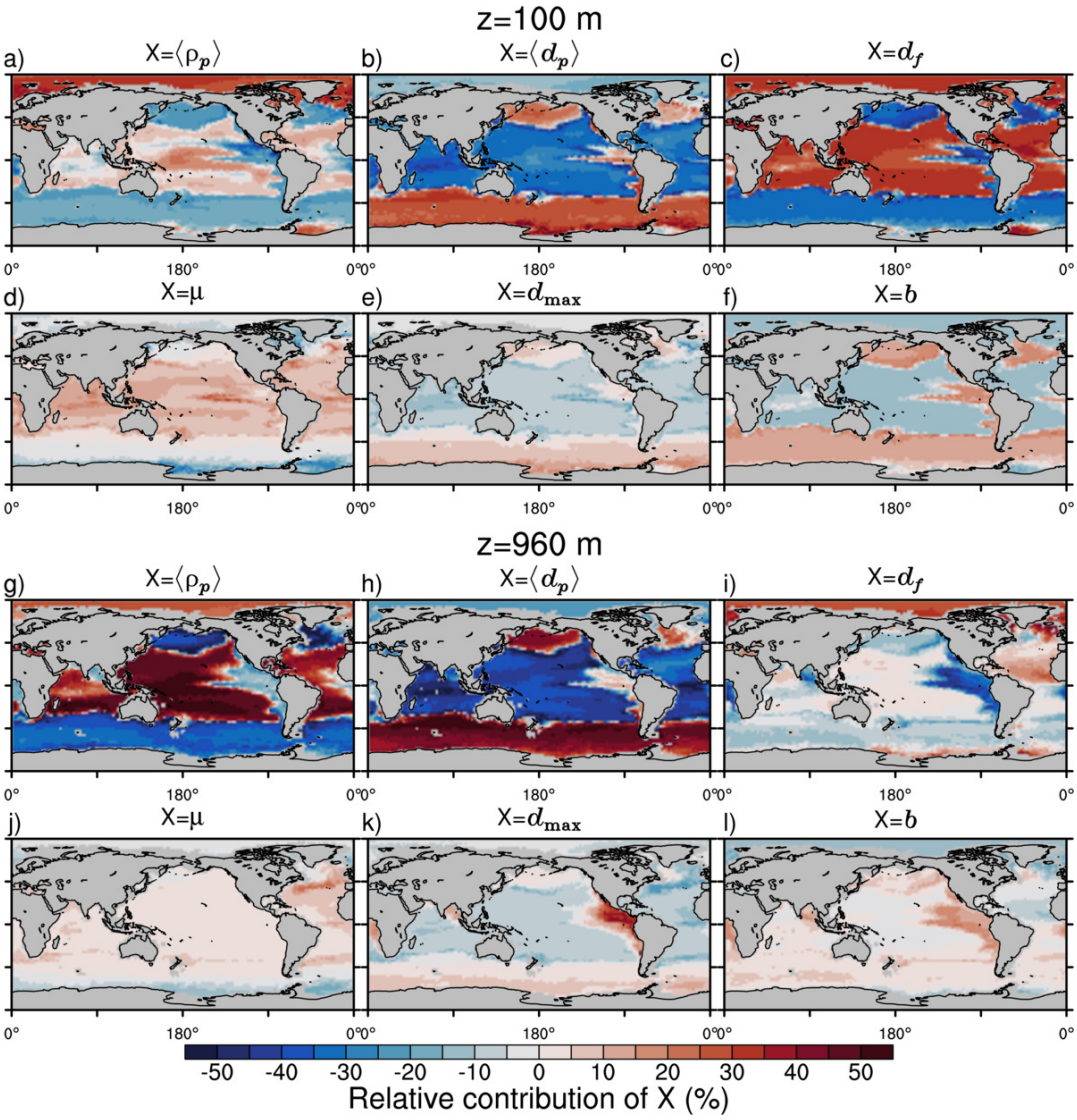

Figure 10. Qualitative first order relative contributions of marine aggregate properties to the change of local mean sinking velocity compared to a global mean aggregate spectrum at depth z. a)-f): 100 m, g)-l) 960 m. Mathematical symbols are: $\langle \rho_p \rangle$: mean primary particle density; $\langle d_p \rangle$: mean primary particle diameter; d_f: fractal dimension; μ: dynamic molecular viscosity; $d_{\max}$: maximum aggregate diameter; b: aggregate number distribution slope.

Previous studies support our finding that $CaCO_3$ act as a strong ballasting agent (e. g. Francois et al., 2002; Balch et al., 2010; Cram et al., 2018). By contrast, opal density of the hollow silicate structures have less effect on $\langle \rho_p \rangle$ (see Fig. 7 a). Instead, silicate frustule size of diatoms significantly affects $\langle w_s \rangle$ (see Fig. 10 b, h and 7 b). This contrasts the assumption of opal acting solely as ballasting material (Cram et al., 2018) and is congruent with Francois et al. (2002) who noticed that factors

other than particle density likely play a role. As indicated by Eq. (5) and (6), primary particle size affects the excess density and porosity of aggregates, which have decisive effects on sinking velocity (Laurenceau-Cornec et al., 2019). Deciphering the size effect of primary particles on *in situ* $\langle w_s \rangle$ and fluxes might be particularly challenging in regions with a diverse size structure of phytoplankton community. Oligotrophic regions typically harbor a narrower size distribution of phytoplankton (see e. g. size ranges and standing stocks in Kostadinov et al., 2016), which may produce more homogeneous aggregates and thus more predictable POC fluxes as found by Guidi et al. (2016) who correlated POC fluxes to the oligotrophic phytoplankton community. In addition, interannual variability of the dominant size of primary producers have been suggested to drive the interannual change in export fluxes (Boyd and Newton, 1995). In contrast to oligotrophic phytoplankton communities, diatom-dominated communities feature a higher size diversity (Tréguer et al., 2018) and different morphologies, which both affect the sinking velocity of aggregates (Laurenceau-Cornec et al., 2015; Bach et al., 2016). Phytoplankton community size structure and morphology thus introduces higher variability to sinking velocity which complicates attribution of cell size and morphology effects on POC fluxes. The higher size and morphology variability in diatom-dominated phytoplankton communities, together with variable cellular silicate to carbon ratios (Brzezinski, 1985), likely explains the poor correlations of opal to POC fluxes (e. g. found by Francois et al., 2002). Similarly, the correlation between POC fluxes and, by number and size, more variable foraminiferal $CaCO_3$ is weaker than for coccolith fluxes (De La Rocha and Passow, 2007). We therefore suggest to factor in, or even focus on, frustule sizes and morphology as explanatory variables for POC fluxes when carrying out mineral ballasting and rain ratio studies in diatom-dominated regions.

3.6 Regional fluxes & rain ratios

Biogenic minerals, dust particles, and detritus are tied together in M^4AGO and define the composition, microstructure and thus sinking velocity of aggregates. In turn, the tracers are independently remineralized or dissolved. Both processes affect $\langle w_s \rangle$ and thus the e-folding depth of tracers. For example, the remineralization of POC increases $\langle w_s \rangle$ of diatom-dominated aggregates and thus increases the dissolution length scale of opal, which we refer to as 'opal RLS'. The combined sinking thus i) affects the RLS of POC and opal (and $CaCO_3$ when dissolution takes place) and ii) couples the timing of mineral and POC fluxes at depth.

The Martin curve concept can be applied to represent the effective attenuation of opal fluxes. The effective Martin curve slope for opal, β'_{opal}, exhibits similar regional variability in the M^4AGO run as in the standard run (Fig. 11). However, the Equatorial Tropical Pacific (ETP) region shows higher spatial variability. The low POC remineralization in OMZs leads to small $\langle w_s \rangle$ of aggregates and decreases the opal RLS and thus increases β'_{opal}. ~~Similar to the POC remineralization length scales, opal fluxes exhibit shorter opal RLS in the surface waters, while they exceed the standard RLS in the mesopelagic zone and below (not shown).~~Similar to POC fluxes, opal fluxes exhibit shorter opal RLSs in the surface waters, while they exceed the standard RLSs in the mesopelagic zone and below (not shown). Particularly in the deep waters of the high latitudes, the opal RLSs are longer than in the standard run. This is due to the aggregates higher sinking velocity than the $25\,\mathrm{m\,d^{-1}}$ opal sinking speed in the standard run and partially to the reformulation of temperature-dependent opal dissolution. In the subtropical regions, opal is remineralized faster below 2000 m and fluxes are generally small (see Fig. 5 a,b).

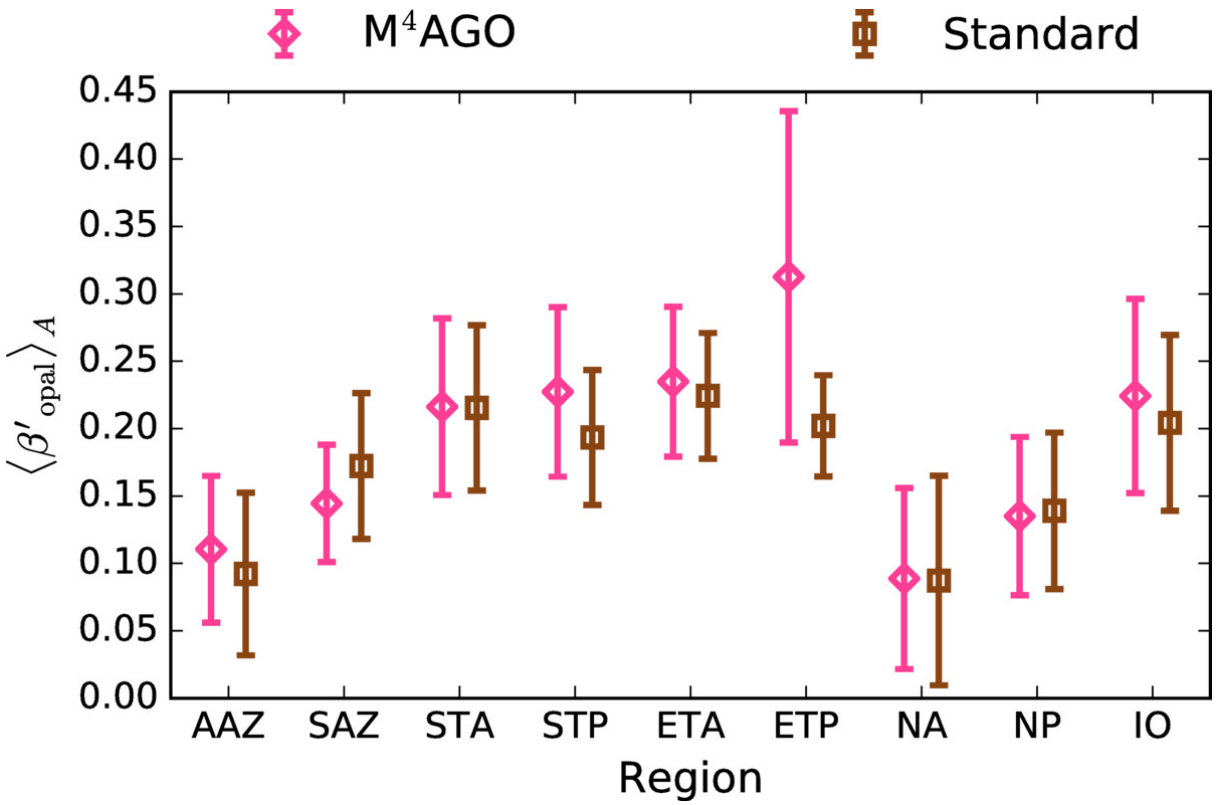

Figure 11. Area-weighted mean effective power function slopes for opal fluxes, $\langle\beta'_{\mathrm{opal}}\rangle_{\mathrm{A}}$, in the regions defined in Fig. 8. Calculated for opal fluxes below 100 m. Error bars show regional standard deviation.

In sum, M^{4}AGO estimates globally ~~~ 1.03 Gt Si per year~~ ~ 1.03 Gt Si per year (~ 1.04 Gt Si per year in the standard run) reaches the seafloor which is in good agreement with present estimates of about 1 Gt Si per year (Tréguer, 2002). Generally, the modelled β'_{opal} is well within the range of observations with estimates of $\beta'_{\mathrm{opal}} = 0.22 \pm 0.53$ (Boyd et al., 2017). In M^{4}AGO, dissolution of opal has the implication that ballasting mineral ratios between opal and $CaCO_3$ shift towards higher importance of $CaCO_3$ with depth. Since the dissolution of opal is temperature-dependent, the preservation efficiency for opal to $CaCO_3$ ratios is thus lowest in regions with strong vertical temperature gradients.

The direct coupling of POC and biogenic mineral fluxes through marine aggregates potentially enhances the models ability to represent rain ratios in space and time. We therefore aggregated the sediment trap data set of Mouw et al. (2016a, b) with 15792 individual POC flux measurements at 673 unique locations to a monthly climatology of POC, particulate inorganic carbon (PIC) and silicate fluxes. We accounted for the time spans of sediment trap deployment ranging from hours to years by time-weighting with a minimum weight of one day per month in cases of few hours measurement, and for each covered month the full monthly weight in cases of a yearly measurement. We compared the climatologies to modeled monthly mean flux ratios

at the stations at their respective depths. The M^{4}AGO run represents the POC/PIC flux ratio equally well as the standard run (not shown). For POC/Si fluxes, the scatter around the 1:1 line is reduced in M^{4}AGO compared to the standard run (Fig. 12).

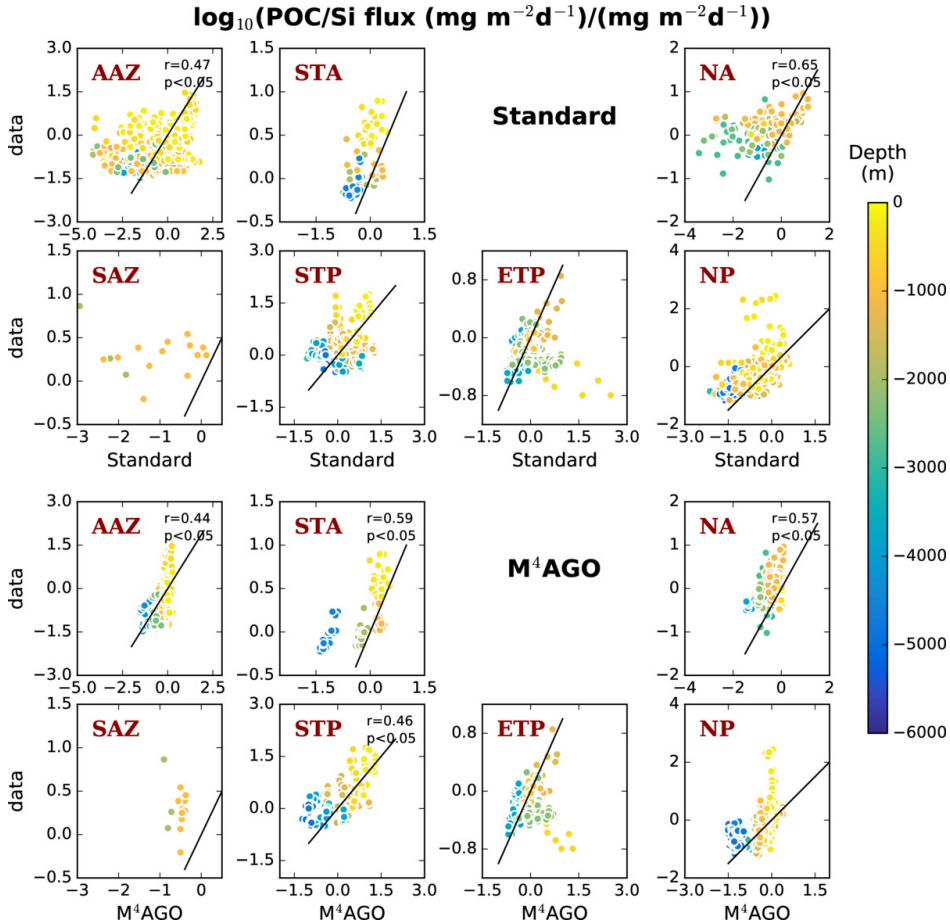

Figure 12. ~~POC/Si rain ratios in the standard run and M^{4}AGO compared to the~~Monthly POC/Si rain ratios in the standard run and in M^{4}AGO compared to the monthly climatological mean derived from the Mouw et al. (2016a, b) data set. The black line denotes the 1:1 line. Notice that the axes are in log and have different limits among regions, but are comparable between runs. No data are available for opal fluxes in the equatorial tropical Atlantic (ETA) where opal fluxes are small (refer to Fig. 5 a, b). Correlation coefficient, r, and significance value, p, are given, if r>0.4.

However, M^{4}AGO introduces a bias in regions deeper than ∼4000 m towards smaller POC/Si ratios. The RLSs in the deep ocean are hence too short in M^{4}AGO. While the scatter of the POC/Si ratio reduces in M^{4}AGO, the overall variability of the flux ratios becomes compressed compared to the measured variability. This compression might be caused by several factors. First, we assume a tight connection of aggregate components and ignore heterogeneous composition among a local particle size spectra which would potentially cause different sinking velocities among the different components. Second, HAMOCC ignores changing diatom silification caused by temperature (see Ragueneau et al., 2006, and references therein) and by seasonal

changes in nutrient availability (Assmy et al., 2013). Generally, deficits exist in both the model runs and sediment trap data. The lack of resolving small scale variability through eddies and their role in shaping the phytoplankton community, as well as general timing, internal variability and spatial current shifts, limits the global models ability to represent local features. Measurement limitations of sediment traps have the potential to additionally increase the mismatch (see e. g. Usbeck et al., 2003, and references therein).

3.7 Evaluation of biogeochemical tracer distributions

We evaluate the simulated spatial distribution of nutrients, oxygen, and alkalinity by comparison to gridded observation climatologies. Silicate, phosphate, nitrate, and oxygen are compared to the World Ocean Atlas (WOA; Boyer et al., 2013; Garcia et al., 2014b). Alkalinity, A_{T}, is compared to the Global Ocean Data Analysis Project (GLODAPv2) climatology (Lauvset et al., 2016). We present the results in Taylor diagrams (Taylor, 2001), which aggregate correlation, root-mean-square-deviation (RMSD), and standard deviation of simulated and observed variables into distances between model results and the reference observations (Fig. 13 a-d). Here, we use spatial grid-cell-wise statistics derived from temporally averaged (100 year mean) fields for which we interpolated the observational data to the model grid. To be able to show all parameters in one plot we derive normalized standard deviations and RMSD. We evaluate the Atlantic and the Pacific Ocean separately to account for their different hydrographical features. For example, the Atlantic ocean is characterized by ventilation through deep water formation in the high latitudes, a feature that does not exist in the Pacific. Furthermore, we select four depth levels: surface waters (6 m depth), the two depths that determine the transfer efficiency, 100 m and approximately 1000 m, and an intermediate depth in the mesopelagic zone, 362 m.

Generally, the two model runs equally well represent nutrients, silicate and oxygen distributions at these depth (Fig.13 a-d), i.e. differences to observations are larger than among the two models. This is expected, as tracer distributions in the model are predominantly determined by the flow field and both simulations use identical physical model conditions. The Taylor diagram captures matches of spatial pattern such as location of fronts, extension of gyres and the location of water masses in an aggregated form. The ocean model represents such features realistically (Jungclaus et al., 2013), but we cannot expect a perfect match of circulation pattern with *in situ* conditions for multiple reasons. The climatological, simplistic atmospheric forcing damps in particular the interannual variability of ocean currents and can contribute to spatial shifts of e. g. frontal regions with respect to the observed climatology. In addition, the coarse horizontal resolution of the model and atmospheric forcing affects features such as upwelling strength (Milinski et al., 2016) and location. In turn, the spatio-temporal interpolation of data, necessary through scarcity of observations, limits the resolution of nutrient variability and introduces uncertainty, particularly in deeper regions, where the density of observations is lower than in surface waters. As a consequence, a mismatch between modelled biogeochemical tracers and the climatological mean of observations is expected.

Tracers undergoing a less complex biogeochemical cycling, such as phosphate or silicate, reflect the quality of the flow field more directly than tracers such as nitrate, oxygen, or alkalinity (see also England and Maier-Reimer, 2001). The latter ones are therefore generally more prone to biogeochemical models reformulation and larger differences can be expected between M^4AGO and the standard run. In addition, M^4AGO links the cycles of phosphate and silicate closer to nitrate and oxygen

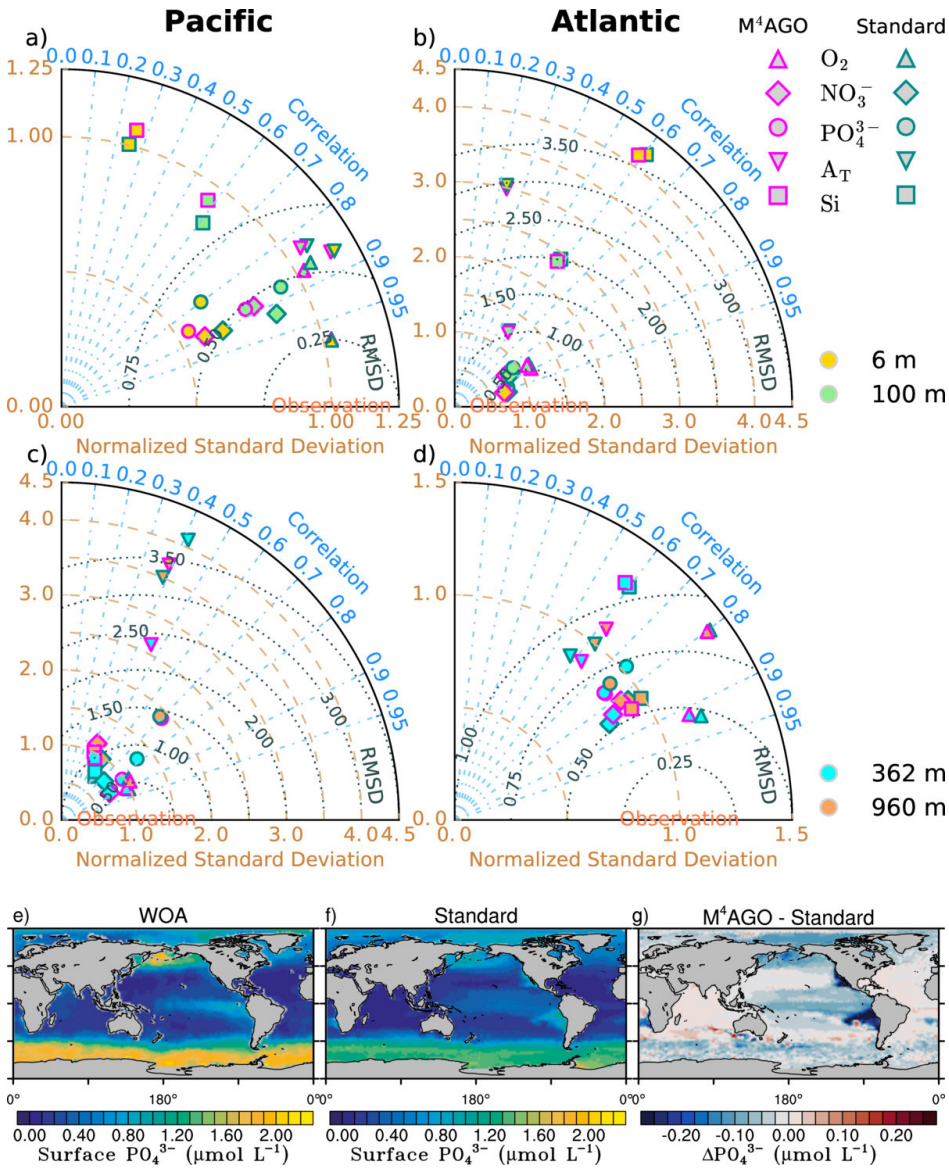

Figure 13. a)-d) Taylor diagram for ~~tracers~~tracers (oxygen, O_2, nitrate, NO_3^-, phosphate, PO_4^{3-}, silicate, Si) in comparison to the World Ocean Atlas data (Boyer et al., 2013; Garcia et al., 2014b) and, in the case of total alkalinity, A_T, to GLODAPv2 data (Lauvset et al., 2016). a) and c): Pacific, b) and d) Atlantic for upper panel 6 m and 100 m. Lower panel 362 m and 960 m. e) surface phosphate concentration in WOA f) in the standard run and g) difference plot between M^{4}AGO and the standard run.

through common sinking of particulate matter. Phosphate and silicate therefore experience an additional biogeochemical cycles imprint in M^{4}AGO compared to the standard run. In surface waters of the Pacific, this led e. g. to a slight improvement of the phosphate correlation with WOA observations, while it increased the normalized standard deviation compared to the standard

run (Fig. 13 a). The improvement is related to the better representation of surface phosphate concentrations off Peru and ~~North America coast~~North American West Coast (see Fig. 13 e-g).

In both simulations, biogeochemical tracer distributions in the Pacific are strongly influenced by the OMZ in the eastern boundary upwelling region. An exception is oxygen in surface waters which is primarily determined by gas exchange processes. As a common feature of all state-of-the-art global ocean biogeochemistry models, OMZs are too large and result from nutrient trapping through a sluggish circulation and associated insufficient supply of oxygen (Dietze and Loeptien, 2013). The sluggish circulation and mixing is likely associated with underrepresented equatorial currents, particularly the equatorial intermediate current system and equatorial deep jets (Brandt et al., 2012; Shigemitsu et al., 2017). The OMZ shape in the eastern Pacific ocean, though, changes between the runs. In M^4AGO, the water column above 800 m is more and below less oxygenated than in the standard run. The change in OMZ shape imprints on A_T, as anaerobic and aerobic remineraliziation processes change alkalinity in a different manner, i.e. denitrification and sulfate reduction increase alkalinity, whereas aerob remineralization decreases alkalinity. While A_T and silicate are generally worst compared to observations, M^4AGO improves the representation of A_T in the Pacific at 360 m compared to the standard run. This is well visible through the higher correlation (~ 0.45 compared to 0.4) and lower RMSD of ~ 2.3 compared to ~ 3.75 in the standard run (Fig. 13 c, 362 m depth). The increased RMSD of silicate in surface waters and 100 m in M^4AGO are associated to the eastern equatorial and upwelling regions in the Pacific. The lower remineralization in OMZs not only decreases sinking velocity of detritus, but also increases the retention time of the tightly coupled opal in M^4AGO and thus enhances the opal dissolution and silicate concentration. In general, the tighter coupling of silicate to nutrients through common sinking in aggregates leads to a higher sensitivity of silicate to ocean circulation and temperature deficiencies in M^4AGO than in the standard run. The high RMSD and low correlation for silicate compared to observations, particularly in the euphotic zone, can have additional implications for M^4AGO, since the silicate distribution in the euphotic zone directly affects opal production and thus the sinking velocity of aggregates, transfer efficiency and nutrient distributions. The tighter coupling of silicate to other biogeochemical cycles in M^4AGO therefore warrants further future investigation.

3.8 Regional CO_2 ~~uptake~~fluxes

In a 100-year climatological steady state, both model runs show the southern hemisphere ocean acting as a net source of CO_2 to the atmosphere while the northern hemisphere acts as a net sink (Fig. 14 a). Consequently, a net oceanic CO_2 transport across the equator from the northern to the southern hemisphere exists. In the simulation with M^4AGO, a stronger CO_2 uptake compared to the standard run occurs in the region between 60 °S and 45 °S which coincides with deeper transfer of POM reflected by an increased transfer efficiency (Fig. 8). In both model runs, the ~~sub~~tropical regions outgas CO_2 to the atmosphere. As visible from the decreasing difference between the cumulative zonal CO_2 fluxes, M^4AGO exhibits a stronger outgassing in the ~~sub~~tropical region, particularly in the northern hemisphere (Fig.14 a). Even though a small residual of zonally integrated fluxes of about $0.02\,\mathrm{Gt\,C\,yr^{-1}}$ between the two model runs remains, the small residual CO_2 flux imbalance of $0.07\,\mathrm{Gt\,C\,yr^{-1}}$ and $0.05\,\mathrm{Gt\,C\,yr^{-1}}$ in M^4AGO and the standard run, respectively, indicate well spun-up model runs. In general, the latitudinal zonal CO_2 fluxes and the cross-equatorial southward oceanic CO_2 transport agree qualitatively and quantitatively well with

former forward-integrated models for pre-industrial conditions (e. g Sarmiento et al., 2000; Gloor et al., 2003; Mikaloff Fletcher et al., 2007).

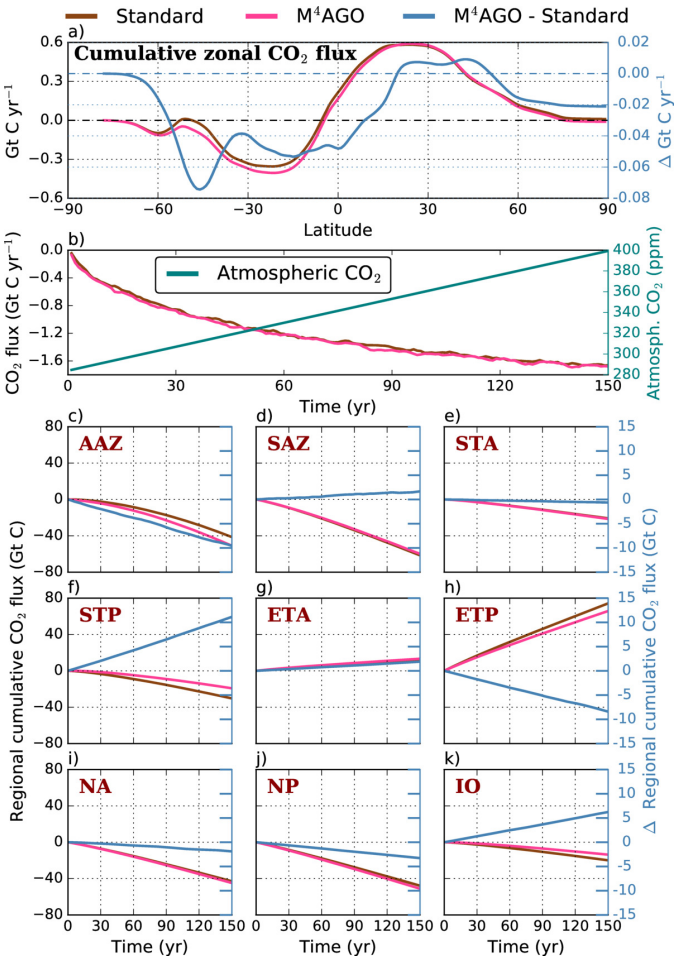

Figure 14. a) Climatological cumulative zonal CO_2 flux in the standard and the M^4AGO run (from south to north). Generally, negative fluxes represent net-CO_2 uptake by the ocean. Note the second y-axis for the difference between the two runs (also in c) - k)). b) Global annual net CO_2 flux under linearly increasing atmospheric CO_2 concentration. c) - k) Regional cumulative CO_2 fluxes under increasing atmospheric CO_2 (regions as defined in Fig. 8).

To study the effect of the changed transfer efficiency in M^4GO on the CO_2 uptake without indirect climate effects, we perform model runs in which we linearly increase the atmospheric CO_2 concentration with a yearly increment from ∼285 ppm to 400 ppm within 150 years. The transient forcing does not feed back onto the physical climate state. We therefore emphasize that no climate feedback on e. g. ocean temperature, stratification, and thus primary production and remineralization occurs in these model runs.

During the atmospheric CO_2 increase, both model runs show similar global annual oceanic CO_2 uptake (Fig. 14 b). About 181-185 Gt C are taken up by the global ocean throughout the 150 year period. The discrepancy of ≈ 4 Gt C between the two runs arises to a large extent from the residual imbalance of 0.02 Gt C yr^{-1} uptake, cumulated over 150 years.

The general trends in the regional cumulative fluxes remain the same between the two model runs (Fig. 14 c-k) and most regions act as net sinks of CO_2. Only the upwelling regions of the equatorial tropical Atlantic (ETA) and Pacific (ETP) are net sources of CO_2 to the atmosphere at the end of the 150 yr period. The magnitude of the regional cumulative fluxes, however, varies among the two model runs.

Since we can rule out temperature-driven effects on the differences in CO_2 uptake when comparing the two climatologically forced runs, a different state and/or changes in A_T and dissolved inorganic carbon (DIC) concentration determine the partial pressure of CO_2, pCO_2, and thus CO_2 fluxes. In our runs, major changes in A_T and DIC can locally occur due to a change in, first, the $CaCO_3$ to detritus rain ratio as a result of varying $CaCO_3$ and POM production and remineralization, or, second, e. g. an increase of the POC transfer efficiency, which reflects a transfer of carbon to deeper waters where CO_2 is withdrawn from immediate exchange with the atmosphere. In addition, such different signals can be transported by the flow field and remote effects can appear. Quantitatively, differences of regional cumulative CO_2 fluxes larger than 5 Gt C appear in the Antarctic Zone (AAZ), the Subtropical Pacific (STP), the Equatorial Tropical Pacific (ETP), and the Indic Ocean (IO) (Fig. 14 c-k). In the upwelling and high latitude regions, the pCO_2 is lower in M^4AGO than in the standard run, which translates to higher oceanic uptake (in AAZ, NP) or less outgassing (in ETP). ~~Qualitatively, this coincides well with the higher transfer efficiencies in these regions (cmp. to Fig. 8).~~Qualitatively, this coincides well with the primary production, respective export and the higher transfer efficiencies in these regions (cmp. to Fig. 4 and 8). In regions of higher transfer efficiency, but similar CO_2 fluxes as compared to the standard run, either POC export fluxes are small (e. g. in the Arctic Ocean) or physical processes such as mixing or upwelling dominate over biologically induced CO_2 fluxes (e. g. in the SAZ). In the STP region, where high $CaCO_3$ to detritus rain ratios occur (refer to Fig. 5), A_T is about 0.2 % lower in M^4AGO than in the standard run, which enhances pCO_2 by about 2 % and thus decreases the CO_2 uptake.

In summary, under linearly increasing CO_2 in a non-interactive mode, the global CO_2 fluxes remain similar for the standard and the M^4AGO run. However, regional CO_2 fluxes change, which is potentially linked to the changing pattern of transfer efficiency and the $CaCO_3$ to detritus rain ratio. A detailed study on the feedbacks between the transfer efficiency, represented by M^4AGO, and a transient climate on oceanic CO_2 uptake is out of the scope of this manuscript and will be part of future investigations.

3.9 Sensitivity analysis

With M^4AGO, the processes of temperature-dependent remineralization and a number of new model parameters to represent variable sinking velocity of marine aggregates were introduced to HAMOCC. We carried out three sensitivity experiments to provide insights into HAMOCCs response to the uncertainty of selected parameters (see below for the criteria). As target variables, we chose i) the transfer efficiency, ii) phosphate as essential nutrient for primary production, and iii) silicate as nutrient and circulation-reflecting agent.

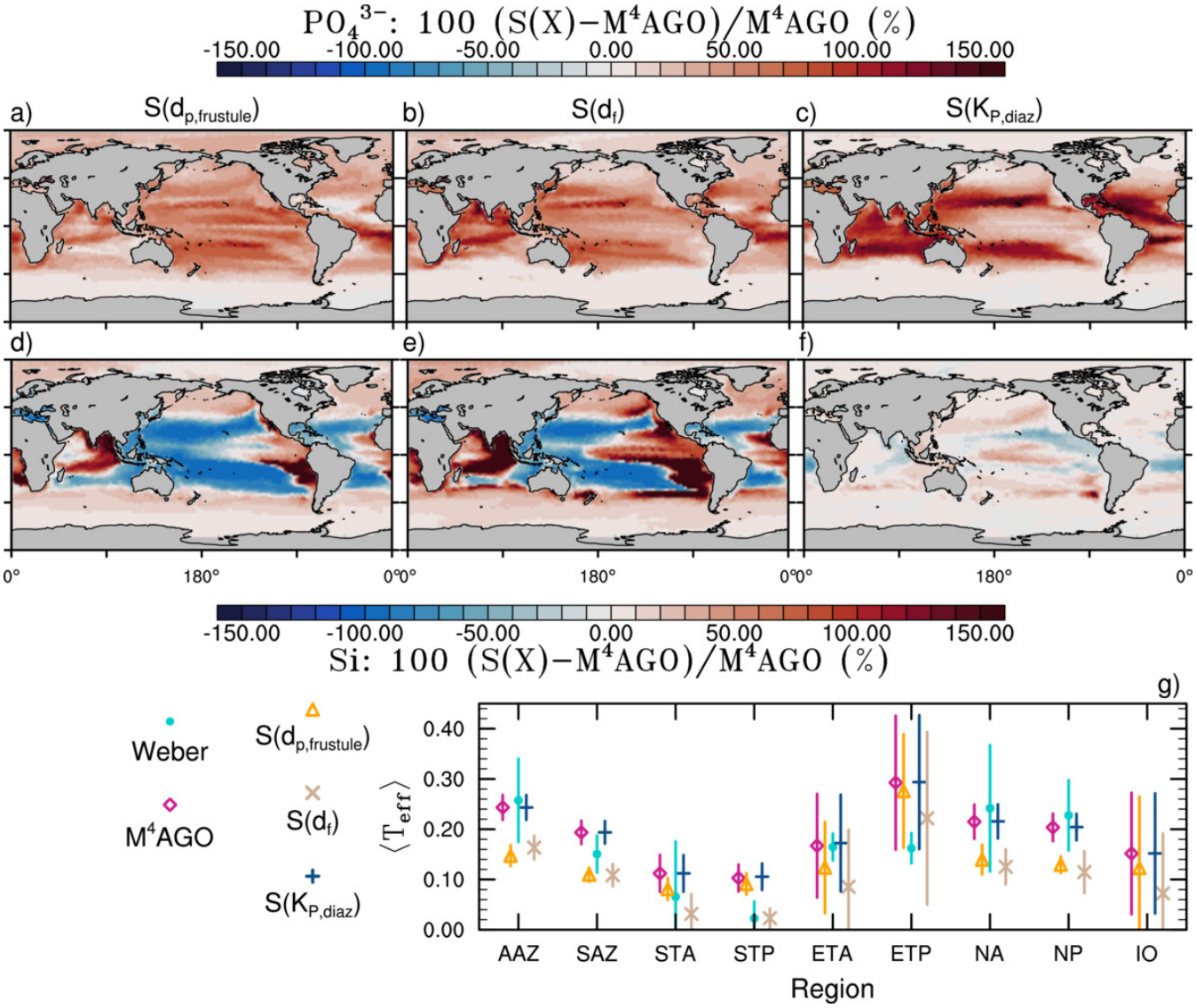

Figure 15. Sensitivity of a)-c) surface phosphate, d)-f) silicate concentrations, and g) ~~POC transfer efficiency to $d_{p,\mathrm{frustule}}$~~POC transfer efficiency to diatom frustule size, $d_{p,\mathrm{frustule}}$ ($S(d_{p,\mathrm{frustule}})$, modified from 20 µm to 10 µm), the half-saturation constant for phosphate uptake by diazotrophs ($S(K_{P,\mathrm{diaz}})$, modified from 0.05 µmol L^{-1} to 0.1 µmol L^{-1}), ~~and d_f~~and fractal dimension, d_f ($S(d_f)$, from variable to constant $d_f = 2$). Error bars in g) represent regional standard deviation and for Weber et al. the uncertainty for the reconstruction of the regional transfer efficiency.

~~We suggested~~Previously in Sect. 3.5, we suggested the size of primary particles, particularly that of opal frustules, as an important factor for regulating $\langle w_s \rangle$ and thus the transfer efficiency. We thus study the effect of primary particle size in the sensitivity experiment $S(d_{p,\mathrm{frustule}})$ exemplarily for diatom frustules because: i) diatom size is highly variable, ii) HAMOCC

does not explicitly represent algae size classes and iii) algae body size is expected to decrease with rising water temperatures (Daufresne et al., 2009). We decrease their size by 50 % from $d_{p,\mathrm{frustule}}$ =20 µm to $d_{p,\mathrm{frustule}}$ =10 µm. In the second sensitivity experiment, $S(d_f)$, the varying fractal dimension, ranging between 1.6 and 2.4 in the M^{4}AGO run, is set to a constant, $d_f = 2$, to eliminate its variable effect on b and $\langle w_s \rangle$. In the third experiment, S($\mathrm{K_{P,diaz}}$), we showcase the sensitivity of phosphate concentration in the subtropical gyres to diazotrophs standing stock which we noticed during the process of tuning the M^{4}AGO run. Here, we increase the half-saturation constant for phosphate uptake by diazotrophs from 0.05 µmol L^{-1} to 0.10 µmol L^{-1}. All sensitivity runs are in quasi-steady state with shown surface properties.

Decreasing the opal frustule size by 50 % compared to the M^{4}AGO run reduces $\langle w_s \rangle$ and thus the RLS in diatom-dominated regions. ~~As a consequence, the transfer efficiency in silicifier-dominated regions is low (Fig. 15 g)~~As a consequence, the transfer efficiency in silicifier-dominated regions is lower in $S(d_{p,\mathrm{frustule}})$ than in M^{4}AGO (Fig. 15 g). ~~Accordingly, opal dissolves closer to surface waters and the silicate concentration increases with respect to the M^{4}AGO run in silicifier-dominated regions (Fig. 15 d)~~Accordingly, opal dissolves closer to surface waters and the silicate concentration increases compared to the M^{4}AGO run in silicifier-dominated regions, particularly in and downstream of coastal upwelling regions (Fig. 15 d). In the subtropical gyres, where silicate is diminished, it further decreases in $S(d_{p,\mathrm{frustule}})$. The higher remineralization in the euphotic zone in upwelling regions increases the phosphate concentrations downstream in the subtropical gyres (Fig. 15 a). In sum, the sensitivity to $d_{p,\mathrm{frustule}}$ underpins the potential importance of primary particle size for $\langle w_s \rangle$ and thus for biogeochemical cycling.

Generally, eco-physiological responses of primary producers are typically neglected in ESM-type models such as HAMOCC. Under the premise that the size of primary particles is of importance to represent $\langle w_s \rangle$ as depicted by M^{4}AGO, changes of the phytoplankton size structure with ongoing ocean warming could affect RLSs, transfer ~~efficieny~~efficiency, and thus the biological carbon pump. Indeed, body size decreases with increasing water temperature (Daufresne et al., 2009)~~ which is suggested~~. The increasing water temperature has been suggested to shift eco-physiological regions polewards by rates of about 22 to 36 km per decade (Lefort et al., 2015, and references therein). $S(d_{p,\mathrm{frustule}})$ shows that decreasing primary particle size reduces the transfer efficiency and thus likely weakens the biological carbon pump. Yet, the net-effect of such eco-physiological responses and adaptability of primary producers on transfer efficiency and CO_2 uptake under ongoing climate change remains elusive and thus demands for further future investigation.

In the sensitivity study $S(d_f)$, d_f in surface waters is increased in diatom-dominated and reduced in calcifier-dominated waters compared to the M^{4}AGO run (cmp. to Fig 6 c). In the M^{4}AGO run, aggregates experience rapid compaction within the depth of about 150 m to 250 m in diatom-dominated regions, d_f increases rapidly (see Fig. 7 c), and hence, $\langle w_s \rangle$. By contrast, $\langle w_s \rangle$ is only enhanced in the productive surface waters of the SAZ, upwelling regions and the associated OMZs due to the larger d_f and the dependent smaller b in $S(d_f)$. The lower $\langle w_s \rangle$ in large parts of the mesopelagic zone and below lead to a generally decreased transfer efficiency in $S(d_f)$ (Fig. 15 g). Consequently, the RLSs are shorter and enhance the silicate concentrations in surface waters in diatom-dominated regions (Fig. 15 e). In the subtropical gyres, the silicate diminishes even further, which is likely related to the enhanced bulk phytoplankton growth through higher phosphate concentrations. Phosphate is remineralized more rapidly than silicate and thus can be transported downstream the equatorial current into the subtropical gyres, where it is enhanced in $S(d_f)$ compared to M^{4}AGO (Fig. 15 b). As a consequence of the potential sensitivity of biogeochemical cycles

on d_f, more knowledge of processes affecting the aggregate microstructure is required, among them e. g. compaction through repacking and zooplankton egestion of fecal pellets.

Diazotrophs in HAMOCC can grow independently of nitrate on phosphate. They are regionally confined to warm tropical and subtropical regions (Paulsen et al., 2017, 2018). Diazotrophs modulate the phosphate concentration in the subtropical gyres. The diazotrophs global primary production increases from about $2.2\,\mathrm{Gt\,C\,yr^{-1}}$ in the standard run to $\approx 2.9\,\mathrm{Gt\,C\,yr^{-1}}$ in the M^{4}AGO run. A slower growth response to phosphate concentrations, enforced by raising the half-saturation constant from $0.05\,\mathrm{\mu mol\,L^{-1}}$ to $0.10\,\mathrm{\mu mol\,L^{-1}}$ in $S(K_{\mathrm{P,diaz}})$, increases the phosphate concentrations in the subtropical gyres as to more than 150 % (Fig. 15 c). The primary production through diazotrophs reduces significantly from formerly global $\approx 2.9\,\mathrm{Gt\,C\,yr^{-1}}$ to $\approx 1.9\,\mathrm{Gt\,C\,yr^{-1}}$ in $S(K_{\mathrm{P,diaz}})$, and regionally particularly in the equatorial Panama basin. By contrast, diazotrophs feature a primary production of more than $5\,\mathrm{Gt\,C\,yr^{-1}}$ and $7\,\mathrm{Gt\,C\,yr^{-1}}$ in $S(d_{p,\mathrm{frustule}})$ and $S(d_f)$, respectively, due to the increased phosphate concentrations in the subtropical gyres. Diazotrophs in the model only produce organic matter. In $S(K_{\mathrm{P,diaz}})$, the lower diazotrophs primary production ~~in the~~ in the equatorial upwelling regions (ETA and ETP) thus leads to a shift of the aggregate composition towards higher opal to detritus ratios which slightly increases the transfer efficiency and reduces the available silicate (Fig. 15 f). ~~Phosphate previously utilized by diazotrophs in the Panama basin now partially populates the downstream equatorial current and increases the subtropical gyres phosphate concentrations.~~Phosphate previously utilized by diazotrophs in the Panama basin now partially populates the downstream equatorial current and reaches the subtropical gyres. In comparison to the standard run, this phenomenon is generally intensified in M^{4}AGO through the shallower remineralization and lower transfer efficiency in the subtropical gyres (Fig. 8 c). In conclusion, the representation and effects of diazotrophs in HAMOCC, particularly in conjunction with M^{4}AGO, require further future evaluation.

3.10 Current limitations of M^{4}AGO

Developing M^{4}AGO, we followed a process-oriented approach and explicitly incorporated ballasting and microstrucure of aggregates of heterogeneous composition to calculate the mean sinking velocity. Introducing such complexity in ESMs typically comes at the cost of high computational efforts. This is a non-negligible factor for model development which we reduce to a minimum with M^{4}AGO. Acknowledging the trade-off between increasing model complexity and computational limitations let us to deploy a number of simplifying assumptions that we critically review in the following.

In the euphotic zone of the oceans, changing phytoplankton community structure, phytoplankton growth, decay, and grazing through zooplankton leads to a dynamic supply of various small particles that potentially aggregate and eventually sink and become remineralized. Assuming homogeneous composition of aggregates throughout a dynamic steady state size distribution is therefore only the first step to a model representation of marine snow, where local diversity of particles and the processes of aggregation and fragmentation are explicitly resolved. By assuming a dynamic steady state for the size distribution, we only represent the characteristic processes within the system and underestimate the variability of the number distribution slope which ranges between $b \approx 3.19 - 3.76$ compared to measurements, where $b \approx 2$ to 5 (Guidi et al., 2009). As a consequence, M^{4}AGO probably underestimates the variability of sinking velocity, particularly in the upper ocean, where the size distribution dynamically evolves.

In M^4AGO, TEPs are simplistically considered. In agreement with Mari et al. (2017), TEPs act as microstructure-loosening and buoyancy-adding for diatom-dominated aggregates. For $CaCO_3$, we only considered the coccolith size which decreases sinking velocity compared to an aggregate composed of intact coccospheres. For simplicity, we assumed that aggregated TEP and intact cells sink as fast as coccoliths and detritus. To decipher the role of TEPs for aggregate formation (Passow, 2002; Mari et al., 2017), our model would require i) to represent TEPs and disintegrating coccospheres, and ii) to consider aggregation and fragmentation processes explicitly to depict the dynamic evolution of marine aggregate distributions. Such dynamic approach is necessary to e. g. study short term events of high POC export hypothesized to be driven by silicate depletion and TEP release by diatoms and their subsequent aggregation (Martin et al., 2011). More detailed models, such as e. g. the 1-D Lagrangian approach of Jokulsdottir and Archer (2016), can likely provide more insights into aggregate dynamics and can help to further improve the aggregate representation in ESM frameworks. Furthermore, an explicit representation of aggregation and fragmentation enables transient size distributions and would allow for a direct comparison to a growing number of particle distribution slope measurements (e. g. Guidi et al., 2009).

4 Summary & Conclusions

We implemented the novel, *Microstructure, Multiscale, Mechanistic, Marine Aggregates in the Global Ocean* (M^4AGO) scheme in HAMOCC to improve the representation of the biological carbon pump in an Earth System Model framework. M^4AGO accounts for the heterogeneity and microstructure of aggregates and thus clearly defines measurable statistic aggregate properties in HAMOCC. M^4AGO links the nutrient and silicate cycle closer together by incorporating opal and other ballasting minerals in aggregate formation and sinking. This lets us to introduce a consistent Q_{10} temperature-dependent dissolution and aerobic remineralization of opal and POC, respectively.

In contrast to the standard HAMOCC version, M^4AGO well represents and provides a mechanistic understanding for the recently published global transfer efficiency pattern. We identify primary particle size, particularly of diatom frustules, and the compaction of aggregates with depth as strong driving factors for sinking velocity that, in combination with temperature-dependent remineralization, co-determines the high POC transfer efficiency in high latitudes and upwelling regions. Our model results support previous findings that $CaCO_3$ with its high density acts as ballasting mineral in calcifier-dominated regions of the ocean. The changed transfer efficiency pattern in combination with the $CaCO_3$ to detritus rain ratio alters regional CO_2 fluxes, while the global uptake remains the same as in the standard run when atmospheric CO_2 is linearly increased without climate feedbacks.

Highest uncertainties in parametrizing M^4AGO are with respect to the weakly constrained primary particle surface properties and their likely effect on the related microstructure of aggregates. Since sinking velocity and transfer efficiency are highly sensitive to microstructure of aggregates, gaining insights into the controlling factors and processes for microstructure is desirable. Future model development for the representation of marine aggregates would highly benefit from sub-aggregate scale measurements of microstructure, adhesive surface properties, and primary particle composition.

Our findings and the underlying model concept suggest a number of implications. ~~First, size of aggregate constituents, particularly of diatom frustules, as potential factor for high sinking velocity suggest to widen the perspective of mineral ballast studies towards a size-and-ballast hypothesis.~~First, the finding that the size of aggregate constituents, particularly of diatom frustules, act as potential factor for high sinking velocities, suggests to widen the perspective of mineral ballast studies towards a size-and-ballast hypothesis. Further, ~~it requires~~such extended size-and-ballast hypothesis requires to factor in the different temperature-dependent remineralization and dissolution rates that aggregates experience during their descend. Accounting for cell size and morphology will aid to better assess the role of the phytoplankton community size structures on POC fluxes, particularly in nutrient-rich upwelling regions, where a wide, variable size spectrum of diatoms prevail. Second, the indirect temperature effect on phytoplankton cell size (e. g. Daufresne et al., 2009) poses the challenging task to resolve the temperature-adapting cell size structure of the phytoplankton community in global carbon cycle models to depict the potential effect on sinking velocity and thus the biological feedback on rising CO_2 in the atmosphere.

In conclusion, M^4AGO provides well-defined aggregate properties in an ESM framework and can thus serve as a testbed to upscale aggregate-associated processes to potential global impacts on biogeochemical cycles, and, in particular, on the biological carbon pump.

Code availability. -none-

Data availability. -none-

Code and data availability. Primary data and code for this study is stored and made available through the Max-Planck-Gesellschaft Publications Repository: https://pure.mpg.de. The respective MPI-OM and HAMOCC model code (revision numbers: r4981 and r5003) is available on request after agreeing to the MPI-ESM license agreement and registering at the MPI-ESM-Forum (https://www.mpimet.mpg.de/en/science/models/licenses/).

.

Sample availability. -none-

Video supplement. -none-

Appendix A: Additional aggregate properties

In addition to the aggregate properties presented in Fig. 6, M^{4}AGO involves the aggregate mean stickiness and the number distribution slope that are tightly connected to each other via d_f (Fig. A1). In addition, the porosity of aggregates, Eq. (6), can be deduced from aggregate size, primary particle size, and d_f. Porosity is frequently calculated for aggregates (Alldredge and Gotschalk, 1988; Ploug et al., 2008). Its potential dependency on the microstructure and primary particle size is, however, seldom covered. We therefore calculated the mean volume-weighted porosity of aggregates, $\langle\phi\rangle_\mathrm{V}$, to provide a perspective on how aggregate porosity varies with the aggregate properties shown in Fig. 6 in the global ocean (Fig. A1).

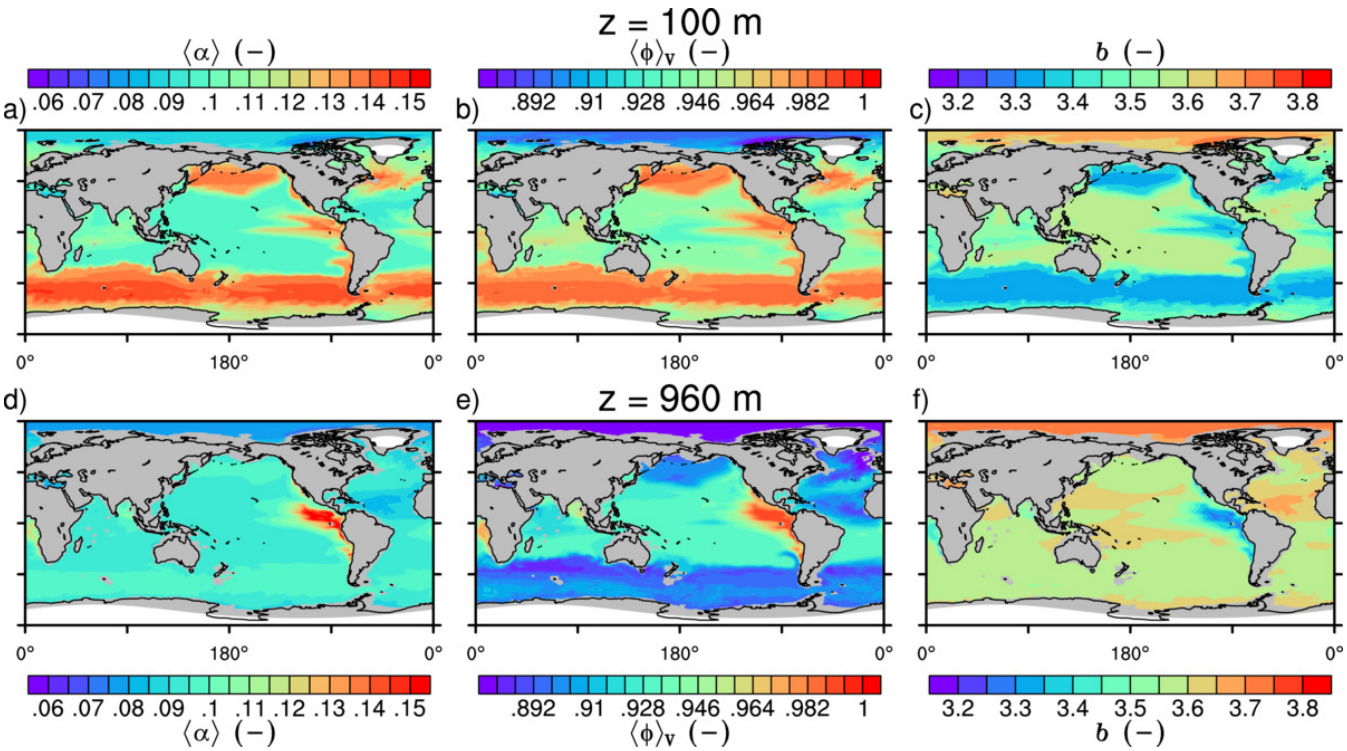

Figure A1. Mean stickiness $\langle\alpha\rangle$, Eq. (22), volume-weighted porosity, $\langle\phi\rangle_\mathrm{V}$, and the number distribution slope, b, Eq. (21).

As defined by the attributed primary particle stickiness, aggregates in diatom-dominated regions show the highest stickiness values in surface waters since the virtual TEP particles linked to detritus increase the $\langle\alpha\rangle$ in M^{4}AGO (Fig. A1). At the bottom of the mesopelagic zone, $\langle\alpha\rangle$ is almost homogeneous apart from the OMZ regions, where the lower anaerobic remineralization retain higher detritus concentration that lead to higher $\langle\alpha\rangle$ in conjunction with diatom frustules. The number distribution shows an inverted picture compared to $\langle\alpha\rangle$ with smallest decay slope, b, in diatom-dominated and OMZ regions and strongest decline in calcifier-dominated surface waters (Fig. A1 c,f). In M^{4}AGO, $\langle\phi\rangle_\mathrm{V}$ is tightly connected to $\langle\alpha\rangle$ in the euphotic zone (Fig. A1 b). With increasing depth, aggregates get compacted, d_f increases, and the maximum size of aggregates decrease. Both lead to lower $\langle\phi\rangle_\mathrm{V}$ particularly in the diatom-dominated regions. In OMZs, however, $\langle\phi\rangle_\mathrm{V}$ is undiminished high. Generally, the

exceptional behavior of aggregate properties in OMZs due to implicitly modelled TEPs is likely overestimated. TEPs possess higher remineralization rate than detritus (Mari et al., 2017), which likely reduces the TEPs occurrence in deep OMZs and thus their influence on aggregate properties.

Appendix B: Effective Martins slope in M^{4}AGO

The effective Martin curve slope β' provides a meaningful measure on the attenuation of POC fluxes. This made β' to be a widely used measure to evaluate POC concentration and flux observations (e. g. Lutz et al., 2007; Lam et al., 2011; Marsay et al., 2015). In M^{4}AGO, we found a β' pattern similar to the inverse of the transfer efficiency (Fig. B1 compared to Fig. 8,

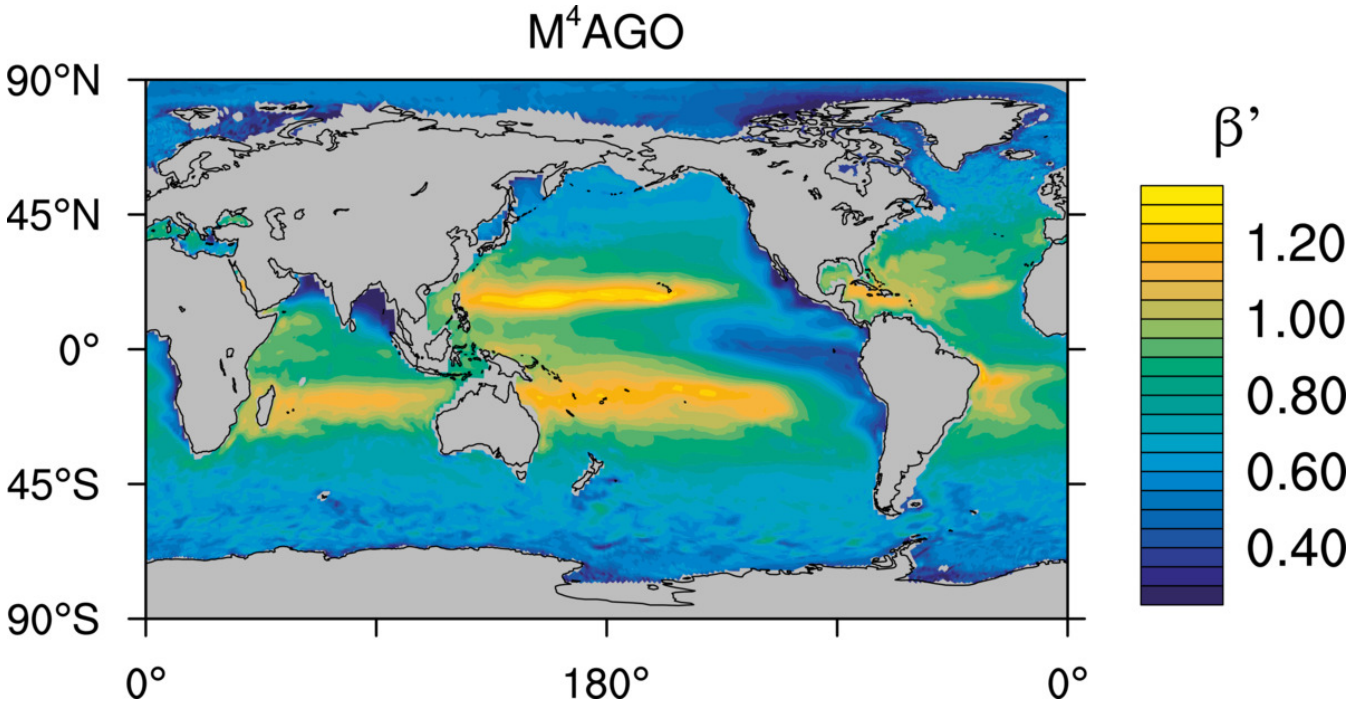

Figure B1. Effective Martin curve slope for POC in M^{4}AGO, β'.

respectively). The smallest β' are found in the models OMZ regions and the shallow Arctic shelf regions. In the North Pacific and North Atlantic, β' features values of about 0.47 to 0.60 and reaches maximum values of about 1.31 in the subtropical gyres. Qualitatively, the pattern thus follows and underpins the previously suggested POC flux attenuation pattern (Marsay et al., 2015; Weber et al., 2016; DeVries and Weber, 2017). By contrast, in our standard run, we found, apart from OMZs, a rather homogeneous β' with a global value of $\langle\beta'\rangle_{\mathrm{A,Martin}} \approx 0.82$ that is smaller than the prescribed value of $\beta = 1.00$ in oxygen-saturated waters. This discrepancy can be attributed to a number of processes. First, the global $\langle\beta'\rangle_{\mathrm{A,Martin}}$ is reduced by the lower anaerobic remineralization in OMZs. Second, turbulent diffusion and vertical transport processes represented by MPI-OM in addition to sinking contribute to vertical POC concentration profiles and fluxes (Boyd et al., 2019). Third, the

artificial numerical diffusion inherent to HAMOCCs implicit upstream scheme for particle sinking contributes to higher mass transport to depth than prescribed by $\beta = 1$. This inherent numerical diffusion is, however, implicitly accounted for during the process of tuning β in the model.

Appendix C: Seasonal transfer efficiency

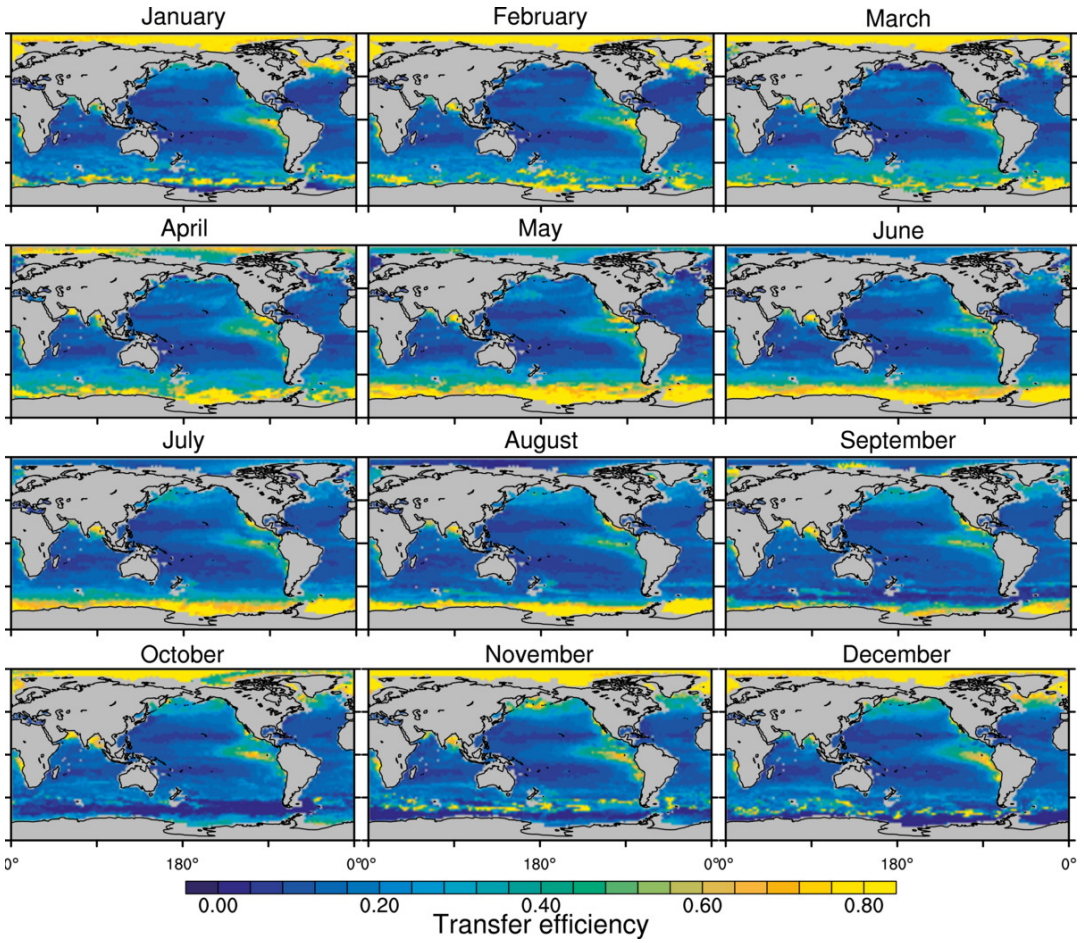

Figure C1. Seasonal evolution of the transfer efficiency in M^4AGO. Note the difference of the colorbar values compared to Fig. 8.

The inversely identified transfer efficiency pattern by Weber et al. (2016) provides an estimate on time-integrated climatological POC fluxes. In regions of high seasonal variability in primary production, POC fluxes can undergo strong seasonal variation and so does transfer efficiency (Lutz et al., 2007). For example, if we assume an average sinking speed of about 25 m d^{-1}, a pulsed flux at 100 m reaches the depth of 1000 m about a month later and can strongly alter flux and concentration profiles (Lam et al., 2011; Giering et al., 2017). Accordingly, single measured POC concentration profiles can even show higher

concentration at depth than in surface waters which results in negative β' values and thus higher transfer efficiency than one. In turn, transfer efficiency can be extremely small at the beginning of a phytoplankton bloom. Seasonal transfer efficiency can thus heavily deviate from the climatological state. This seasonal behavior is reflected in M^{4}AGO which shows high transfer efficiency in late autumn and early times of low primary production after the bloom in high latitudes (Fig. C1). Even though the standard run exhibits a similar qualitative pattern, the seasonal amplitude of the transfer efficiency in high latitudes is lower in M^{4}AGO compared to the standard run.

Appendix D: Mathematical symbols

Table D1. Mathematical symbols and their description.

Symbol	Description	Units
$\langle\alpha\rangle$	mean aggregate stickiness	$[-]$
α_{diatom}	stickiness of a diatom frustule	$[-]$
α_i	stickiness of primary particle type i	$[-]$
α_{max}	maximum stickiness of primary particles	$[-]$
$\langle\alpha\rangle_{\mathrm{map}}$	mapped mean stickiness	$[-]$
α_{min}	minimum stickiness of primary particles	$[-]$
α_{opal}	stickiness of opal	$[-]$
α_{TEP}	stickiness of TEPs	$[-]$
A	total surface area of primary particles in an aggregate	$[\mathrm{m}^2]$
a	power law factor for the aggregate number distribution	$[\mathrm{m}^{b-4}]$
A_i	surface area of a primary particle of type i	$[\mathrm{m}^2]$
a_j	drag approximation factor	$[-]$
b	slope of the aggregate number distribution	$[-]$
β	Martin curve POC flux slope	$[-]$
β'	effective Martin curve slope	$[-]$
β_f	slope of fractal dimension-mapping function	$[-]$
b_J	drag approximation power slope for b calculation	$[-]$
b_j	drag approximation power slope	$[-]$
c_D	drag coefficient for sinking	$[-]$
C_i	concentration of HAMOCC tracer i	$[\mathrm{kmol\,m^{-3}}]$
d	diameter of an aggregate	$[\mathrm{m}]$
d_f	3-D mass fractal dimension	$[-]$
$d_{f,\mathrm{max}}$	maximum fractal dimension	$[-]$
$d_{f,\mathrm{min}}$	minimum fractal dimension	$[-]$
d_j	aggregate diameter at integration boundary	$[\mathrm{m}]$
d_{max}	maximum aggregate diameter	$[\mathrm{m}]$
d_{min}	minimum aggregate diameter	$[\mathrm{m}]$
$\langle d_p\rangle$	primary particle diameter	$[\mathrm{m}]$
$\langle d_p\rangle$	mean primary particle diameter	$[\mathrm{m}]$
$d_{p,\mathrm{frustule}}$	outer diameter of diatom frustule	$[\mathrm{m}]$
$d_{p,i}$	primary particle diameter of primary particle type i	$[\mathrm{m}]$

continued . . .

$\Delta\rho_f$	aggregate excess density	$[\mathrm{kg\,m^{-3}}]$
$\langle\Delta\rho_f\rangle_\mathrm{V}$	volume-weighted mean aggregate excess density	$[\mathrm{kg\,m^{-3}}]$
F_0	POC flux at export depth z_0	$[\mathrm{kmol\,m^{-2}\,s^{-1}}]$
F_i	flux of tracer $i = \{\mathrm{CaCO_3, opal, POC}\}$	$[\mathrm{kg\,m^{-2}\,s^{-1}}]$ or $[\mathrm{kmol\,m^{-2}\,s^{-1}}]$
g	gravitational acceleration constant	$[\mathrm{m\,s^{-2}}]$
K_i	primary particle number ratio	$[-]$
K_{O_2}	half saturation constant for oxygen	$[\mathrm{kmol\,m^{-3}}]$
l	diatom shell thickness	$[\mathrm{m}]$
μ	molecular dynamic viscosity	$[\mathrm{kg\,m^{-1}\,s^{-1}}]$
$m(d)$	mass of an aggregate of diameter d	$[\mathrm{kg}]$
m_e	actual mass of detritus in diatom frustules	$[\mathrm{kg}]$
m_f	mass-factor for smallest entity	$[\mathrm{kg\,m^{-d_f}}]$
$m_\mathrm{potential}$	mass of detritus that could fill the void in diatom frustules	$[\mathrm{kg}]$
$n(d)$	aggregate number distribution	$[\#\,\mathrm{m^{-4}}]$
n_i	number of primary particles of type i in an aggregate	$[-]$
$n_{i,\mathrm{tot}}$	number of primary particles of type i per unit volume	$[\mathrm{m^{-3}}]$
n_frustule	number of diatom frustules per unit volume	$[\mathrm{m^{-3}}]$
n_p	total number of primary particles in an aggregate	$[-]$
ν	molecular kinematic viscosity	$[\mathrm{m^2\,s^{-1}}]$
ϕ	aggregate porosity	$[-]$
$\langle\phi\rangle_\mathrm{V}$	volume-weighted mean aggregate porosity	$[-]$
$Q_{10,\mathrm{opal}}$	Q_{10} factor for opal dissolution	$[-]$
$Q_{10,\mathrm{POC}}$	Q_{10} factor for POC remineralization	$[-]$
ρ	ambient water density	$[\mathrm{kg\,m^{-3}}]$
ρ_calc	density of $CaCO_3$	$[\mathrm{kg\,m^{-3}}]$
ρ_det	density of detritus (POM)	$[\mathrm{kg\,m^{-3}}]$
ρ_dust	density of dust	$[\mathrm{kg\,m^{-3}}]$
ρ_f	aggregate density	$[\mathrm{kg\,m^{-3}}]$
ρ_diatom	density of a diatom frustule incl. TEP	$[\mathrm{kg\,m^{-3}}]$
ρ_frustule	density of a diatom frustule incl. water and POM	$[\mathrm{kg\,m^{-3}}]$
ρ_opal	density of opal	$[\mathrm{kg\,m^{-3}}]$
r_opal	dissolution rate of opal	$[\mathrm{s^{-1}}]$
ρ_p	primary particle density	$[\mathrm{kg\,m^{-3}}]$

continued . . .

. . . Table D1 continued

$\langle \rho_p \rangle$	mean primary particle density	$[\mathrm{kg\,m^{-3}}]$
$\rho_{p,i}$	primary particle density of primary particle type i	$[\mathrm{kg\,m^{-3}}]$
Re_p	particle Reynolds number	$[-]$
Re_crit	critical particle Reynolds number for fragmentation	$[-]$
R_calc	carbon mol-to-$CaCO_3$-mass factor	$[\mathrm{kg\,mol^{-1}}]$
R_det	P mol-to-detritus-mass factor	$[\mathrm{kg\,mol^{-1}}]$
R_i	mol-to-mass factor for tracer i	$[\mathrm{kg\,mol^{-1}}]$
R_opal	silicon mol-to-opal-mass factor	$[\mathrm{kg\,mol^{-1}}]$
r_POC	specific POC remineralization rate at reference temperature $T_\mathrm{ref,POC}$	$[\mathrm{s^{-1}}]$
$R_\mathrm{POC,remin}$	total POC remineralization rate	$[\mathrm{s^{-1}}]$
$R_\mathrm{Si:P}$	silicate to phosphate production ratio	$[\mathrm{mol\,mol^{-1}}]$
T	temperature	$[^\circ\mathrm{C}]$
T_eff	transfer efficiency	$[-]$
$T_\mathrm{ref,opal}$	reference temperature for opal dissolution	$[^\circ\mathrm{C}]$
$T_\mathrm{ref,POC}$	reference temperature for POC remineralization	$[^\circ\mathrm{C}]$
V_aq	volume of water in the void of the diatom frustule	$[\mathrm{m^3}]$
V_opal	volume of the opal spherical shell of the diatom frustule	$[\mathrm{m^3}]$
V_POM	volume of POM in the void of the diatom frustule	$[\mathrm{m^3}]$
$V_{p,i}$	volume of primary particle of type i	$[\mathrm{m^3}]$
$w_s(d)$	terminal sinking velocity of aggregates of diameter d	$[\mathrm{m\,s^{-1}}]$
$\bar{w_s}$	concentration-weighted mean sinking velocity for the Martin curve parametrization	$[\mathrm{m\,s^{-1}}]$
$\langle w_s \rangle$	concentration-weighted mean sinking velocity of aggregates	$[\mathrm{m\,s^{-1}}]$
z	depth	$[\mathrm{m}]$
z_0	export depth ($z_0 = 100\,\mathrm{m}$)	$[\mathrm{m}]$
z^*_POC	remineralization length scale for POC	$[\mathrm{m}]$

Author contributions. Joeran Maerz performed the M^{4}AGO model development, the HAMOCC model runs and wrote the manuscript. Katharina D. Six and Irene Stemmler significantly contributed in tuning the M^{4}AGO sinking scheme in HAMOCC and aided during implementation. Soeren Ahmerkamp contributed by significant discussions on aggregates microphysics. All authors of the manuscript critically discussed the presented results and contributed by providing valuable feedback during the manuscript compilation.

Competing interests. The authors declare that they have no conflict of interest.

Disclaimer. -none-

Acknowledgements. The authors thank Thomas Weber for sharing the results on the transfer efficiency, and Adrian Burd for discussion on fractal dimension of aggregates. The authors thank Bo Liu for the internal review and comments on the manuscript. The authors thank the two anonymous reviewers for their constructive and valuable comments on the manuscript. J. Maerz thanks U. Feudel for earlier discussions on the topic of marine aggregates. The *Multiscale Approach on the Role of Marine Aggregates (MARMA)* project is funded by the Max-Planck-Society (MPG). We acknowledge funding from European Union Horizon 2020 research and innovation programme under grant agreement No 641816 (CRESCENDO). This work contributes to the project PalMod of the German Federal Ministry of Education and Research (BMBF) as Research for Sustainability initiative (FONA). Thanks to Thyng et al. (2016) for providing the cmocean colormap. All simulations were performed at the German Climate Computing Center (DKRZ).

References

Adler, P. M.: A study of disaggregation effects in sedimentation, AlChE Journal, 25, 487–493, 1979.

Alldredge, A.: The carbon, nitrogen and mass content of marine snow as a function of aggregate size, Deep-Sea Research I, 45, 529–541, 1998.

Alldredge, A. L. and Gotschalk, C.: In situ settling behaviour of marine snow, Limnol. Oceanogr., 33, 339–351, 1988.

Alldredge, A. L. and Gotschalk, C. C.: The relative contribution of marine snow of different origins to biological processes in coastal waters., Continental Shelf Research, 10, 41–58, 1990.

Alldredge, A. L. and McGillivary, P.: The attachment probabilities of marine snow and their implications for particle coagulation in the ocean, Deep-Sea Research, 38, 431–443, 1991.

Alldredge, A. L., Granata, T. C., Gotschalk, C. C., and Dickey, T. D.: The physical strength of marine snow and its implications for particle disaggregation in the ocean, Limnology and Oceanography, 35, 1415–1428, 1990.

Alldredge, A. L., Passow, U., and Logan, B. E.: The abundance and significance of a class of large, transparent organic particles in the ocean, Deep-Sea Research I, 40, 1131–1140, 1993.

Armbrecht, L. H., Smetacek, V., Assmy, P., and Klaas, C.: Cell death and aggregate formation in the giant diatom Coscinodiscus wailesii (Gran & Angst, 1931), Journal of Experimental Marine Biology and Ecology, 452, 31–39, 2014.

Armbrust, E. V.: The life of diatoms in the world's ocean, Nature, 459, 185–192, 2009.

Armstrong, R. A., Lee, C., Hedges, J. I., Honjo, S., and Wakeham, S. G.: A new, mechanistic model for organic carbon fluxes in the ocean based on the quantitative association of POC with ballast minerals, Deep-Sea Research II, 49, 219–236, 2002.

Assmy, P., Smetacek, V., Montresor, M., Klaas, C., Henjes, J., Strass, V. H., Arieta, J. M., Bathmann, U., Berg, G. M., Breitbarth, E., Cisewski, B., Friedrichs, L., Fuchs, N., Herndl, G. J., Jansen, S., Krägefsky, S., Latasa, M., Peeken, I., Röttgers, R., Scharek, R., Schüller, S. E., Steigenberger, S., Webb, A., and Wolf-Gladrow, D.: Thick-shelled, grazer protected diatoms decouple ocean carbon and silicon cycles in the iron-limited Antarctic Circumpolar Current, PNAS, 2013.

Azam, F. and Malfatti, F.: Microbial structuring of marine ecosystems, Nature, 5, 782–791, 2007.

Azetsu-Scott, K. and Passow, U.: Ascending marine particles: Significance of transparent exopolymer particles (TEP) in the upper ocean, Limnol. Oceanogr., 49, 741–748, 2004.

Bach, L. T., Boxhammer, T., Larsen, A., Hildebrandt, N., Schulz, K. G., and Riebesell, U.: Influence of plankton community structure on the sinking velocity of marine aggregates, Global Biogeochemical Cycles, 30, 2016.

Bagster, D. F. and Tomi, D.: The stresses within a sphere in simple flow fields, Chemical Engineering Science, 29, 1773–1783, 1974.

Balch, W. M., Bowler, B. C., Drapeau, D. T., Poulton, A. J., and Holligan, P. M.: Biominerals and the vertical flux of particulate organic carbon from the surface ocean, Geophysical Research Letters, 37, L22 605, 2010.

Berelson, W. M., Balch, W. M., Najjar, R., Feely, R. A., Sabine, C., and Lee, K.: Relating estimates of $CaCO_3$ production, export, and dissolution in the water column to measurements of $CaCO_3$ rain into sediment traps and dissolution on the sea floor: A revised global carbonate budget, Global Biogeochemical Cycles, 21, GB1024, https://doi.org/10.1029/2006GB002803, 2007.

Bidle, K. D., Manganelli, M., and Azam, F.: Regulation of oceanic silicon and carbon preservation by temperature control on bacteria, Science, 298, 1980–1984, 2002.

Biermann, A. and Engel, A.: Effect of CO_2 on the properties and sinking velocity of aggregates of the coccolithophore *Emiliana huxleyi*, Biogeosciences, 7, 1017–1029, 2010.

Bisson, K. M., Siegel, D. A., DeVries, T., Cael, B. B., and Buesseler, K. O.: How data set characteristics influence ocean carbon export models, Global Biogeochemical Cycles, 32, https://doi.org/10.1029/2018GB005934, 2018.

Block, A., von Bloh, W., and Schellnhuber, H. J.: Aggregation by attractive particle-cluster interaction, J. Phys. A: Math. Gen, 24, L1037–L1044, 1991.

Bopp, L., Resplandy, L., Orr, J. C., Doney, S. C., Dunne, J. P., Gehlen, M., Halloran, P., Heinze, C., Ilyina, T., Séférian, R., Tjiputra, J., and Vichi, M.: Multiple stressors of ocean ecosystems in the 21st century: projections with CMIP5 models, Biogeosciences, 10, 6225–6245, 2013.

Boyd, P. and Newton, P.: Evidence of the potential influence of planctonic community structure on the interannual variability of particulate organic carbon flux, Deep-Sea Research I, 42, 619–639, 1995.

Boyd, P. W., Ellwood, M. J., Tagliabue, A., and Twining, B. S.: Biotic and abiotic retention, recycling and remineralization of metals in the ocean, Nature Geoscience, 10, 167–174, 2017.

Boyd, P. W., Claustre, H., Levy, M., Siegel, D. A., and Weber, T.: Multi-faceted particle pumps drive carbon sequestration in the ocean , Nature, 568, 327–335, 2019.

Boyer, T. P., Antonov, J. I., Baranova, O. K., Coleman, C., Garcia, H. E., Grodsky, A., Johnson, D. R., Locarnini, R. A., Mishonov, A. V., O'Brien, T. D., Paver, C. R., Reagan, J. R., Seidov, D., Smolyar, I. V., and Zweng, M. M.: World Ocean Database 2013, Tech. rep., NOAA National Oceanic and Atmospheric Administration, http://doi.org/10.7289/V5NZ85MT, 2013.

Brakalov, L. B.: A connection between the orthokinetic coagulation capture efficiency of aggregates and their maximum size, Chemical Engineering Science, 42, 2373–2383, 1987.

Brandt, P., Greatbatch, R. J., Claus, M., Didwischus, S.-H., Hormann, V., Funk, A., Hahn, J., Krahmann, G., Fischer, J., and Körtzinger, A.: Ventilation of the equatorial Atlantic by the equatorial deep jets, Journal of Geophysical Research, 117, https://doi.org/10.1029/2012JC008118, 2012.

Brzezinski, M. A.: The Si:C:N ratio of marine diatoms: interspecific variability and the effect of some environmental variables, J. Phycol., 21, 347–357, 1985.

Buesseler, K. O.: The decoupling of production and particulate export in the surface ocean, Global Biogeochemical Cycles, 12, 297–310, 1998.

Buesseler, K. O. and Boyd, P. W.: Shedding light on processes that control particle export and flux attenuation in the twilight zone of the open ocean, Limnol. Oceanogr., 54, 1210–1232, 2009.

Bushell, G. and Amal, R.: Fractal aggregates of polydisperse particles, Journal of Colloid and Interface Science, 205, 459–469, 1998.

Cael, B. B. and Bisson, K.: Particle flux parameterizations: quantitative and mechanistic similarities and differences, frontiers in MARINE SCIENCE, 5, 395, https://doi.org/10.3389/fmars.2018.00395, 2018.

Carr, M.-E., Friedrich, M. A. M., Schmeltz, M., Aita, M. N., Antoine, D., Arrigo, K. R., Asanuma, I., Aumont, O., Barber, R., Behrenfeld, M., Bidigare, R. E. T., Campbell, J., Ciotti, A., Dierssen, H., Dowell, M., Dunne, J., Esaias, W., Gentili, B., Gregg, W., Groom, S., Hoepffner, N., Ishizaka, J., Kameda, T., Le Quéré, C., Lohrenz, S., Marra, J., Mélin, F., Moore, K., Morel, A., Reddy, T. E., Ryan, J., Scardi, M., Smyth, T., Turpie, K., Tilstone, G., Waters, K., and Yamanaka, Y.: A comparison of global estimates of marine primary production from ocean color, Deep-Sea Research, 53, 741–770, 2006.

Cram, J. A., Weber, T., Leung, S. W., McDonnell, A. M. P., Liang, J.-H., and Deutsch, C.: The role of particle size, ballast, temperature, and oxygen in the sinking flux to the deep sea, Global Biogeochemical Cycles, 2018.

Dam, H. G. and Drapeau, D. T.: Coagulation efficiency, organic-matter glues and the dynamics of particles during a phytoplankton bloom in a mesocoms study, Deep-Sea Research II, 42, 111–123, 1995.

Daufresne, M., Lengfeller, K., and Sommer, U.: Global warming benefits the small in aquatic ecosystems, PNAS, 106, 12 788–12 793, 2009.

De La Rocha, C. L. and Passow, U.: Factors influencing the sinking of POC and the efficiency of the biological carbon pump, Deep-Sea Research II, 54, 639–658, 2007.

De La Rocha, C. L., Nowald, N., and Passow, U.: Interactions between diatom aggregates, minerals, particulate organic carbon, and dissolved organic matter: Further implications for the ballast hypothesis, Global Biogeochemical Cycles, 22, 2008.

Decho, A. W.: Microbial exopolymer secretions in oceanic environments: their role(s) in food webs and marine processes, Oceanogr. Mar. Biol. Annu. Rev., 28, 73–153, 1990.

Dell, A. I., Pawar, S., and Savage, V. M.: Systematic variation in the temperature dependence of physiological and ecological traits, PNAS, 108, 10 591–10 596, 2011.

DeVries, T. and Weber, T.: The export and fate of organic matter in the ocean: New constraints from combining satellite and oceanographic tracer observations, Global Biogeochemical Cycles, 31, 535–555, 2017.

DeVries, T., Liang, J.-H., and Deutsch, C.: A mechanistic particle flux model applied to the oceanic phosporus cycle, Biogeosciences, 11, 5381–5398, 2014.

Dietze, H. and Loeptien, U.: Revisiting "nutrient trapping" in global coupled biogeochemical ocean circulation models, Global Biogeochemical Cycles, 27, 1–20, https://doi.org/10.1002/gbc.20029, 2013.

Dilling, L. and Alldredge, A. L.: Fragmentation of marine snow by swimming macrozooplankton: A new process impacting carbon cycling in the sea, Deep-Sea Research I, 47, 1227–1245, 2000.

Dunne, J. P., Armstrong, R. A., Gnanadesikan, A., and Sarmiento, J. L.: Empirical and mechanistic models for the particle export ratio, Global Biogeochemical Cycles, 19, GB4026, 2005.

Eisma, D.: Flocculation and de-flocculation of suspended matter in estuaries, Netherlands Journal of Sea Research, 20, 183–199, 1986.

Engel, A., Thoms, S., Riebesell, U., Rochelle-Newall, E., and Zondervan, I.: Polysaccharide aggregation as a potential sink of marine dissolved organic carbon, Nature, 428, 929–932, 2004.

Engel, A., Szlosek, J., Abramson, L., Liu, Z., and Lee, C.: Investigating the effect of ballasting by $CaCO_3$ in *Emiliania huxleyi*, I. Formation, settling velocities and physical properties of aggregates, Deep-Sea Research II, 56, 1396–1407, 2009.

England, M. H. and Maier-Reimer, E.: Using chemical tracers to assess ocean models, Reviews of Geophysics, 39, 29–70, 2001.

Falkowski, P. G., Barber, R. T., and Smetacek, V.: Biogeochemical Controls and Feedbacks on Ocean Primary Productivity, Science, 281, 200–206, 1998.

Fettweis, M.: Uncertainty of excess density and settling velocity of mud flocs derived from in situ measurements, Estuar Coast Shelf S, 78, 426–436, 2008.

Filella, M.: Colloidal properties of submicron particles in natural waters, in: Environmental Colloids and Particles: Behaviour, Separation and Characterisation, IUPAC Series on Analytical and Physical Chemistry of Environmental Systems, chap. 2, pp. 17–93, John Wiley & Sons, Inc., 2007.

Fischer, G. and Karakaş, G.: Sinking rates and ballast composition of particles in the Atlantic Ocean: implications for the organic carbon fluxes to the deep ocean, Biogeosciences, 6, 85–102, 2009.

Fischer, G., Romero, O., Merkel, U., Donner, B., Iversen, M., Nowald, N., Ratmeyer, V., Ruhland, G., Klann, M., and Wefer, G.: Deep ocean mass fluxes in the coastal upwelling off Mauritania from 1988 to 2012: variability on seasonal to decadal timescales, Biogeosciences, 13, 3071 – 3090, 2016.

Francois, R., Honjo, S., Krishfield, R., and Manganini, S.: Factors controlling the flux of organic carbon to the bathypelagic zone of the ocean, Global Biogeochemical Cycles, 16, 2002.

Garcia, H. E., Locarnini, R. A., Boyer, T. P., Antonov, J. I., Baranova, O. K., Zweng, M. M., Reagan, J. R., and Johnson, D. R.: World Ocean Atlas 2013, NOAA Atlas NESDIS 75, Volume 3: Dissolved Oxygen, Apparent Oxygen Utilization, and Oxygen Saturation, 27pp, 2014a.

Garcia, H. E., Locarnini, R. A., Boyer, T. P., Antonov, J. I., Baranova, O. K., Zweng, M. M., Reagan, J. R., and Reagan, D. R.: World Ocean Atlas 2013, NOAA Atlas NESDIS 76, Volume 4: Dissolved Inorganic Nutrients (phosphate, nitrate, silicate), 25pp, 2014b.

Gehlen, M., Bopp, L., Emprin, N., Aumont, O., Heinze, C., and Ragueneau, O.: Reconciling surface ocean productivity, export fluxes and sediment composition in a global biogeochemical ocean model, Biogeosciences, 3, 521–537, 2006.

Giering, S. L. C., Sanders, R., Martin, A. P., Henson, S. A., Riley, J. S., Marsay, C. M., and Johns, D. G.: Particle flux in the oceans: Callenging the steady state assumption, Global Biogeochemical Cycles, 31, 159–171, 2017.

Gloor, M., Gruber, N., Sarmiento, J., Sabine, C. L., Feely, R. A., and Rödenbeck, C.: A first estimate of present and preindustrial air-sea CO_2 flux patterns based on ocean interior carbon measurements and models, Geophysical Research Letters, 30, 1010, https://doi.org/10.1029/2002GL015594, 2003.

Guidi, L., Jackson, G. A., Stemmann, L., Miquel, J. C., Picheral, M., and Gorsky, G.: Relationship between particle size distribution and flux in the mesopelagic zone, Deep-Sea Research I, 55, 1364–1374, 2008.

Guidi, L., Stemmann, L., Jackson, G. A., Ibanez, F., Claustre, H., Legendre, L., Picheral, M., and Gorsky, G.: Effects of phytoplankton community on production, size and export of large aggregates: A world-ocean analysis, Limnol. Oceanogr., 54, 1951–1963, 2009.

Guidi, L., Chaffron, S., Bittner, L., Eveillard, D., Larhlimi, A., Roux, S., Darzi, Y., Audic, S., Berline, L., Brum, J. R., Coelho, L. P., Espinoza, J. C. I., Malviya, S., Sunagawa, S., Dimier, C., Kandels-Lewis, S., Picheral, M., Poulain, J., Searson, S., *Tara* Oceans Consortium Coordinators, Stemmann, L., Not, F., Hingamp, P., Speich, S., Follows, M., Karp-Boss, L., Boss, E., Ogata, H., Pesant, S., Weissenbach, J., Wincker, P., Acinas, S. G., Bork, P., de Vargas, C., Iudicone, D., Sullivan, M. B., Raes, J., Karsenti, E., Bowler, C., and Gorsky, G.: Plankton networks driving carbon export in the oligotrophic ocean, Nature, 532, 465–481, 2016.

Hamm, C. E.: Interactive aggregation and sedimentation of diatoms and clay-sized lithogenic material, Limnol. Oceanogr., 47, 1790–1795, 2002.

Hansen, J. L. S. and Kiørboe, T.: Quantifying interspecific coagulation efficiency of phytoplankton, Marine Ecology Progress Series, 159, 75–79, 1997.

Hedges, J. L., Baldock, J. A., Gélinas, Y., Lee, C., Peterson, M., and Wakeham, S. G.: Evidence for non-selective preservation of organic matter in sinking marine particles, Nature, 409, 801–804, 2001.

Heinemann, M., Segschneider, J., and Schneider, B.: CO_2 drawdown due to particle ballasting by glacial aeolian dust: an estimate based on the ocean carbon cycle model MPIOM/HAMOCC version 1.6.2p3, Geoscientific Model Development, 12, 1869–1883, https://doi.org/10.5194/gmd-2018-137, 2019.

Heinze, C., Maier-Reimer, E., Winguth, A. M. E., and Archer, D.: A global oceanic sediment model for long-term climate studies, Global Biogeochemical Cycles, 13, 221–250, 1999.

Henderiks, J.: Coccolithophore size rules - Reconstructing ancient cell geometry and cellular calcite quota from fossil coccoliths, Marine Micropaleontology, 67, 143–154, 2008.

Henderiks, J. and Pagani, M.: Coccolithophore cell size and the Paleogene decline in atmopheric CO_2, Earth and Planetary Science Letters, 269, 576–584, 2008.

Henson, S. A., Sanders, R., Madsen, E., Morris, P. J., Le Moigne, F., and Quartly, G. D.: A reduced estimate of the strength of the ocean's biological carbon pump, Geophysical Research Letters, 38, L04 606, 2011.

Henson, S. A., Sanders, R., and Madsen, E.: Global patterns in efficiency of particulate organic carbon export and transfer to the deep ocean, Global Biogeochemical Cycles, 265, 2012.

Hill, P. S.: Controls on floc size in the sea, Oceanography, 11, 13–18, 1998.

Honjo, S.: Coccoliths: Production, transportation and sedimentation, Marine Micropaleontology, 1, 65–79, 1976.

Ilyina, T. and Friedlingstein, P.: WCRP Grand Challenge - Carbon feedbacks in the climate system, Tech. rep., WCRP, https://www.wcrp-climate.org/JSC37/Documents/BGCGC_whitepaper_submission.pdf, 2016.

Ilyina, T., Six, K. D., Segschneider, J., Maier-Reimer, E., Li, H., and Núñez-Riboni, I.: Global ocean biogeochemistry model HAMOCC: Model architecture and performance as component of the MPI-Earth system model in different CMIP5 experimental realizations, Journal of Advances in Modeling Earth Systems, 5, 1–29, 2013.

Iversen, M. H. and Ploug, H.: Ballast minerals and the sinking carbon flux in the ocean: carbon-specific respiration rates and sinking velocity of marine snow aggregates, Biogeosciences, 7, 2613–2624, 2010.

Iversen, M. H. and Ploug, H.: Temperature effects on carbon-specific respiration rate and sinking velocity of diatom aggregates – potential implications deep ocean export processes, Biogeosciences, 10, 4073–4085, 2013.

Iversen, M. H. and Robert, M. L.: Ballasting effects of smectite on aggregate formation and export from a natural plankton community, Marine Chemistry, 175, 18–27, 2015.

Jackson, G. A.: A model of the formation of marine algal flocs by physical coagulation processes, Deep-Sea Research, 37, 1197–1211, 1990.

Jackson, G. A.: Using fractal scaling and two-dimensional particle size spectra to calculate coagulation rates for heterogeneous systems, Journal of Colloid and Interface Science, 202, 20–29, 1998.

Jiang, Q. and Logan, B. E.: Fractal dimension of aggregates determined from steady-state size distributions., Environ. Sci. Technol., 25, 2031–2038, 1991.

Jokulsdottir, T. and Archer, D.: A stochastic, Lagrangian model of sinking biogenic aggregates in the ocean (SLAMS 1.0): model formulation, validation and sensitivity , Geoscientific Model Development, 9, 1455–1476, https://doi.org/10.5194/gmd-9-1455-2016, 2016.

Jungclaus, J. H., Fischer, N., Haak, H., Lohmann, K., Marotzke, J., Matei, D., Mikolajewicz, U., Notz, D., and von Storch, J. S.: Characteristics of the ocean simulations in the Max Planck Institute Ocean Model (MPIOM) the ocean component of the MPI-Earth system model, Journal of Advances in Modeling Earth Systems, 5, 422–446, https://doi.org/10.1002/jame.20023, 2013.

Khelifa, A. and Hill, P. S.: Models for effective density and settling velocity of flocs, Journal of Hydraulic Research, 44, 390–401, 2006.

Kiørboe, T., Andersen, K. P., and Dam, H. G.: Coagulation efficiency and aggregate formation in marine phytoplankton, Marine Biology, 107, 235–245, 1990.

Kiørboe, T., Ploug, H., and Thygesen, U. H.: Fluid motion and solute distribution around sinking aggregates. I. Small-scale fluxes and heterogeneity of nutrients in the pelagic environment, Marine Ecology Progress Series, 211, 1–13, 2001.

Klaas, C. and Archer, D. E.: Association of sinking organic matter with various types of mineral ballast in the deep sea: Implications for the rain ratio, Global Biogeochemical Cycles, 16, 2002.

Kostadinov, T. S., Milutinović, S., Marinov, I., and Cabré, A.: Carbon-based phytoplankton size classes retrieved via ocean color estimates of the particle size distribution, Ocean Science Discussions, 12, 561–575, 2016.

Kranenburg, C.: The fractal structure of cohesive sediment aggregates, Estuarine, Coastal and Shelf Science, 39, 451–460, 1994.

Kranenburg, C.: Effects of floc strength on viscosity and deposition of cohesive sediment suspensions, Continental Shelf Research, 19, 1665–1680, 1999.

Kriest, I. and Evans, G. T.: Representing phytoplankton aggregates in biogeochemical models, Deep-Sea Research I, 46, 1841–1859, 1999.

Kriest, I. and Oschlies, A.: On the treatment of particulate organic matter sinking in large-scale models of marine biogeochemical cycles, Biogeosciences, 5, 55–72, 2008.

Lam, P. J. and Marchal, O.: Insights into particle cycling from thorium and particle data, Ann. Rev. Mar. Sci., 7, 159–184, 2015.

Lam, P. J., Doney, S. C., and Bishop, J. K. B.: The dynamic ocean biological pump: Insights from a global compilation of particulate organic carbon, $CaCO_3$, and opal concentration profiles from the mesopelagic, Global Biogeochemical Cycles, 25, http://dx.doi.org/10.1029/2010GB003868, 2011.

Laurenceau-Cornec, E. C., Trull, T. W., Davies, D. M., De La Rocha, C. L., and Blain, S.: Phytoplankton morphology controls on marine snow sinking velocity, Marine Ecology Progress Series, 520, 35–56, 2015.

Laurenceau-Cornec, E. C., Le Moigne, F. A. C., Gallinari, M., Moriceau, B., Toullec, J., Iversen, M. H., Engel, A., and De La Rocha, C. L.: New guidelines for the application of Stokes' models to the sinking velocity of marine aggregates, Limnol. Oceanogr., https://doi.org/10.1002/lno.11388, 2019.

Lauvset, S. K., Key, R. M., Olsen, A., van Heuven, S., Velo, A., Lin, X., Schirnick, C., Kozyr, A., Tanhua, T., Hoppema, M., Jutterström, S., Steinfeldt, R., Jeansson, E., Ishii, M., Perez, F. F., Suzuki, T., and Watelet, S.: A new global interior ocean mapped climatology: the 1 ° x 1 ° GLODAP version 2, Earth Syst. Sci. Data, 8, 325–340, https://doi.org/10.5194/essd-8-325-2016, 2016.

Laws, E. A., Falkowski, P. G., Smith Jr., W. O., Ducklow, H., and McCarthy, J. J.: Temperature effects on export production in the open ocean, Global Biogeochemical Cycles, 14, 1231–1246, 2000.

Le Moigne, F. A. C., Cisternas-Novoa, C., Piontek, J., Maßmig, M., and Engel, A.: On the effect of low oxygen concentrations on bacterial degradation of sinking particles, Scientific Reports, 7, 16 722, https://doi.org/10.1038/s41598-017-16903-3, 2017.

Lefort, S., Aumont, O., Bopp, L., Arsouze, T., Gehlen, M., and Maury, O.: Spatial and body-size dependent response of marine pelagic communities to projected global climate change, Global Change Biology, 21, 154–164, https://doi.org/10.1111/gcb.12679, 2015.

Lewin, J. C.: The dissolution of silica from diatom walls, Geochimica et Cosmochimica Acta, 21, 182–198, 1961.

Li, X. and Logan, B. E.: Size distributions and fractal properties of particles during a simulated phytoplankton bloom in a mesocosm, Deep-Sea Research II, 42, 125–138, 1995.

Litchman, E., Klausmeier, C. A., and Yoshiyama, K.: Contrasting size evolution in marine and freshwater diatoms , PNAS, 106, 2665–2670, 2009.

Liu, J., Shih, W. Y., Sarikaya, M., and Aksay, I. A.: Fractal colloidal aggregates with finite interparticle interactions: Energy dependence of the fractal dimension, Physical Review A, 41, 1990.

Logan, B. E. and Alldredge, A. L.: Potential for increased nutrient uptake by flocculating diatoms, Marine Biology, 101, 443–450, 1989.

Logan, B. E. and Wilkinson, D. B.: Fractal geometry of marine snow and other biological aggregates, Limnol. Oceanogr., 35, 130–136, 1990.

Löscher, C. R., Bange, H. W., Schmitz, R. A., Callbeck, C. M., Engel, A., Hauss, H., Kanzow, T., Kiko, R., Lavik, G., Loginova, A., Melzner, F., Meyer, J., Neulinger, S. C., Pahlow, M., Riebesell, U., Schunck, H., Thomsen, S., and Wagner, H.: Water column biogeochemistry of oxygen minimum zones in the eastern tropical North Atlantic and eastern tropical South Pacific oceans, Biogeosciences, 13, 3585–3606, 2016.

Lutz, M., Dunbar, R., and Caldeira, K.: Regional variability in the vertical flux of particulate organic carbon in the ocean interior, Global Biogeochemical Cycles, 16, 2002.

Lutz, M. J., Caldeira, K., Dunbar, R. B., and Behrenfeld, M. J.: Seasonal rhythms of net primary production and particulate organic carbon flux to depth describe the efficiency of biological pump in the global ocean, Journal of Geophysical Research, 112, https://doi.org/10.1029/2006JC003706, 2007.

Maggi, F.: Biological flocculation of suspended particles in nutrient-rich aqueous ecosystems, Journal of Hydrology, 376, 116–125, 2009.

Maher, B. A., Prospero, J. M., Mackie, D., Gaiero, D., Hesse, P. P., and Balkanski, Y.: Global connections between aeolian dust, climate and ocean biogeochemistry at the present day and at the last glacial maximum , Earth-Science Reviews, 99, 61–97, 2010.

Mahowald, N., Albani, S., Kok, J. F., Engelstaeder, S., Scanza, R., Ward, D. S., and Flanner, M. G.: The size distribution of desert dust aerosols and its impact on the Earth system, Aeolian Research, 15, 53–71, 2014.

Mari, X., Passow, U., Migon, C., Burd, A. B., and Legendre, L.: Transparent exopolymer particles: Effects on carbon cycling in the ocean, Progress in Oceanography, 151, 13–37, 2017.

Marsay, C. M., Sanders, R. J., Henson, S. A., Pabortsava, K., Achterberg, E. P., and Lampitt, R. S.: Attenuation of sinking particulate organic carbon flux through the mesopelagic ocean, PNAS, 112, 1089–1094, 2015.

Marsland, S. J., Haak, H., Jungclaus, J. H., Latif, M., and Röske, F.: The Max-Planck-Institute global ocean/sea ice model with orthogonal curvilinear coordinates, Ocean Modelling, 5, 91–127, 2003.

Martin, J. H., Knauer, G. A., Karl, D. M., and Broenkow, W. W.: VERTEX: carbon cycling in the northeast Pacific, Deep-Sea Research, 34, 267–285, 1987.

Martin, P., Lampitt, R. S., Perry, M. J., Sanders, R., Lee, C., and D'Asaro, E.: Export and mesopelagic particle flux during a North Atlantic spring diatom bloom, Deep-Sea Research I, 58, 338–349, 2011.

Matthäus, W.: Die Viskosität des Meerwassers. , Beiträge zur Meereskunde, 29 (in German), 1972.

Mauritsen, T., Bader, J., Becker, T., Behrens, J., Bittner, M., Brokopf, R., Brovkin, V., Claussen, M., Crueger, T., Esch, M., Fast, I., Fiedler, S., Fläschner, D., Gayler, V., Giorgetta, M., Goll, D. S., Haak, H., Hagemann, S., Hedemann, C., Hohenegger, C., Ilyina, T., Jahns, T., Jimenéz-de-la Cuesta, D., Jungclaus, J., Kleinen, T., Kloster, S., Kracher, D., Kinne, S., Kleberg, D., Lasslop, G., Kornblueh, L., Marotzke, J., Matei, D., Meraner, K., Mikolajewicz, U., Modali, K., Möbis, B., Müller, W. A., Nabel, J. E. M. S., Nam, C. C. W., Notz, D., Nyawira, S.-S., Paulsen, H., Peters, K., Pincus, R., Pohlmann, H., Pongratz, J., Popp, M., Raddatz, T. J., Rast, S., Redler, R., Reick, C. H., Rohrschneider, T., Schemann, V., Schmidt, H., Schnur, R., Schulzweida, U., Six, K. D., Stein, L., Stemmler, I., Stevens, B., von Storch, J.-S., Tian, F., Voigt, A., Vrese, P., Wieners, K.-H., Wilkenskjeld, S., Winkler, A., and Roeckner, E.: Developments in the MPI-M Earth System Model version 1.2 (MPI-ESM1.2) and Its Response to Increasing CO_2, Journal of Advances in Modeling Earth Systems, 11, 1–41, https://doi.org/10.1029/2018MS001400, 2019.

McCave, I. N.: Size spectra and aggregation of suspended particles in the deep ocean, Deep-Sea Research, 31, 329–352, 1984.

Meakin, P.: Models for colloidal aggregation, Ann. Rev. Phys. Chem., 39, 237–267, 1988.

Mikaloff Fletcher, S. E., Gruber, N., Jacobson, A. R., Gloor, M., Doney, S. C., Dutkiewicz, S., Gerber, M., Follows, M., Joos, F., Lindsay, K., Menemenlis, D., Mouchet, A., Müller, S. A., and Sarmiento, J. L.: Inverse estimates of the oceanic sources and sinks of natural CO_2 and the implied oceanic carbon transport, Global Biogeochemical Cycles, 21, https://doi.org/10.1029/2006GB002751, 2007.

Miklasz, K. A. and Denny, M. W.: Diatom sinking speeds: Improved predictions and insights from a modified Stokes' law, Limnol. Oceanogr., 55, 2513–2525, 2010.

Milinski, S., Bader, J., Haak, H., Siongco, A. C., and Jungclaus, J. H.: High atmospheric horizontal resolution eliminates the wind-driven coastal warm bias in the southeastern tropical Atlantic, Geophysical Research Letters, 43, 10 455–10 462, https://doi.org/10.1002/2016GL070530, 2016.

Mislan, K. A. S., Stock, C. A., Dunne, J. P., and Sarmiento, J.: Group behaviour among model bacteria influences particulate carbon mineralization depths, Journal of Marine Research, 72, 183–218, 2014.

Mouw, C. B., Barnett, A., McKinley, G. A., Gloege, L., and Pilcher, D.: Global ocean particulate organic carbon flux merged with satellite parameters, Earth Syst. Sci. Data, 8, 531–541, 2016a.

Mouw, C. B., Barnett, A., McKinley, G. A., Gloege, L., and Pilcher, D.: Global Ocean Particulate Organic Carbon flux merged with satellite parameters. , PANGAEA, https://doi.org/10.1594/PANGAEA.855600, 2016b.

Najjar, R. G., Jin, X., Louanchi, F., Aumont, O., Caldeira, K., Doney, S. C., Dutay, J.-C., Follows, M., Gruber, N., Joos, F., Lindsay, K., Maier-Reimer, E., Matear, R. J., Matsumoto, K., Monfray, P., Mouchet, A., Orr, J. C., Plattner, G.-K., Sarmiento, J. L., Schlitzer, R., Slater, R. D., Weirig, M. F., Yamanaka, Y., and Yool, A.: Impact of circulation on export production, dissolved organic matter, and dissolved oxygen in the ocean: Results from Phase II of the Ocean Carbon-cycle Model Intercomparison Project (OCMIP-2), Global Biogeochemical Cycles, 21, 2007.

Neuer, S., Davenport, R., Freudenthal, T., Wefer, G., Llinás, O., Rueda, M.-J., Steinberg, D. K., and Karl, D. M.: Differences in the biological carbon pump at three subtropical ocean sites, Geophysical Research Letters, 29, 1885, 2002.

Nicolás-Carlock, J. R., J.L.Carrillo-Estrada, and Dossetti, V.: Fractality à la carte: a general particle aggregation model, Scientific Reports, 6, 19 505, 2016.

Passow, U.: Transparent exopolymer particles (TEP) in aquatic environments, Progress in Oceanography, 55, 287–333, 2002.

Passow, U.: Switching perspectives: Do mineral fluxes determine particulate organic carbon fluxes or vice versa?, Geochemistry Geophysics Geosystems, 5, 2004.

Passow, U. and De La Rocha, C. L.: Accumulation of mineral ballast on organic aggregates, Global Biogeochemical Cycles, 20, 2006.

Paulsen, H., Ilyina, T., Six, K. D., and Stemmler, I.: Incorporating a prognostic representation of marine nitrogen fixers into the global ocean biogeochemical model HAMOCC , Journal of Advances in Modeling Earth Systems, 9, 2017.

Paulsen, H., Ilyina, T., Jungclaus, J. H., Six, K. D., and Stemmler, I.: Light absorption by marine cyanobacteria affects tropical climate mean state and variability, Earth Syst. Dynam., 9, 1283–1300, https://doi.org/10.5194/esd-9-1283-2018, 2018.

Ploug, H., Iversen, M. H., and Fischer, G.: Ballast, sinking velocity, and apparent diffusivity within marine snow and zooplankton fecal pellets: Implications for substrate turnover by attached bacteria, Limnol. Oceanogr., 53, 1878–1886, 2008.

Ragueneau, O., Teguér, P., Leynaert, A., Anderson, R. F., Brzezinski, M. A., DeMaster, D. J., Dugdale, R. C., Dymond, J., Fischer, G., François, R., Heinze, C., Maier-Reimer, E., Martin-Jézéquel, V., Nelson, D. M., and Quéguiner, B.: A review of the Si cycle in the modern ocean: recent progress and missing gaps in the application of biogenic opal as a paleoproductivity proxy, Global and Planetary Change, 26, 317–365, 2000.

Ragueneau, O., Schultes, S., Bidle, K., Claquin, P., and Moriceau, B.: Si and C interactions in the world ocean: Importance of ecological processes and implications for the role of diatoms in the biological pump, Global Biogeochemical Cycles, 20, 2006.

Read, B. A., Kegel, J., Klute, M. J., Kuo, A., Lefebvre, S. C., Maumus, F., Mayer, C., Miller, J., Monier, A., Salamov, A., Young, J., Aguilar, M., Claverie, J.-M., Frickenhaus, S., Gonzalez, K., Herman, E. K., Lin, Y.-C., Napier, J., Ogata, H., Sarno, A. F., Shmutz, J., Schroeder, D., de Vargas, C., Verret, F., von Dassow, P., Valentin, K., Van de Peer, Y., Wheeler, G., Consortium, E. h. A., Allen, A. E., Bidle, K., Borodovsky, M., Bowler, C., Brownlee, C., Mark, C. J., Elias, M., Gladyshev, V. N., Groth, M., Guda, C., Hadaegh,

A., Debora Iglesias-Rodriguez, M., Jenkins, J., Jones, B. M., Lawson, T., Leese, F., Lindquist, E., Lobanov, A., Lomsadze, A., Malik, S.-B., Marsh, M. E., Mackinder, L., Mock, T., Mueller-Roeber, B., Pagarete, A., Parker, M., Probert, I., Quesneville, H., Raines, C., Rensing, S. A., Riaño-Pachón, D. M., Richier, S., Rokitta, S., Shiraiwa, Y., Soanes, D. M., van der Giezen, M., Wahlund, T. M., Williams, B., Wilson, W., Wolfe, G., Wurch, L. L., Dacks, J. B., Delwiche, C. F., Dyhrman, S. T., Glöckner, G., John, U., Richards, T., Worden, A. Z., Zhang, X., and Grigoriev, I. V.: Pan genome of the phytoplankton Emiliania underpins its global distribution, Nature, 499, 209, https://doi.org/10.1038/nature12221, https://www.nature.com/articles/nature12221#supplementary-information, 2013.

Röske, F.: Global oceanic heat and fresh water forcing datasets based on ERA-40 and ERA-15, Tech. Rep. 13, Max Planck Institue for Meteorology, 2005.

Roullier, F., Berline, L., Guidi, L., Durrieu De Madron, X., Picheral, M., Sciandra, A., Pesant, S., and Stemmann, L.: Particle size distribution and estimated carbon flux across the Arabian Sea oxygen minimum zone, Biogeosciences, 11, 4541–4557, 2014.

Sarmiento, J. L., Monfray, P., Maier-Reimer, E., Aumont, O., Murnane, R. J., and Orr, J. C.: Sea-air CO_2 fluxes and carbon transport: A comparison of three ocean general circulation models, Global Biogeochemical Cycles, 14, 1267–1281, 2000.

Schwinger, J., Goris, N., Tjiputra, J. F., Kriest, I., Bentsen, M., Bethke, I., Ilicak, M., Assmann, K. M., and Heinze, C.: Evaluation of NorESM-OC (versions 1 and 1.2), the ocean carbon-cycle stand-alone configuration of the Norwegian Earth System Model (NorESM1), Geoscientific Model Development, 9, 2589–2633, 2016.

Segschneider, J. and Bendtsen, J.: Temperature-dependent remineralization in a warming ocean increases surface pCO_2 through changes in marine ecosystem composition, Global Biogeochemical Cycles, 27, 1214–1225, 2013.

Sherwood, C. R., Aretxabaleta, A. L., Harris, C. K., Rinehimer, J. P., Verney, R., and Ferré, B.: Cohesive and mixed sediment in the Regional Ocean Modeling System (ROMS v3.6) implemented in the Coupled Ocean-Athmosphere-Wave-Sediment Transport Modeling System (COAWST r1234), Geoscientific Model Development, 11, 1849–1871, 2018.

Shigemitsu, M., Yamamoto, A., Oka, A., and Yamanaka, Y.: One possible uncertainty in CMIP5 projections of low-oxygen water volume in the Eastern Tropical Pacific, Global Biogeochemical Cycles, 31, 804–820, https://doi.org/10.1002/2016GB005447, 2017.

Siegel, D. A., Buesseler, K. O., Doney, S. C., Sailley, S. F., Behrenfeld, M. J., and Boyd, P. W.: Global assessment of ocean carbon export by combining satellite observations and food-web models, Global Biogeochemical Cycles, 28, 181–196, 2014.

Simmons, A. J. and Gibson, J. K.: The ERA-40 Project Report Series 1, Tech. rep., ECMWF, 2000.

Simon, H., Lipsewers, Y. A., Giebel, H.-A., Wiltshire, K. H., and Simon, M.: Temperature effects on aggregation during a spring diatom bloom, Limnol. Oceanogr., 59, 2089–2100, 2014.

Six, K. D. and Maier-Reimer, E.: Effects of plankton dynamics on seasonal carbon fluxes in an ocean general circulation model, Global Biogeochemical Cycles, 10, 559–583, 1996.

Stemmann, L., Jackson, G. A., and Ianson, D.: A vertical model of particle size distributions and fluxes in the midwater column that includes biological and physical processes—Part I: model formulation, Deep-Sea Research I, 51, 865–884, 2004.

Stokes, G. G.: On the effect of the internal friction of fluids on the motion of pendulums, Cambridge Philos Trans, IX, 8–106, reprinted in Mathematical and Physical Papers, 2nd ed., Vol. 3 New York: Johnson Reprint Corp., p 1, 1966, 1851.

Takahashi, T., Broecker, W. S., and Langer, S.: Redfield ratio based on chemical data from isopycnical surfaces, Journal of Geophysical Research, 90, 6907–6924, 1985.

Tambo, N. and Hozumi, H.: Physical aspect of flocculation process-II. Contact flocculation, Water Research, 13, 441–448, 1979.

Taylor, K. E.: Summarizing multiple aspects of model performance in a single diagram, Journal of Geophysical Research, 106, 7183–7192, 2001.

Thornton, D. C. O.: Diatom aggregation in the sea: mechanisms and ecological implications, Eur. J. Phycol., 37, 149–161, 2002.

Thyng, K. M., Greene, C. A., Hetland, R. D., Zimmerle, H. M., and DiMarco, S. F.: True colors of oceanography: Guidelines for effective and accurate colormap selection, Oceanography, 29, 9–13, 2016.

Tréguer, P.: Silica and the cycle of carbon in the ocean, Comptes Rendus Geoscience, 334, 3–11, 2002.

Tréguer, P., Bowler, C., Moriceau, B., Dutkiewicz, S., Gehlen, M., Aumont, O., Bittner, L., Dugdale, R., Finkel, Z., Iudicone, D., Jahn, O., Guidi, L., Lasbleiz, M., Leblanc, K., Levy, M., and Pondaven, P.: Influence of diatom diversity on the ocean biological carbon pump, Nature Geoscience, 11, 27–37, 2018.

Usbeck, R., Schlitzer, R., Fischer, G., and Wefer, G.: Particle fluxes in the ocean: comparison of sediment trap data with results from inverse modeling, Journal of Marine Systems, 39, 167–183, 2003.

Verdugo, P., Alldredge, A. L., Azam, F., Kirchman, D. L., Passow, U., and Santschi, P. H.: The oceanic gel phase: a bridge in the DOM-POM continuum, Marine Chemistry, 92, 67–85, 2004.

Villa-Alfagame, M., de Soto, F. C., Ceballos, E., Giering, S. L. C., Le Moigne, F. A. C., Henson, S., Mas, J. L., and Sanders, R. J.: Geographical, seasonal, and depth variation in sinking particle speeds in the North Atlantic, Geophysical Research Letters, 43, 8609–8616, https://doi.org/10.1002/2016GL069233, 2016.

Waterhouse, A. F., MacJinnon, J. A., Nash, J. D., Alford, M. H., Kunze, E., Simmons, H. L., Polzin, K. L., Laurent, L. C. S., Sun, O. M., Pinkel, R., Talley, L. D., Whalen, C. B., Huussen, T. N., Carter, G. S., Fer, I., Waterman, S., Naveira Garabato, A. C., Sanford, T. B., and Lee, C. M.: Global Patterns of Diapycnal Mixing from Measurements of the Turbulent Dissipation Rate, Journal of Physical Oceanography, 44, 1854–1872, 2014.

Weber, T., Cram, J. A., Leung, S. W., DeVries, T., and Deutsch, C.: Deep ocean nutrients imply large latitudinal variation in particle transfer efficiency, PNAS, 113, 8606–8611, 2016.

White, F. M.: Viscous Fluid Flow, McGraw-Hill, 3rd edition edn., 2005.

White, M. M., Waller, J. D., Lubelczyk, L., Drapeau, D. T., Bowler, B. C., Balch, W. M., and Fields, D. M.: Coccolith dissolution within copepod guts affects fecal pellet density and sinking rate, Scientific Reports, 8, 9758, https://doi.org/10.1038/s41598-018-28073-x, 2018.

Williams, R. G. and Follows, M. J.: Ocean Dynamics and the Carbon Cycle: Principles and Mechanisms, Cambridge University Press, 2011.

Wilson, J. D., Barker, S., and Ridgwell, A.: Assessment of the spatial variability in particulate organic matter and mineral sinking fluxes in the ocean interior: Implications for the ballast hypothesis, Global Biogeochemical Cycles, 26, GB4011, 2012.

Winterwerp, J. C.: A simple model for turbulence induced flocculation of cohesive sediment, Journal of Hydraulic Research, 36, 309–326, 1998.

Young, J. R. and Ziveri, P.: Calculation of coccolith volume and its use in calibration of carbonate flux estimates, Deep-Sea Research II, 47, 1679–1700, 2000.

Ziveri, P., de Bernardi, B., Baumann, K.-H., Stoll, H. M., and Mortyn, P. G.: Sinking of coccolith carbonate and potential contribution to organic carbon ballasting in the deep ocean, Deep-Sea Research II, 54, 659–675, 2007.